Westinghouse Non-Proprietary Class 3

WCAP-7401

LOSS-OF-COOLANT ANALYSIS: COMPARISON BETWEEN BLOWDN-2 CODE RESULTS AND TEST DATA

Westinghouse Electric Company LLC

NES Proprietary Class 3

WCAP-7401

LOSS-OF-COOLANT ANALYSIS:

COMPARISON BETWEEN BLODWN-2 CODE RESULTS AND TEST DATA

by

Stanislav Fabic

November 1969

APPROVED: L. S. Tong
L. S. Tong, Manager
Engineering Development

APPROVED: W G Brussalis
W. G. Brussalis, Manager
Engineering Mechanics

Westinghouse Electric Corporation
PWR Systems Division
P. O. Box 355
Pittsburgh, Pennsylvania 15230

INTERNAL DISTRIBUTION

G. J. Bohm

W. G. Brussalis

J. O. Cermak

L. Chajson

A. R. Collier

R. A. Dean (2)

J. W. Dorrycott (2)

S. Fabic (2)

R. J. French

P. B. Haga

J. D. McAdoo

J. S. Moore

C. W. Solbrig (2)

T. Stern

J. J. Taylor

D. E. Thorn

L. S. Tong

H. J. von Hollen

R. A. Wiesemann

Library (2)

Engineering Mechanics (60)

ACKNOWLEDGMENTS

The help given to the author by the following persons in procuring various test data is acknowledged:

- H. D. Curet - Idaho Nuclear Corporation
- G. H. Hanson - Idaho Nuclear Corporation
- E. V. Gallagher - IIT Research Institute
- W. C. Townsend - Batelle-Northwest National Laboratory

TABLE OF CONTENTS

TABLE OF CONTENTS

LIST OF ILLUSTRATIONS

LIST OF ILLUSTRATIONS (Cont)

LIST OF ILLUSTRATIONS (Cont)

LIST OF ILLUSTRATIONS (Cont)

NOMENCLATURE

A	Flow area (ft^2)
a	Velocity of sound (ft/sec)
c	Velocity of sound in Section 4 (ft/sec)
D	Diameter (or equivalent diameter) (ft)
F	Friction force term in the momentum equation
f	Friction coefficient
G	Mass velocity of fluid ($lbs/sec/ft^2$)
g_c	Gravity constant = 32.2 (ft/sec^2)
h	Fluid enthalpy (Btu/lb)
J	Mechanical equivalent of heat (ft-lb)/Btu
J_m	Bessel function of order m
L	Length (ft)
N	Constant defining the degree of thermal non-equilibrium (see Eq. 9 in Section 2)
P	Fluid pressure
R	Vessel radius
r	Radial coordinate
q	Rate of heat addition per unit mass of fluid (Btu/lb/sec)
T	Fluid temperature (°F)
t	Time (sec)
u	Fluid velocity (ft/sec)

NOMENCLATURE (Cont)

V	Volume (ft^3)
v	Specific volume of fluid (ft^3/lb)
z	Spatial coordinate
x	Quality of vapor/liquid mixture ($\frac{lb\ vapor}{lb\ mixture}$); also, spatial (length) coordinate
α	Void fraction ($\frac{ft^2\ vapor}{ft^2\ mixture}$); also zero root of Bessel function
$\frac{\partial}{\partial t}, \frac{\partial}{\partial x}$	Partial derivatives with respect to time, space
ν	Natural frequency of acoustic vibration (c/sec)
π	3.1416
ρ	Fluid density (lb/ft^3)
θ	Angular coordinate
ω	Angular frequency (rad/sec)

SUBSCRIPTS

CRIT	Critical (choked) condition
E	Equilibrium
FROZ	Pertaining to the "Frozen Composition" model
f	Of liquid
H	Homogeneous
HE	Pertaining to the homogeneous, equilibrium model
g	Of vapor
p	At constant pressure
ρ	At constant density

ABSTRACT

Westinghouse BLODWN-2 Code was written to describe the hydraulic transients within the reactor primary coolant system, caused by the loss of coolant through an assumed rupture. Subcooled, transition and two-phase (saturated) blowdown regimes are considered. The code employs the method of characteristics and assumes one-dimensionality of flow and homogeneity of the liquid-vapor mixture. A degree of thermal nonequilibrium is specified through a special manner in which the local velocity of sound in the vapor-liquid mixture is computed. Initial nonuniformities of the liquid temperature distribution can be considered. These were found to be mainly responsible for the observed local pressure undershoots.

The ability to consider multiple flow branches and a large number of mesh points (2400) gives the code the required flexibility to represent the various flow passages within the primary coolant system and in the detail necessary for tracking the acoustic decompression waves. These waves are mainly responsible for the loads on the reactor internals, piping and other system components.

This report documents the various comparisons between test data and BLODWN-2 calculation results. Good comparisons were obtained, starting with the blowdown of a simple pipe and ending with that of a complex primary coolant loop. Analysis of the blowdown of a larger vessel indicated that higher order effects introduced by the multidimensionality of flow and pressure fields cannot be obtained through simple one-dimensional modeling. A synthesis of an equivalent piping network would allow application of the one-dimensional BLODWN-2 program to such cases. Work is presently underway to determine the most suitable method for synthesizing networks that would satisfactorily bring out the effects of multidimensionality.

SECTION 1

INTRODUCTION

As far as the integrity of the primary coolant system is concerned, there are three main problem areas associated with a loss-of-coolant accident. Listed in the order of their occurrence they are:

a. Generation of Hydraulic Forces Acting on the Reactor Internals, Vessel, Steam Generator, Pump and Associated Piping

Here we wish to establish whether:

1. The reactor internals have retained a functional geometry that would allow insertion of the control rods and proper operation of the emergency core cooling system;
2. The vessel, steam generator and pump supports can withstand the impact-type forces and associated moments; and
3. Stresses in the piping, nozzles, steam generator tubing and other primary coolant system components are below the maximum allowable limit.

b. Reduction of the Reactor Core Cooling

In the case of an inlet pipe rupture the coolant flow through the core will decrease and may even reverse direction. The coolant density will also decrease quickly. These effects cause a reduction in the heat removal from the core. The core cladding temperature will start to increase until checked by the decrease in power generation and by operation of the emergency core cooling system. The power decrease will result from the inherent shutdown mechanism associated with the void (steam) formation and from the fuel temperature rise, as well as by the insertion of the control rods and other (liquid) absorbers.

Here we wish to establish:

1. The rate and amount of void formation as functions of time and the location in the core; and

2. The fuel and cladding temperature history throughout the core as associated with the feedback-affected local power generation and local conditions of the coolant, both prior to and after the commencement of emergency core cooling.

c. Generation of Thermal Stresses in the Primary Coolant Piping, Nozzles, Steam Generator Tubing, and Other Components.

These come about as the coolant changes phase and experiences a decrease in both pressure and temperature. The final pressure will be of the order of 40 psi, corresponding to the coolant temperature of about 260° to 270°F.

In the case of a large break, the primary coolant fluid will experience large pressure, flow, and density transients throughout the system. The coolant will depressurize by the passage of rarefaction waves generated at the rupture and traveling with a local speed of sound. Once the local pressures drop below saturation, vapor generation will take place, drastically reducing the speed of sound and hence the local rate of decompression. In fact, once the coolant has become steam, acoustic wave effects responsible for large pressure fluctuations become very small everywhere in the system, and the entire system decompresses rather uniformly (in space).

Analytical modeling of the blowdown regime encompassing the large pressure and flow transients must allow for a very detailed spatial distribution from the standpoint of accuracy of calculation of sonic decompression. Such modeling must also allow detailed evaluation of hydraulic loadings on all reactor internals piping and other loop components. The Westinghouse BLODWN-2 computer program[6] has those capabilities. In contrast to the WHAM[6] program, which also gives a detailed picture of pressure and flow transients while no evaporation has yet occurred anywhere in the system, BLODWN-2 extends the region of validity well into the saturated blowdown regime. The importance of this ability to deal with the subcooled, transition, and the saturated blowdown regimes is threefold:

1. It can correctly compute discharge flows and wave reflections at the rupture when, locally, the water has already flashed into steam. This occurs a few milliseconds after a large rupture has started to "open."

2. It can consider the condition in which one portion of the system is still subcooled while the rest is already steam. The presence of adjacent steam regions will bring about damping and the eventual disappearance of any acoustic waves which may still exist in the subcooled region. The manner in which these transients damp out is important for calculation of the structural response of reactor internals and other components.

3. It can compute core fluid properties (velocity, pressure, density) and heat transfer during the early portion of blowdown when core flow reversal and local void formation takes place before the whole system fluid has become steam.

Once the fluid has become steam everywhere in the system, and when spatial fluctuations of pressure, velocity and density have died out, the subsequent pressure, flow and density changes are devoid enough of spatial variations that a "lumped-parameter" modeling becomes sufficient. Such modeling forms the basis of FLASH 1 and 2, RELAP 2 and 3, and SATAN programs in which the system is subdivided into "lumps" or elements whose decompression is solved simultaneously. These lumped parameter programs are well suited for the description of the saturated blowdown regime in which the whole primary coolant system needs to be subdivided into (at most) 15 to 20 lumps or elements. These programs are preferred to BLODWN-2 in the saturated blowdown regime because of the minimum number of mesh points needed for the system geometry description by the method of characteristics (employed in BLODWN-2). This has proven to be 10 to 20 times larger than the minimum number of "elements" used for the lumped parameter programs. Hence, BLODWN-2 would run some 3 to 5 times longer, despite the fact that for the same number of elements and mesh points, BLODWN-2 runs 3 to 5 times faster. During the subcooled and the transition blowdown regimes information on pressure, etc., is needed at more than 1000 locations; BLODWN-2 can accommodate up to 2400 locations or mesh points.

In view of the above presented arguments, it appears that the best strategy for calculation of thermal-hydraulic effects pertaining to the whole blowdown is as follows:

1. Employ BLODWN-2 program for the duration of (typically) one-tenth of the actual blowdown duration.
2. Employ FLASH-2 or SATAN for the remainder of blowdown, in order to describe the hydraulic transients everywhere except in the reactor core.
3. Use a separate, multidimensional program (such as LOCTA-THINC) for the description of thermal-hydraulic transients in the reactor core. The boundary conditions, at reactor inlet and outlet, would be supplied by the one-dimensional programs listed in (1) and (2) above.

The "core" program is necessary because it must consider multidimensional flow and sophisticated heat transfer routines. It must also merge with the nuclear power transients program.

BLODWN-2 includes heat transfer routines for the core and steam generators. However, their level of sophistication is adequate only for evaluation of the effects of heat transfer on the fluid decompression and phase change, rather than for calculation of the effect of fluid decompression on the fuel and cladding thermal transients.

BLODWN-2 does not include routines that consider the emergency core cooling system. The latter is accounted for in FLASH and SATAN, in a manner sufficient for the description of the effects of ECC on the fluid everywhere except in the core. The "core" program must have the necessary level of sophistication for the thermal-hydraulic description of re-flooding, etc.

The material presented in this report pertains to the examination of the capability of BLODWN-2 in the regimes of blowdown for which the program is best suited. This is accomplished by comparing the results of BLODWN-2 with the existing test data for a variety of situations which gradually increase in geometric complexity. Only test conditions leading to the largest hydraulic transients were chosen for comparison.

The brief description of the BLODWN-2 code presented in Section 2 gives an overall view of the theory on which the code is based. Comparisons with test data are first made for the simplest, truly one-dimensional systems described in Section 3, which starts with a discussion of the pressure undershoots.

Comparisons of results for vessels that introduce a departure from one-dimensionality are presented in Section 4. The small vessels are described first, without and with internals, followed by comparisons involving a relatively large vessel. The latter introduces significant three-dimensional effects which are discussed in some detail. Because the large vessel discussed contained a perforated baffle (core plate), the last portion of Section 4 discusses the computation method and comparison with test data concerning the hydraulic loading such a baffle would experience during blowdown.

Comparisons concerning a reactor primary coolant loop, which introduces a large degree of geometric complexity, are described in Section 5.

Section 6 presents comparisons of results based on two calculational methods pertaining to a highly simplified representation of a full-scale pressurized water reactor.

Conclusions are presented in Section 7.

SECTION 2

BRIEF DESCRIPTION OF BLODWN-2 CODE

The conservation laws on which the BLODWN-2 code is based are the well known, spatially one-dimensional, partial differential equations describing the conservation of mass, momentum, and energy of either a single phase fluid or a two-phase homogeneous mixture, contained within rigid walls. These equations are as follows:

$$\frac{\partial \rho}{\partial t} + \frac{\partial (\rho u)}{\partial x} = 0 \qquad \ldots .(1)$$

$$\rho \left(\frac{\partial u}{\partial t} + u \frac{\partial u}{\partial x}\right) = -g_c \frac{\partial p}{\partial x} - F \qquad \ldots .(2)$$

$$\frac{\partial h}{\partial t} + u \frac{\partial h}{\partial x} = q''' + \frac{1}{\rho J} \left(\frac{\partial p}{\partial t} + u \frac{\partial p}{\partial x}\right) \qquad \ldots .(3)$$

with the friction loss term F being represented by the one-dimensional approximation evaluated in a quasi-steady-state manner:

$$F = \rho \frac{f u |u|}{2 D_e} \qquad \ldots .(4)$$

and the energy addition term in Equation 3:

$$q''' = \left(q + \frac{uF}{g_c J}\right) \qquad \ldots .(5)$$

The equation of state is given in a polynomial form, relating ρ, p, and h.

Utilizing a suitable transformation procedure, the three partial differential equations are changed into a set of three pairs of ordinary differential equations. Two of these pairs describe the relationship between the pressure, velocity and density valid along two characteristic paths. One member of each pair describes the path itself; i.e., the path contours in the space-time plane. The third pair describes the path and the magnitude of the enthalpy change in the x-t plane.

These ordinary differential equations are then solved numerically within the framework of a fixed space-time mesh as described in Section 15 of Reference 10.

The local slopes of the three characteristic paths in the x-t plane are given by

$$\frac{dx}{dt} = u \pm a \qquad \text{. . . . (6)}$$

and

$$\frac{dx}{dt} = u \qquad \text{. . . . (6a)}$$

When $q''' = 0$ in Eq. 3, i.e., when heat transfer and energy of friction dissipation are negligibly small, the term "a" in Eq. 6 reduces to the well known relation for the velocity of sound in the fluid:

$$a_{q'''=0} = a_{HE} = \sqrt{g_c \frac{dp}{d\rho}} \qquad \text{. . . . (7)}$$

With the assumption of thermal equilibrium and using the above-mentioned polynomial relationships for the equation of state, the velocity of sound computed by Eq. 7 has the following properties:

In the subcooled regime it shows a slight effect of pressure and a somewhat stronger effect of temperature. The values of "a" are of the order of 2500-5000 ft/sec, the lower limit pertaining to the high temperature liquid.

As soon as the minute quantities of steam are formed there is a discontinuous drop to very low values of the order of 100 ft/sec. A further increase in the steam quality causes "a_{HE}" to increase rather gradually until the void fraction α becomes about 0.8. After this occurs, further increase in "a_{HE}" is steep, reaching (at $\alpha = 1$) the typical saturated steam velocity of sound of the order of 1600 ft/sec. An increase in pressure leads to an increase in "a_{HE}."

Experimental data on the velocity of sound in the steam/water mixtures exist only for relatively low pressures. These data were obtained by measuring the velocity of propagation of a weak compression wave in a shock tube.[11] The measurements show that the "frozen composition model" for the velocity of sound, which is also obtained from Eq. 7 by deleting the term representing the change in the steam quality, better agrees with the data. The frozen composition model gives a "U" shape to the velocity of sound vs. the void fraction curve. As the void fraction tends to zero, the predicted velocity of sound, a_{FROZ}, experiences a very large increase. At the other end, as void fraction approaches unity, a_{FROZ} approaches a_{HE}. At any given pressure the minimum a_{FROZ} is about twice as large as a_{HE} at the same void fraction.

In Reference 12 Henry contends that compression waves lead to a stable condition which favors prevention of the phase change during passage of the wave. Rarefaction waves, however, cause liquid superheat to occur, leading to an unstable condition in which a phase change is much more likely to occur. A complete, equilibrium-type phase change gives a_{HE}; whereas an incomplete phase change gives $a_{FROZ} > a > a_{HE}$. Henry proposed that

$$a = \{\frac{v_H}{v_{HE}} \frac{a_{HE}}{\sqrt{N}}\} \quad \ldots .(8)$$

where

$$v_H = (1 - N\, x_E)\, v_f + N\, x_E\, v_g \quad \ldots .(9)$$

$$v_{HE} = (1 - x_E)\, v_f + x_E\, v_g \quad \ldots .(10)$$

N = experimentally defined constant

When heat transfer cannot be neglected, as in the reactor core passages and in the steam generator tubing, the term "a" of Eq. 6 is no longer represented by the simple relation given by Eq. 7, but rather by

$$\frac{a^2}{g_c} = \frac{-\left[\frac{\partial h}{\partial \rho}\right]_p}{\left[\left(\frac{\partial h}{\partial p}\right)_\rho - \frac{1}{\rho J}\right]} \qquad \ldots .(11)$$

in which both partial differentials are also functions of the energy addition (or subtraction) term. The heat transfer term in the energy equation denotes the heat addition or subtraction per unit mass of the fluid. In the homogeneous two-phase fluid undergoing an equilibrium expansion process, this energy addition term also denotes the heat transfer between the liquid and the steam phase, which is responsible for growth of the steam phase. In actuality, however, the heat addition takes place at the wetted wall so that the largest effect on the phase change should be near such a wall. This would tend to de-homogenize the fluid/steam mixture, leading to a slip flow condition.

The velocity of wave propagation in the nonhomogeneous fluid flowing in the annular pattern of the phase distribution was experimentally found[13] to be quite different from either a_{HE} or a_{FROZ}, tending to the values of the velocity of sound in the saturated steam.

The calculational labor involved in finding "a" from Eq. 11 for the reactor core and steam generator tubing is therefore not justifiable.

In view of the above presented arguments it was decided to formulate the BLODWN-2 program such that the q''' term is first deleted from the energy equation during the transformation process leading to characteristic equations, but is subsequently added to the characteristic equation describing the enthalpy path. In this manner the partial differentials of Eq. 11 are not heat transfer dependent. This results in the homogeneous-equilibrium values for "a" (= a_{HE}) given by Eq. 7 which, as discussed above, gives unreasonably low values when the void fraction is very small. To compensate for this effect, "a" is updated by setting

$$a = a_{HE}\left[\frac{1}{\sqrt{20\, x_E}}\right] \qquad \ldots . (12)$$

when

$$0 < x_E < 0.05$$

which bears a similarity to Henry's definition for "a" as given by Eq. 8. In fact, the term shown within the square bracket of Eq. 12 is the same as the multiplier for the critical mass velocity which Henry found to best fit his critical flow test data:[14]

$$G^{CRIT} = G_{HE}^{CRIT}\left[\frac{1}{\sqrt{20\, x_E}}\right]$$

$$= \rho_{HE} \cdot a_{HE} \cdot \left[\frac{1}{\sqrt{20\, x_E}}\right] \qquad \ldots . (13)$$

Note that when $x_E = 0.05$, $a = a_{HE}$. For larger qualities of steam/water mixture, BLODWN-2 sets

$$a = a_{HE} \qquad \ldots . (14)$$

The consequences of the above-described assumptions incorporated in BLODWN-2 are as follows:

1. Sharp discontinuity in the behavior of "a" is eliminated, leading to better stability in numerical calculations.
2. The predicted velocity of sound in the low quality region has "more credible" values.
3. Such updating of "a" (see Eq. 12) implies consideration of thermal nonequilibrium despite the fact that the actual heat

transfer between the liquid and the vapor phase is not locally evaluated.

4. Heat transfer in the core and in the steam generator enters only into the evaluation of the local enthalpy, not of the local velocity of sound. This greatly simplifies calculation of a_{HE}.

The value of "a" is recomputed after each time increment and for every mesh point in the system where fluid is in the form of a two-phase mixture. The boundary condition at the exit considers Zaloudek's relation[15] for G_{CRIT} when the fluid, just upstream of the rupture, is in the form of liquid. When this fluid becomes a two-phase mixture

$$G_{EXIT} = \rho . a \leq G_{CRIT}(\text{ZALOUDEK}) \qquad \ldots . (15)$$

In both cases the boundary equation and the equation for the characteristic of the path leading to the boundary are solved simultaneously in order to obtain the appropriate pressure and flow.

The system to be analyzed is subdivided in up to 120 flow channels (or legs), each leg having a uniform cross section area. The boundary conditions between legs may consist of

1. branches joining up 6 legs,
2. area changes (contractions or expansions) with the associated minor losses
3. orifices
4. pumps

The end boundaries could consist of flow valves, dead-ends, or pressurizers.

Discrete values from homologous curves (see Reference 16) are inputed for the description of the pump behavior, with or without power.

Specification of the negative initial time allows the program to adjust flow, enthalpy and pressure distribution, all of which are initialized as rough approximations. Once the "time zero" is reached, the BLODWN-2 code allows specification of the system rupture that initiates the blowdown transients.

The capability of BLODWN-2 to consider many branches allows the analyst to represent three-dimensional flow paths by equivalent piping networks - as in the WHAM program.[16]

SECTION 3

PIPE BLOWDOWN

3.1 DISCUSSION OF PRESSURE UNDERSHOOTS

Pressure undershoots (i.e., the temporary local pressure drops below the saturation pressure corresponding to a given fluid temperature) have been reported by all sources of experimental data on blowdown.[1,2,3]

The previous blowdown analyses, employing the assumption of thermal equilibrium and of uniform fluid temperature, did not predict the observed undershoots.[2,7,8] It was therefore generally believed that thermal nonequilibrium and/or metastability are the responsible mechanisms. Our definition of metastability assumes that the liquid must be superheated by some finite amount before vapor growth is triggered. The superheat is caused by the drop in the liquid pressure which takes a finite length of time to drop a specified amount below saturation. For this reason, the "vapor growth delay time" has often been employed as a measure of metastability.

Once vapor nucleation has occurred, the subsequent rate of vapor growth is determined by the rate with which the heat is transferred from the surrounding liquid to the vapor bubble boundaries. Thus, the larger the local superheat (i.e., the lower the local pressure) the faster will be the rate of bubble growth which, due to significant density changes, will tend to repressurize the fluid to the saturation pressure. Edward's thermal nonequilibrium blowdown analysis[5] considers such a process by actually tracking the growth of vapor bubbles in the nonuniform pressure field. This is accomplished by employing various assumptions as to the nucleation delay time and the number of the active nucleation centers, but at an enormous expense of computer time.

If metastability and thermal nonequilibrium were very important pheonmena, their effects (i.e., pressure undershoots) should be measurable everywhere in the system. An example of Edward's calculation results is illustrated in Figure 3-1 where his model does predict occurrence of undershoots at all locations in the blowdown pipe. Most of the measurements, however, show that pronounced pressure undershoot occurs only at or near the closed end of the pipe (or vessel nozzles). Test data[4] for such a pipe blowdown are also shown in the figure. In view of that disagreement, it becomes worthwhile to examine whether some other phenomena, rather than metastability and thermal nonequilibrium, could explain the discrepancy.

3.2 EFFECT OF TEMPERATURE PROFILE ON PRESSURE UNDERSHOOTS

The most pronounced undershoots occur at closed ends, such as the dead ends of pipes or nozzles (where pressure gages are usually located). It is very likely that these locations act as heat sinks, causing a steep temperature gradient in the adjacent fluid. Such steep temperature gradients have actually been observed,[9] as illustrated in Figure 3-2. On the basis of that observation it became of interest to examine what predictions for pressures at closed ends will result from the BLODWN-2 computer program which does not consider the above described metastability and thermal non-equilibrium. For this purpose, a pipe blowdown geometry of Reference 2 was chosen, with one of the initial conditions noted in that reference.

A horizontal pipe 6 feet long and 2 inches ID contained water initially pressurized to 980 psig. This water was heated by uniformly wrapped heaters to an average temperature of 490°F. One end of this pipe was closed, the other being fitted with a glass diaphragm which was ruptured by an air gun pellet, causing a fluid to discharge into a relatively large container -- initially at ambient pressure and temperature. The rupture area was assumed to open linearly to the full pipe cross section area in 1/2 milliseconds. For purposes of calculation with BLODWN-2 code (which employs the method of characteristics) the pipe was "meshed" with a mesh spacing of 1.7143 inches. Five cases were examined, each differing only in the specification of the initial temperature profile near the closed end of the pipe; the temperature was assumed to be uniform everywhere else.

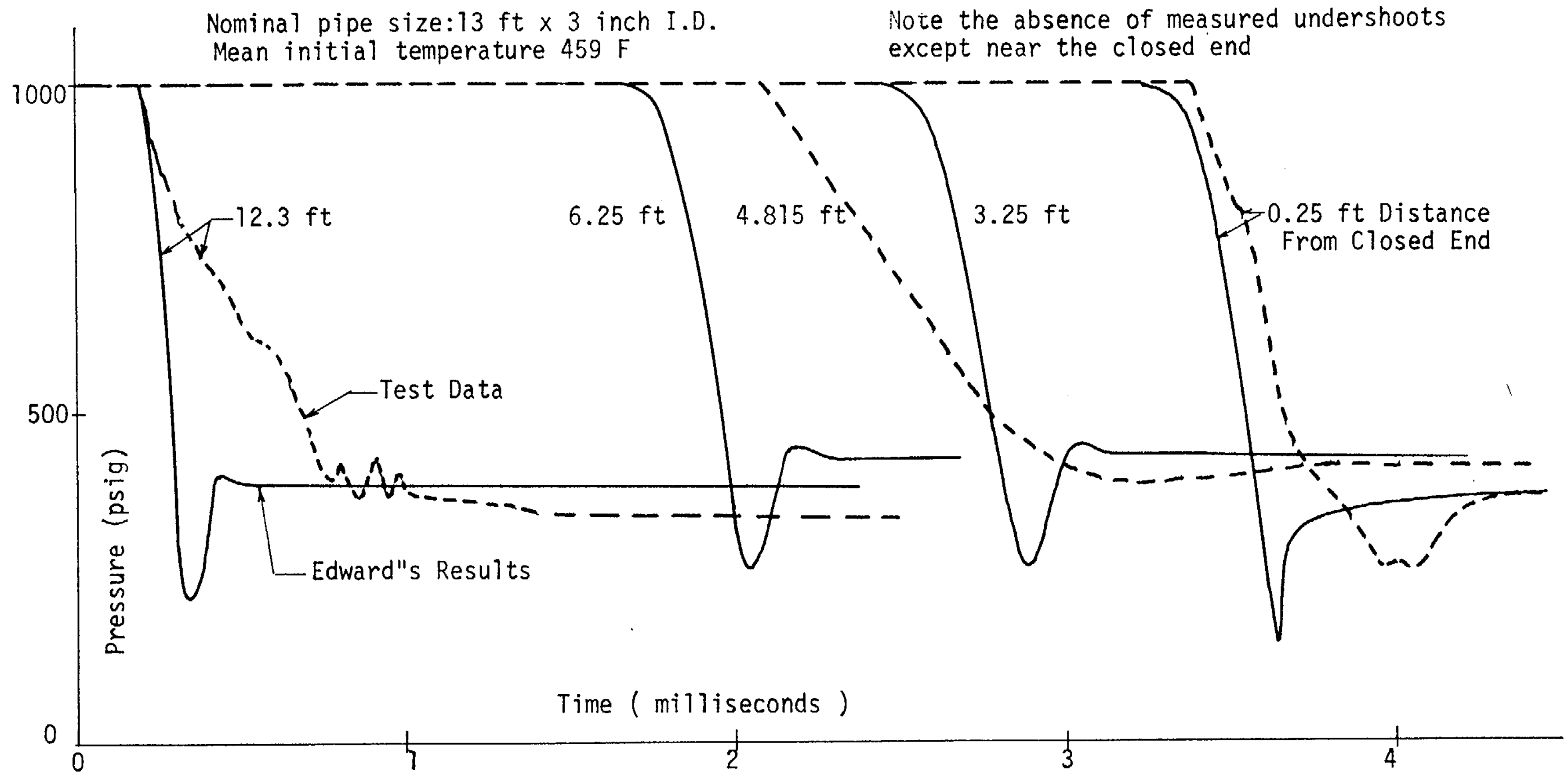

Figure 3-1. Comparison of Measured Pressures Along the Pipe (Ref. 4) With Results of Edward's Non-Equilibrium Analysis (With 10^7 nuclei/lb)

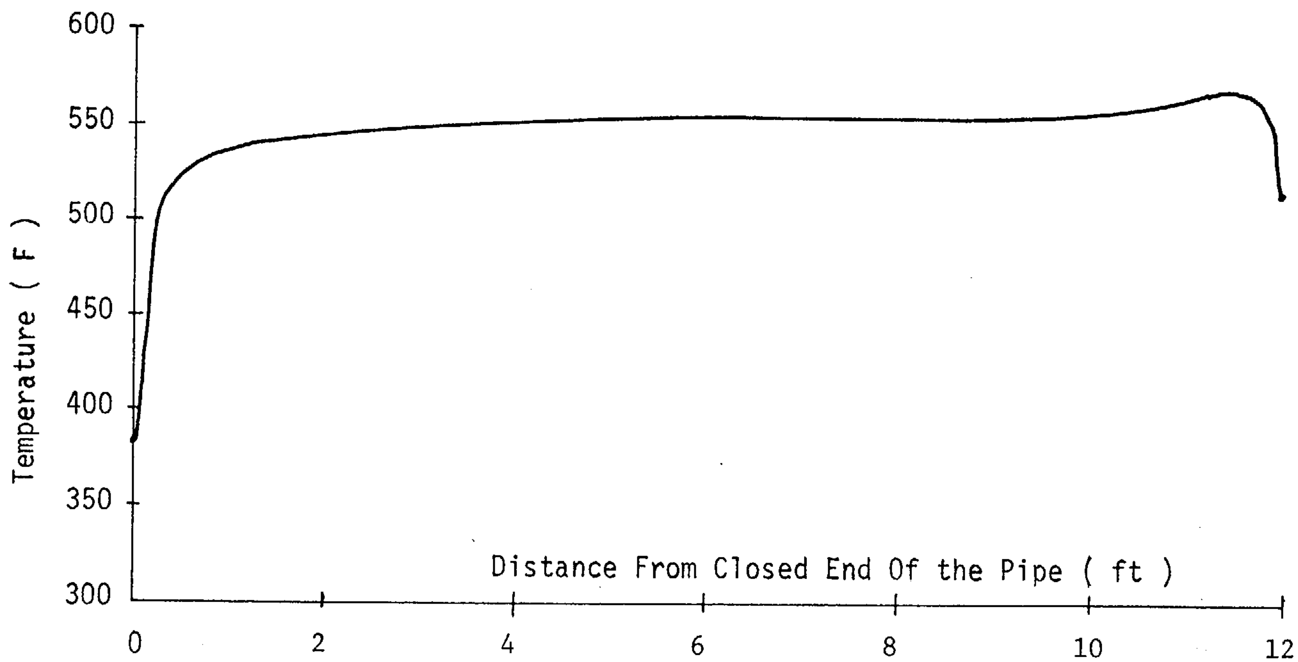

Figure 3-2. Measurement of Initial Temperature Distribution Pressurized Water Contained Within a Uniformly Heated 2" I.D. 12 ft Long Pipe (Ref. 9)

Temperature profiles and the computed pressure histories at the closed end are shown in Figure 3-3. The first case pertains to the uniform water temperature which resulted in no discernible pressure undershoot. In the other four cases, linear temperature profiles were specified, each starting with 330°F at the closed end (arbitrarily assumed) and differing only by the depth of penetration; i.e., by the slope.

The results show that both the strength of the undershoot and its shape depend strongly on the temperature profile penetration. After a certain penetration distance was exceeded (about 5 inches), a simple undershoot changed character and became a pressure oscillation -- its number of cycles increasing with the penetration depth. Other than linear temperature profiles, and with other minimum temperatures (higher or lower than 330°F) only altered the strength and character of the undershoot.

Figure 3-4, taken from Reference 2, shows the measurement of pressure at the closed end of the above-mentioned pipe for two different initial conditions. At the time, the initial temperature was assumed to be uniform and the undershoots were thought to be the consequence of metastability. What the actual temperature profiles were in these tests is not known; it is interesting to note, however, that both cases of Figure 3-4 have their counterparts in one of the cases shown in Figure 3-3.

3.3 COMPARISON WITH TEST DATA

3.3.1 British Pipe Blowdown Tests

Figures 3-5, 3-6 and 3-7 show comparisons between BLODWN-2 results and test data[4] pertaining to the blowdown of water from a horizontal pipe 13.43 feet long and 2.88 inches ID. The initial pressure and mean temperature of the water were 1000 psig and 459°F, respectively. The pressure-time histories are shown at three locations: 1.07 feet from the open end; 4.815 feet from the closed end; and 0.255 feet from the closed end. Only the pressure near the closed end shows a significant undershoot. The assumed temperature profile and geometry for this run are shown in the Appendix.

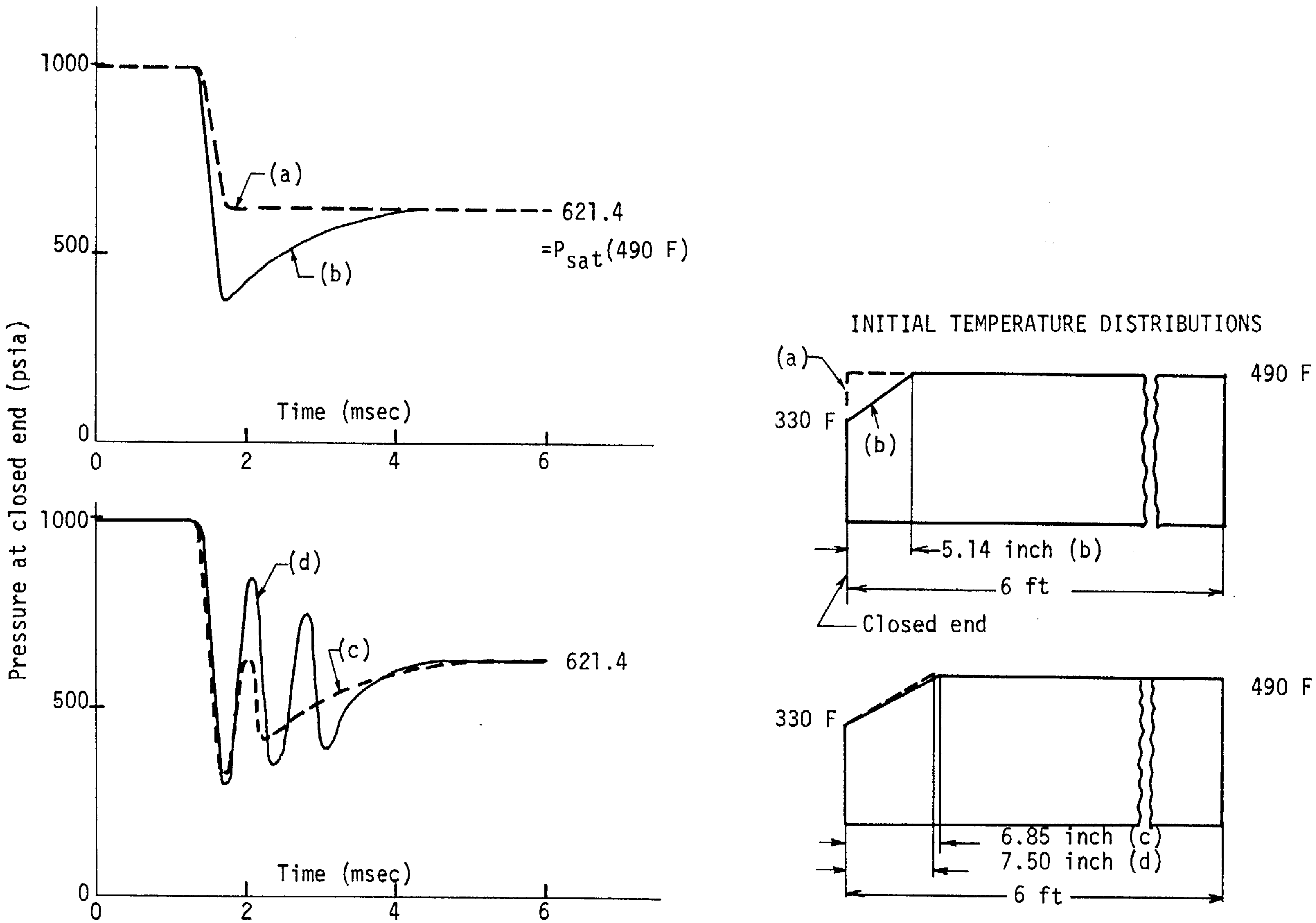

Figure 3-3. Effect of Initial Temperature Distribution on BLODWN-2 Predicted Pressure Undershoot At Closed End of a 2 in. I.D., 6 ft Long Pipe

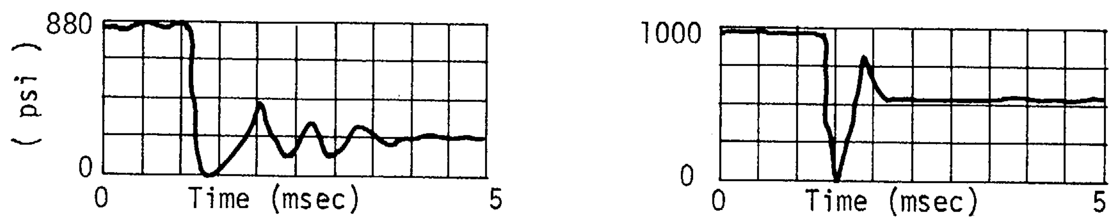

Record 725 A

Initial Temperature 420 F
Initial Pressure 800 psi

Record 727 B

Initial Temperature 490 F
Initial Pressure 980 psi

Figure 3-4. Measurement of Pressure-Time History At Closed End of a Blowdown Pipe (From Ref. 2) Illustrating Pressure Undershoot Types

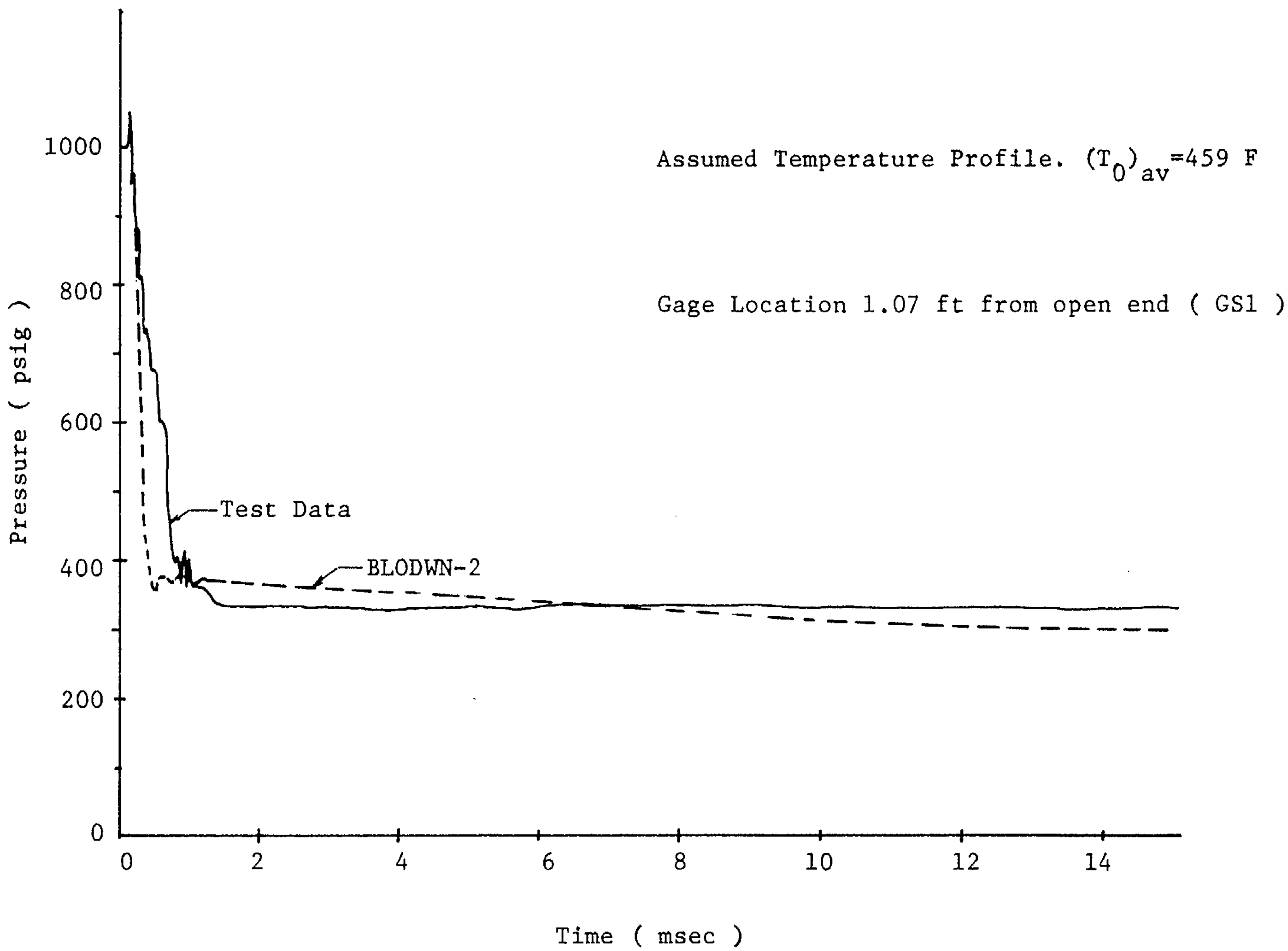

Figure 3-5. Pipe Blowdown; Subcooled and Transition Regimes Comparison Between BLODWN-2 Results and British Test Data (Ref. 4) for Test #53

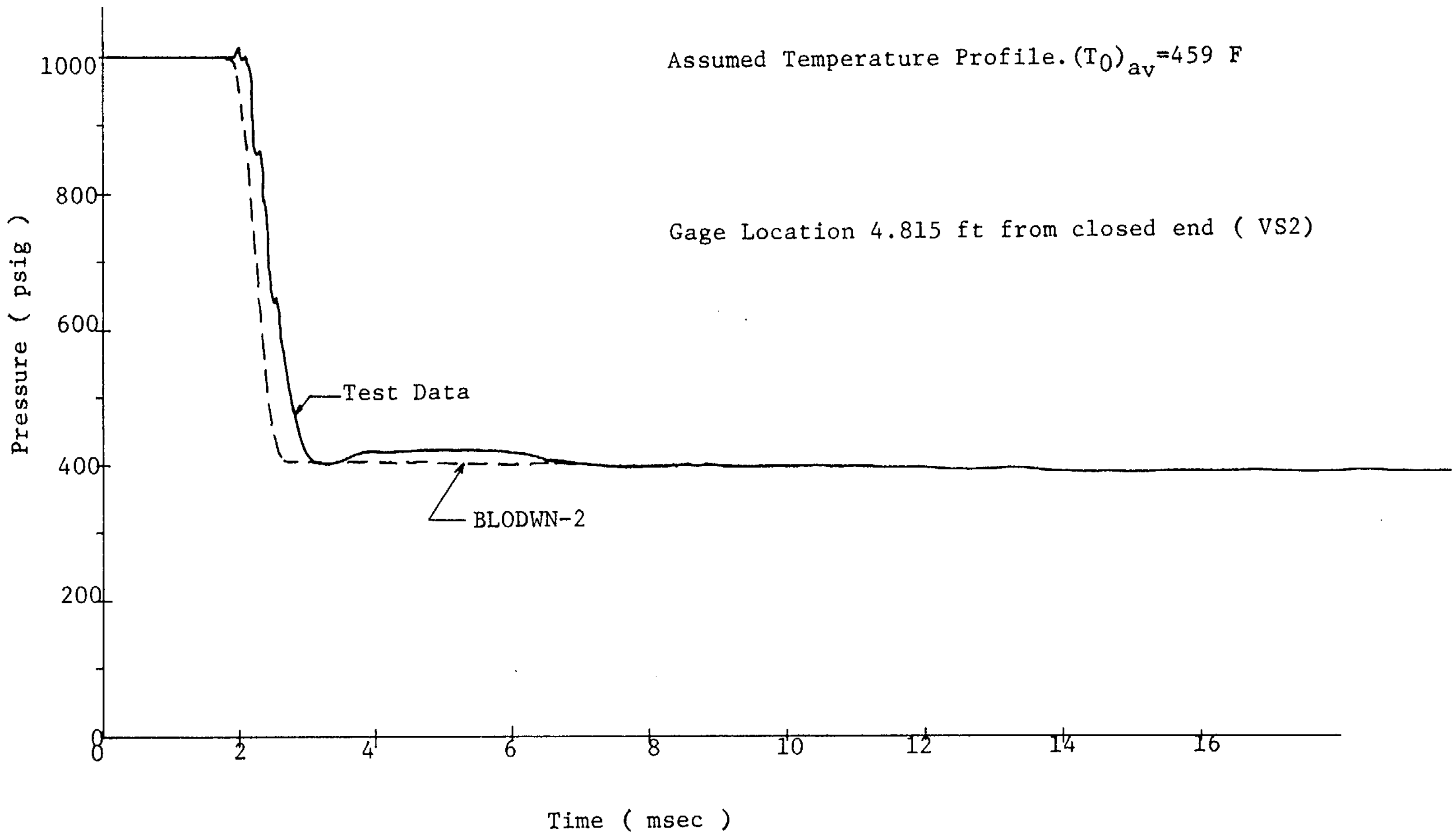

Figure 3-6. Pipe Blowdown; Subcooled and Transition Regime Comparison Between BLODWN-2 Results and British Test Data (Ref. 4) for Test #53

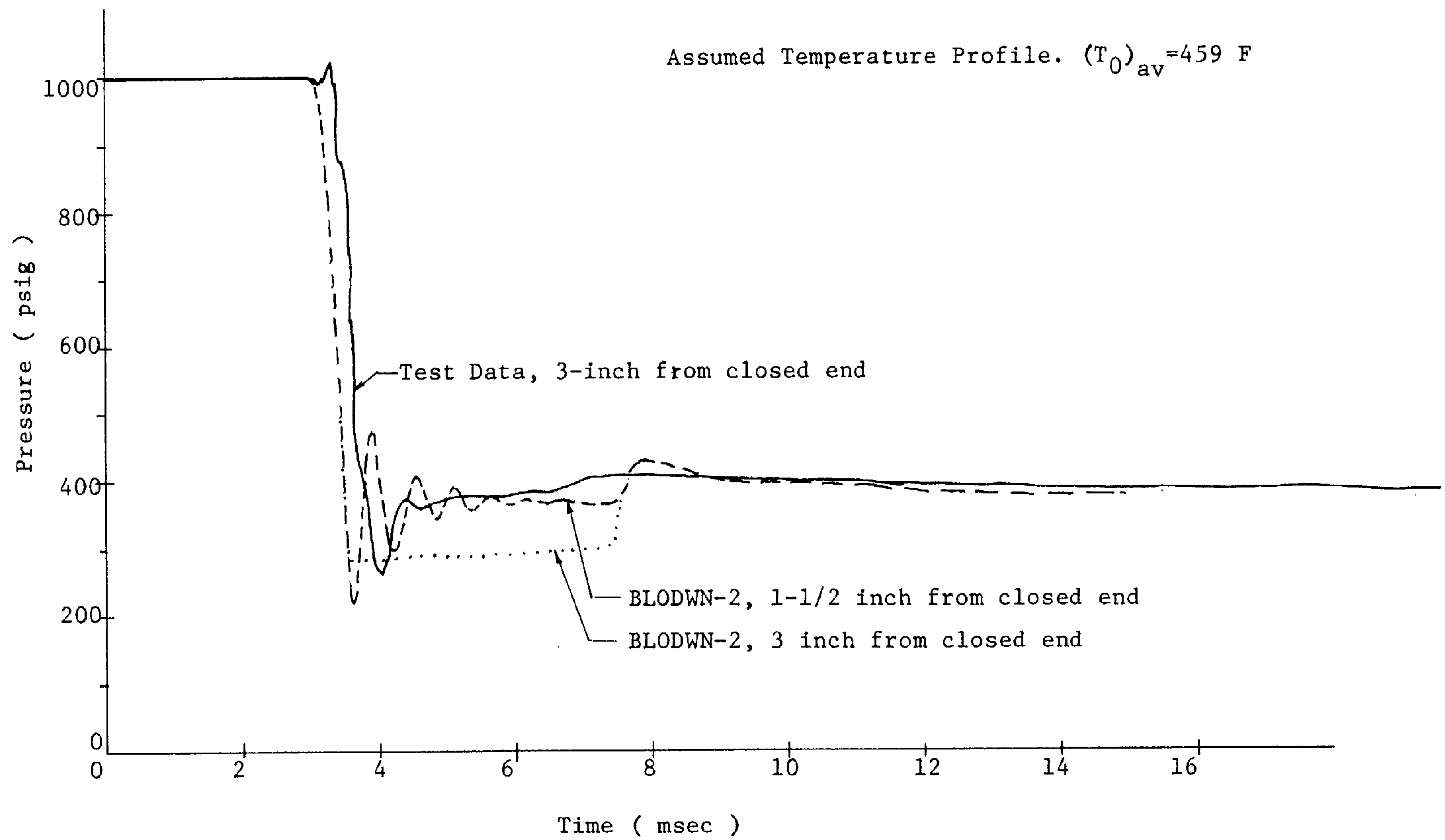

Figure 3-7. Pipe Blowdown; Subcooled and Transition Regimes Comparison Between BLODWN-2 Results and British Test Data (Ref. 4) for Test #53

It cannot be denied that some thermal nonequilibrium must exist in order to cause evaporation of water through the formation and growth of vapor bubbles, and that some degree of local superheat is necessary for vapor nucleation. It is quite likely, however, that vapor bubbles grow to the "thermal equilibrium size" very rapidly. Furthermore, because ordinary tap water was utilized in blowdown experiments it is likely that sufficient noncondensible gas (air) was present at nucleation sites, requiring only rather small amounts of local superheat for vapor nucleation. Consequently, blowdown calculations with a thermal equilibrium modeling are deemed satisfactory, providing that the initial temperature profiles are accounted for when such are either expected or measured.

Local steep temperature profiles appear to be largely responsible for the observed pressure undershoots during blowdown. In Reference 5, Edwards concluded that a detailed thermal nonequilibrium description of blowdown is necessary, both for correct prediction of depressurization of a vessel plus pipe system and for the prediction of pressure undershoots. Our results, however, indicate that such a detailed thermal nonequilibrium description is not necessary.

3.3.2 Illinois Institute of Technology Research Institute (IITRI) Pipe Blowdown

The strong effect of the initial water temperature distribution on local pressure histories during blowdown can be seen from the IITRI pipe blowdown tests.

A 12-foot-long, 2-inch ID pipe containing hot pressurized water was oriented such that its axis formed a 5-degree angle with the horizontal plane -- the uppermost end being provided with a glass diaphragm and the lowermost end being closed off. The center section contained flanges fitted with a viewing window. Heating coils were wrapped around the entire length of the pipe except for the viewing window flanges. A number of pressure and temperature transducers were located along the pipe to obtain data during blowdown initiated by the rupture of the glass diaphragm. The discharge end was connected to a relatively large tank filled with air at ambient pressure and temperature. The small inclination of the pipe axis facilitated venting of air during the heatup process.

While in most previous blowdown tests the assumption was made that the initial water temperature was uniform within the pipe, the recorded local pressure during blowdown indicated that this cannot be true.[9] The best guide as to the temperature of liquid just upstream of any given pressure transducer is the recorded local pressure at the end of subcooled blowdown period; that pressure equals p_{sat}, corresponding to the local liquid temperature. To check this assertion, tests were performed by IITRI in which thermocouples were placed along the pipe in pairs. One member of the pair was at the liquid/wall interface along the top surface of the pipe, the other along the bottom surface.

Figure 3-8 shows the results of such temperature measurements for Run Nos. 3 and 4. The dotted lines give local temperature data of the thermocouple pairs, the solid line is the average liquid temperature (along the pipe axis). Visual observations through the central viewing window indicated the existence of a strong convective flow, wherein top layers of water moved towards the glass diaphragm end while the bottom layers moved towards the low dead-end of the pipe. This dead end acted as a strong heat sink. The viewing port flanges and the glass diaphragm end also acted as heat sinks, although of smaller magnitudes. The buoyancy effect caused by the pipe inclination, coupled with the existence of the heat sinks, created the observed convective currents. The very significant differences between the local temperatures of top and bottom layers of water came as a surprise.

Figures 3-9 and 3-10 show local pressure data recorded along the pipe during blowdown tests Nos. 3 and 4. Although the initial pressure in Test 4 was somewhat higher, the very significant differences in blowdown behavior are mainly attributable to the differences in the local amounts of subcooling -- i.e., of temperature profiles. In Test 4, the water temperature near pressure gages 1 and 2 was very close to the saturation level. The time at which the liquid/vapor mixture pressures dropped to about 50 psi was nearly four times longer for Test 4 as for Test 3.

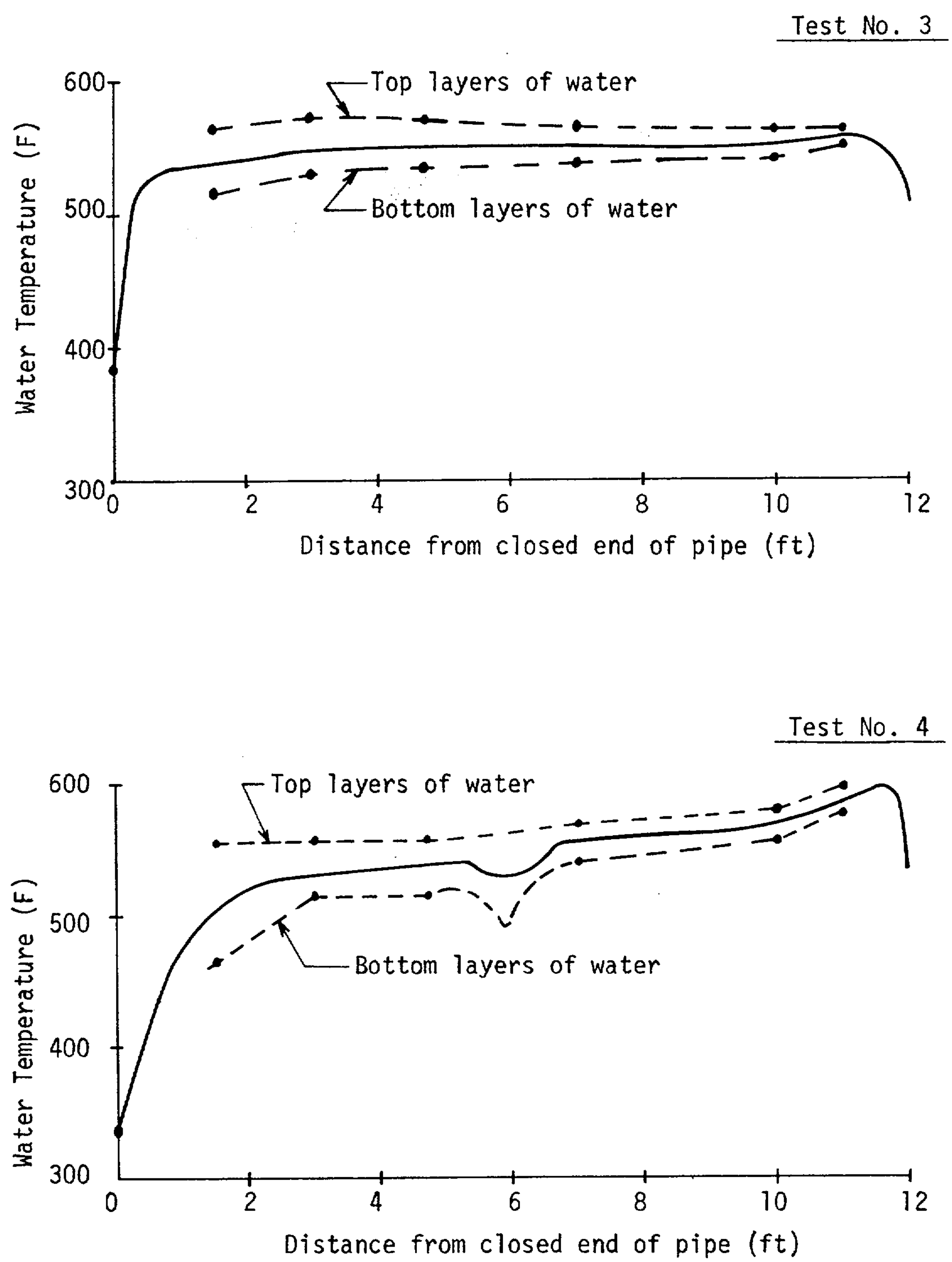

Figure 3-8. IITRI 12-ft x 12 in. ID Pipe Blowdown. Measurement of Initial Temperature Profile Along Pipe

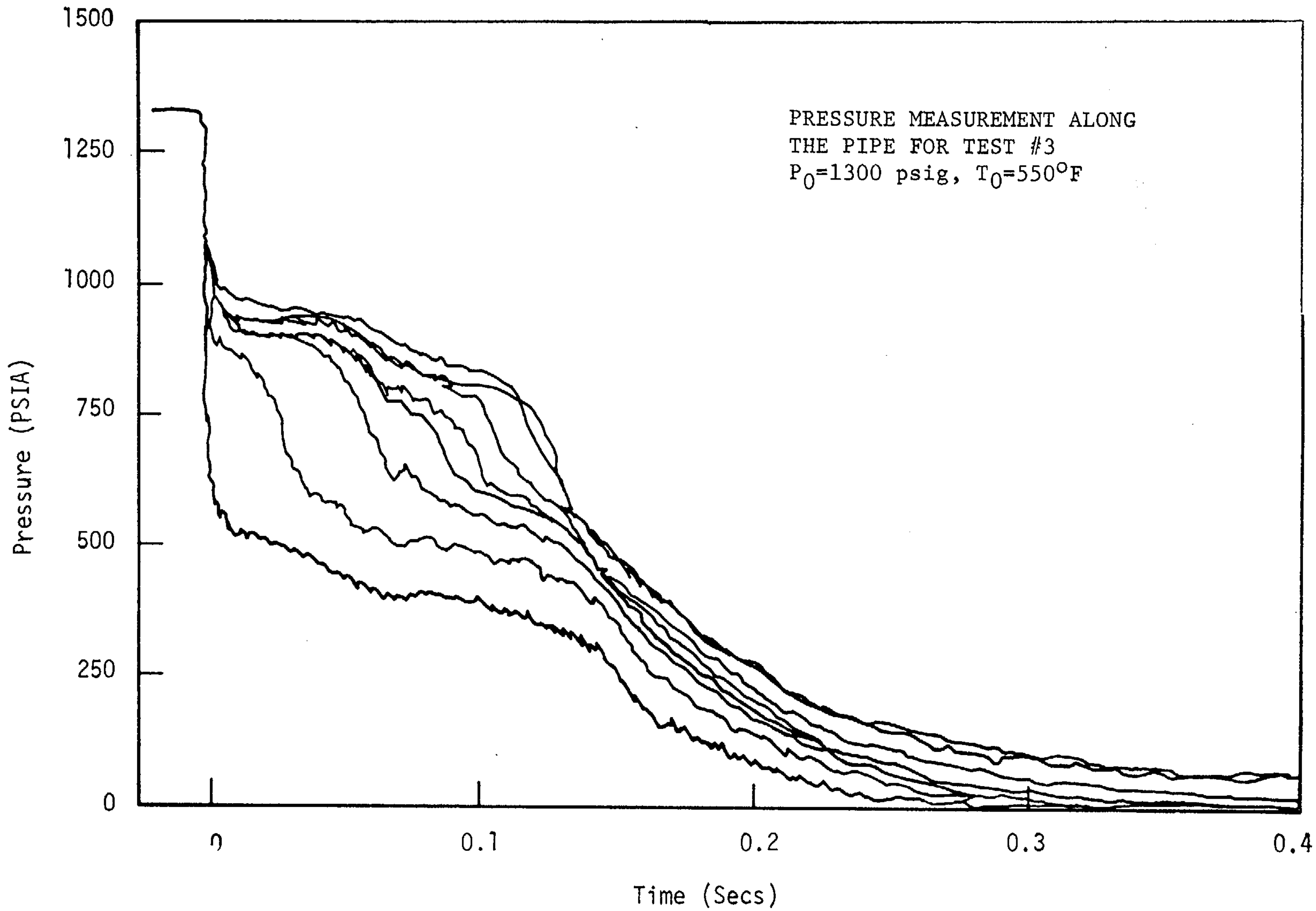

Figure 3-9. IITRI, 12-ft, 2-inch Dia. Pipe Without Internals

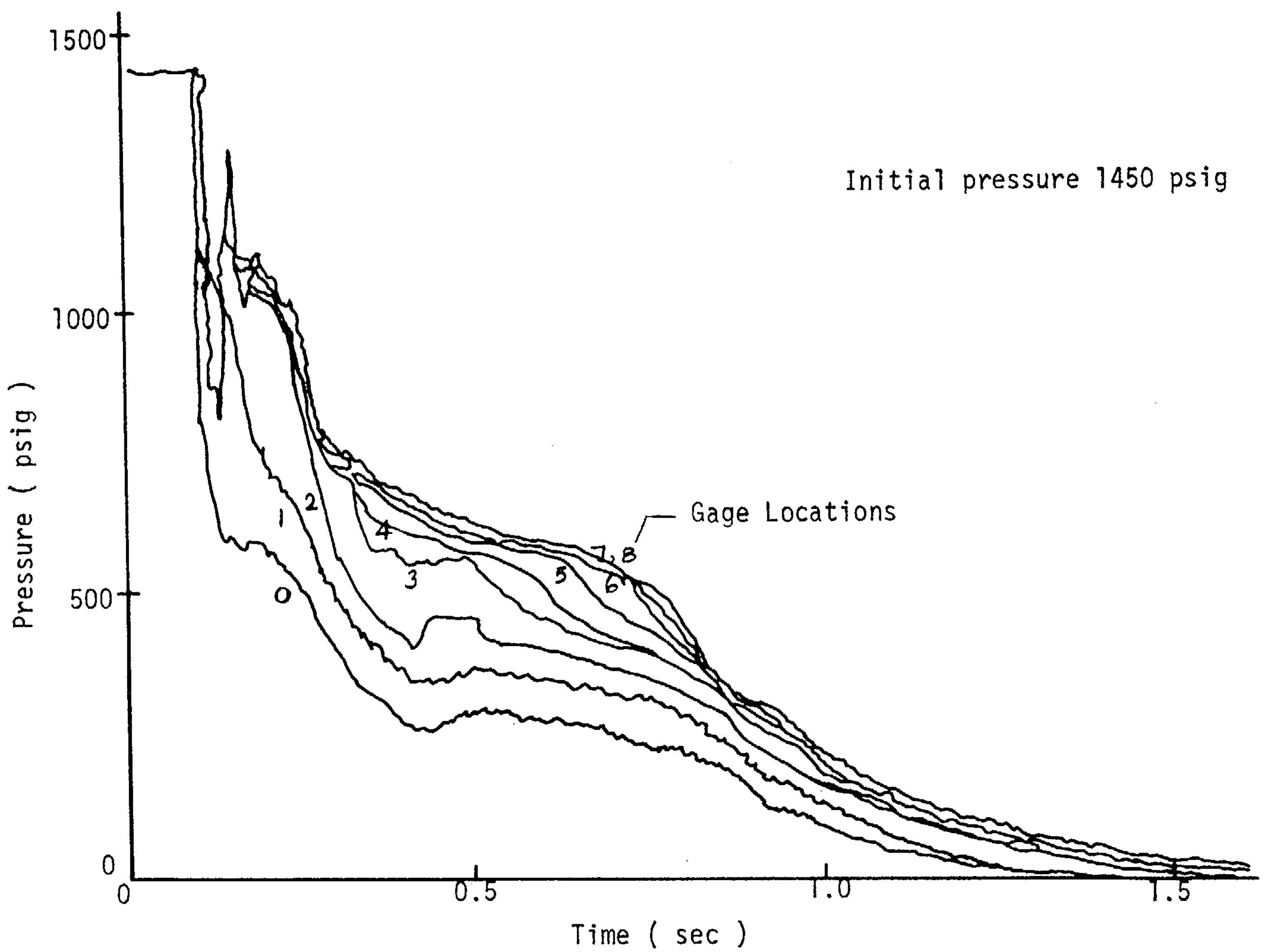

Figure 3-10. IITRI 12-ft x 2 in. ID Pipe Blowdown. Measured Pressure Histories Along the Pipe For Test No. 4

BLODWN-2 calculation results pertaining to Test 3 (shown in Figure 3-9) were based on the temperature profile shown in Figure 3-11. At that time, steep temperature profiles could not be considered in BLODWN-2. Nevertheless, comparison of Figure 3-12 with Figure 3-9 shows that the relative differences between computed pressures for various locations show a distinct similarity with test data. The initial levels of computed pressures in a two-phase blowdown regime are also satisfactory, considering the differences in the initial temperature profiles. The latter effect was responsible for the somewhat faster depressurization computed by BLODWN-2.

This comparison also shows that BLODWN-2 is capable of satisfactory prediction of blowdown phenomena in all blowdown regimes: subcooled, transition, and saturated.

3.3.3 Blowdown of IITRI Pipe Containing a Rod Bundle

A six-foot-long, 2-inch ID pipe was fitted with a rod bundle to simulate the effect of an unheated reactor core on blowdown behavior. Although such internal flow restrictions cause local departures from a one-dimensional flow pattern, such departures are not very significant. Hence, this particular test geometry still falls in the "one-dimensional" category. It does, however, serve to illustrate how the regions connected with high impedance passages depressurize during blowdown.

The rod bundle consisted of seven 1/2-inch-diameter rods provided with perforated plate spacers at each end. Figure 3-13 illustrates the geometry, the local ratio of the flow area over the empty pipe area, locations of pressure transducers, and two assumed temperature profiles. These profiles differ mainly near the two ends of the pipe. The measured initial pressure was 1380 psig and the mean temperature was estimated to be 532°F.

Three cases were examined with the BLODWN-2 code. In the first two runs, the perforated plate spacers were treated as separate flow passages (of small cross section area) connected in series with the regions downstream and upstream of the plate. The assumed temperature profiles in the first and the second run were the profiles "A" and "B" of Figure 3-13.

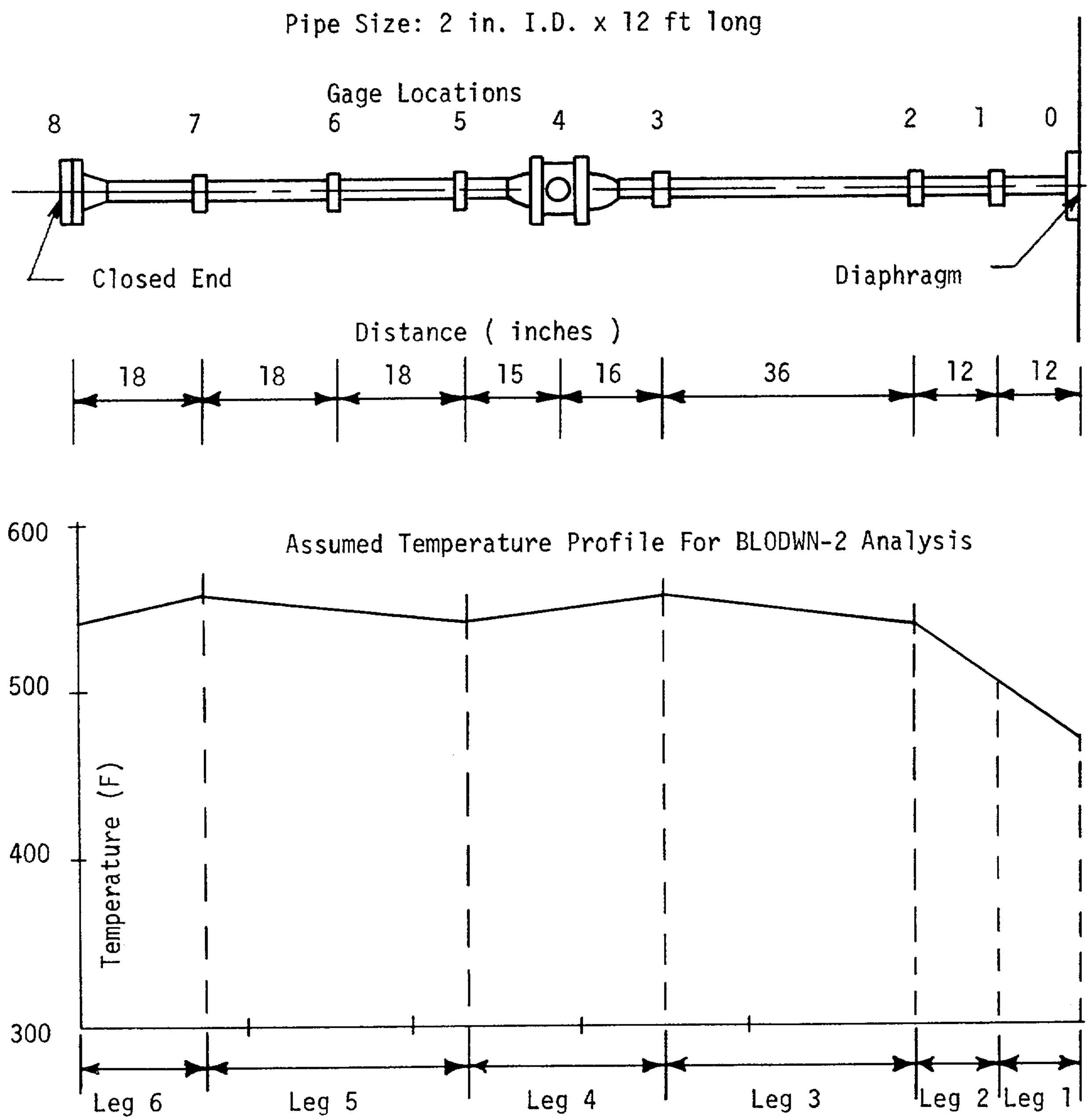

Figure 3-11. Test Geometry, Gage Locations, and Assumed Temperature Profile for BLODWN-2 Calculation of IITRI Pipe Blowdown

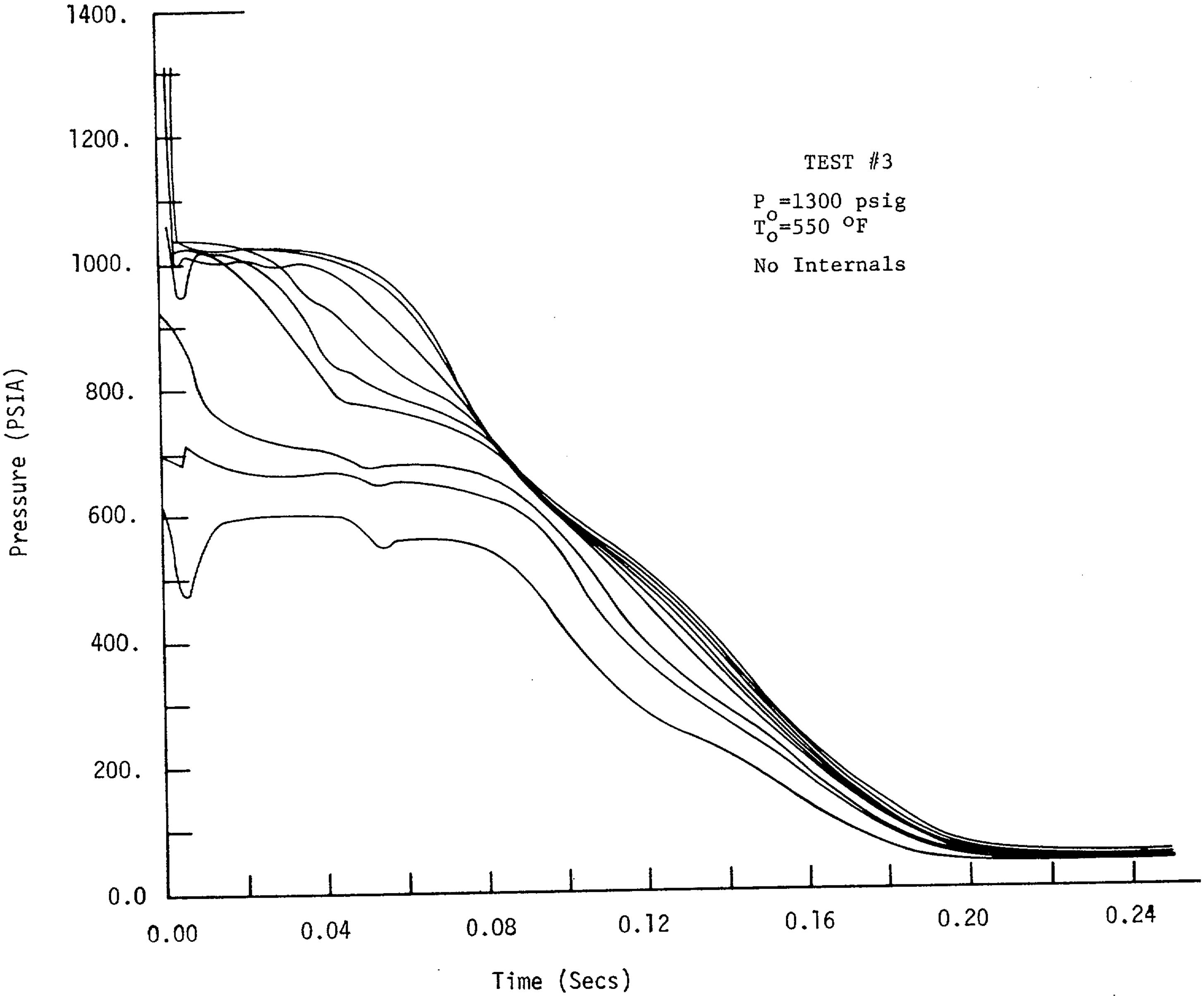

Figure 3-12. BLODWN-2 Results for Pressure Along the IITRI, 12-ft, 2-inch Diameter Pipe

Geometry, Gage Locations, and Assumed Temperature Profiles
For BLODWN-2 Analysis

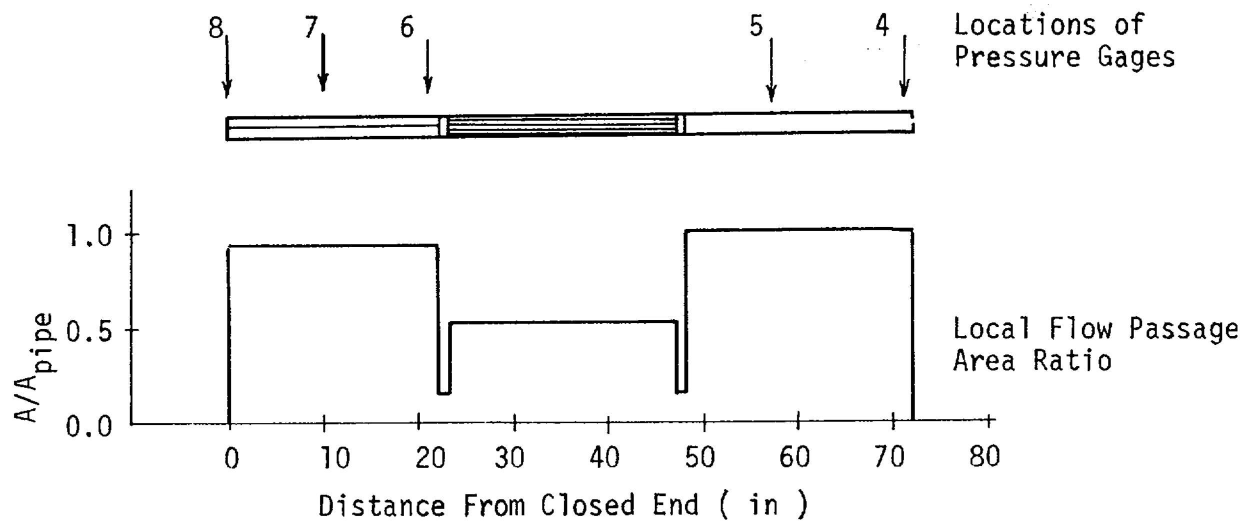

Assumed Temperature Profiles For BLODWN-2 Analysis

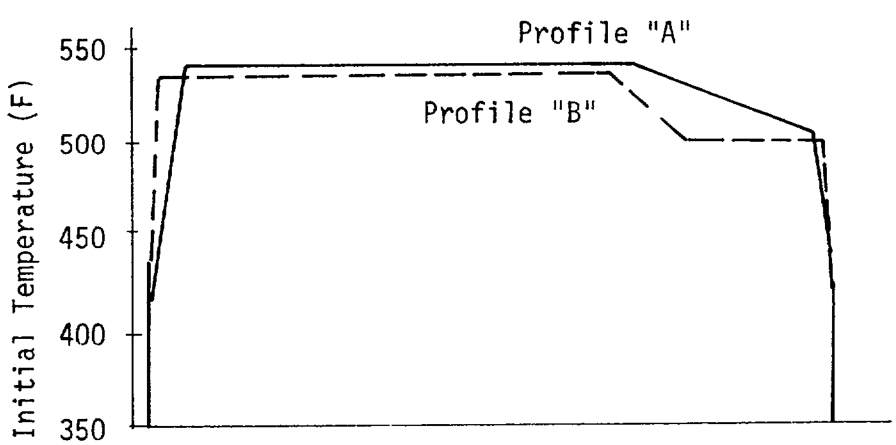

Figure 3-13. IITRI Pipe with Rod Bundle

Figure 3-14 shows the test data and results of the first run. It can be seen that the grouping of pressure traces was correctly predicted; those pertaining to the region upstream of the rod bundle show a rather slow and uniform decompression rate, while the pressures in the region downstream of the rod bundle drop off steeply. The pressure undershoots at the dead end and near the discharge end were predicted, although their magnitudes did not match. The second dip in the computed pressure for Location 4 was attributed to the excessive axial penetration of the temperature profile "A" near the discharge end. The computed pressure at Gage 5 location reached saturation at about 830 psig in contrast to the measured 700 psig, indicating that the initial temperature of the liquid near that location must have been lower than originally assumed. These two corrections were employed in temperature profile B, together with a decrease in the profile penetration depth at the closed end. This latter modification in the profile was in the wrong direction, as illustrated in Figure 3-15a which shows the absence of the pressure undershoot for Location 8. Temperature profile modifications near the discharge end, however, were in the right direction.

In the third run, in which temperature profile "B" was retained, the perforated plate spacers at the two ends of the rod bundle were treated as passages of the same area as that of the section of the pipe containing the rod bundle. A quasi-steady loss coefficient, obtained by standard methods, was applied at each end of the rod bundle to account for the contraction and expansion losses encountered in the true geometry.

Comparison of Figure 15a with Figure 15b shows that the employment of quasi-steady losses and deletion of separate, small area passages were not detrimental. This conclusion is important insofar as such simplification in geometric modeling leads to a significant reduction in computer running time. The latter depends on the smallest mesh spacing anywhere in the system; the thin rod end plates force this mesh to be very small because the minimum of three mesh points are required along any constant flow area segment (or "leg").

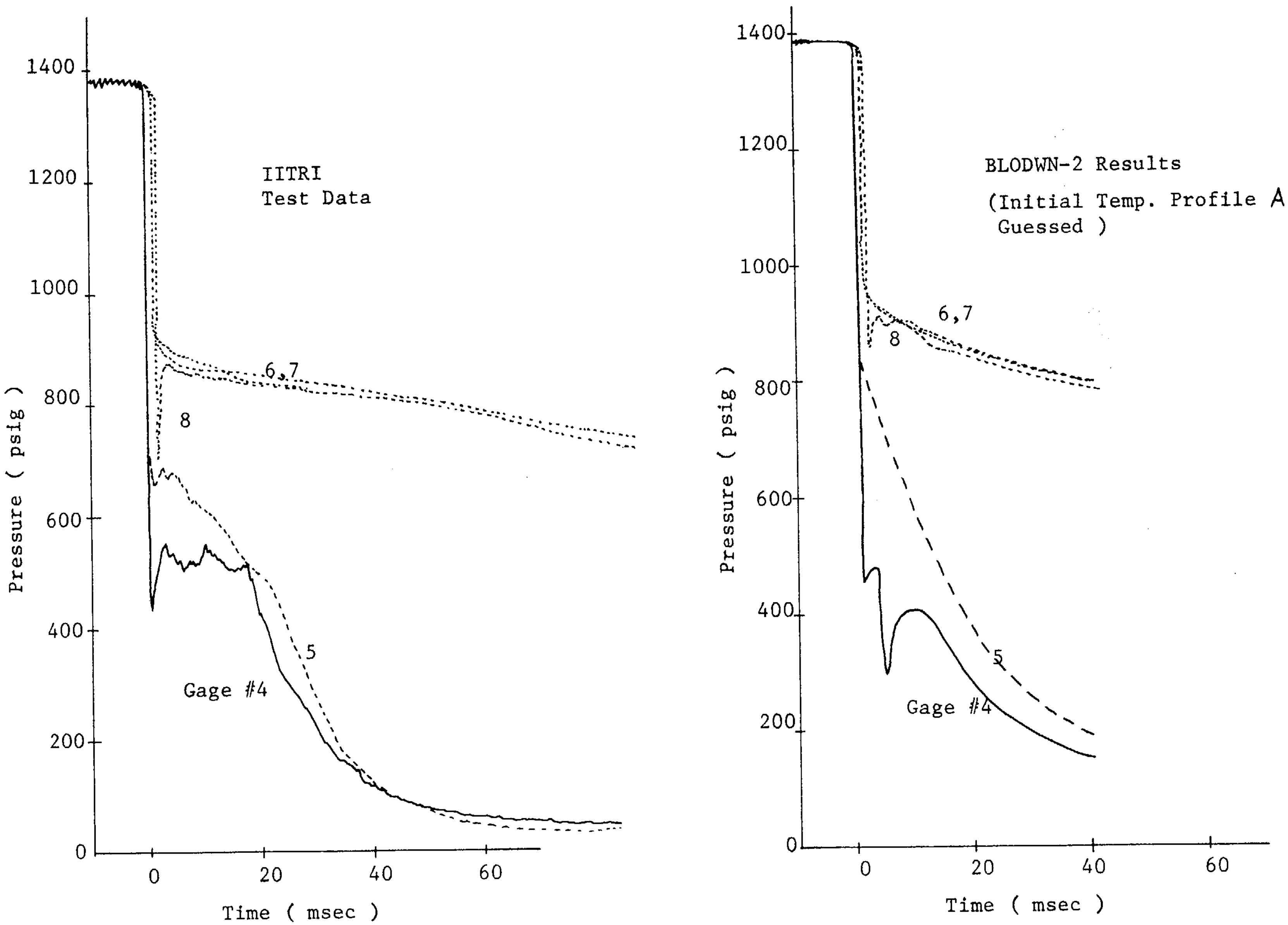

Figure 3-14. Blowdown Of A 6-ft, 2-in. I.D. Pipe Containing A Rod Bundle

TEMPERATURE PROFILE "B"; COMPARISON OF COMPUTED PRESSURES

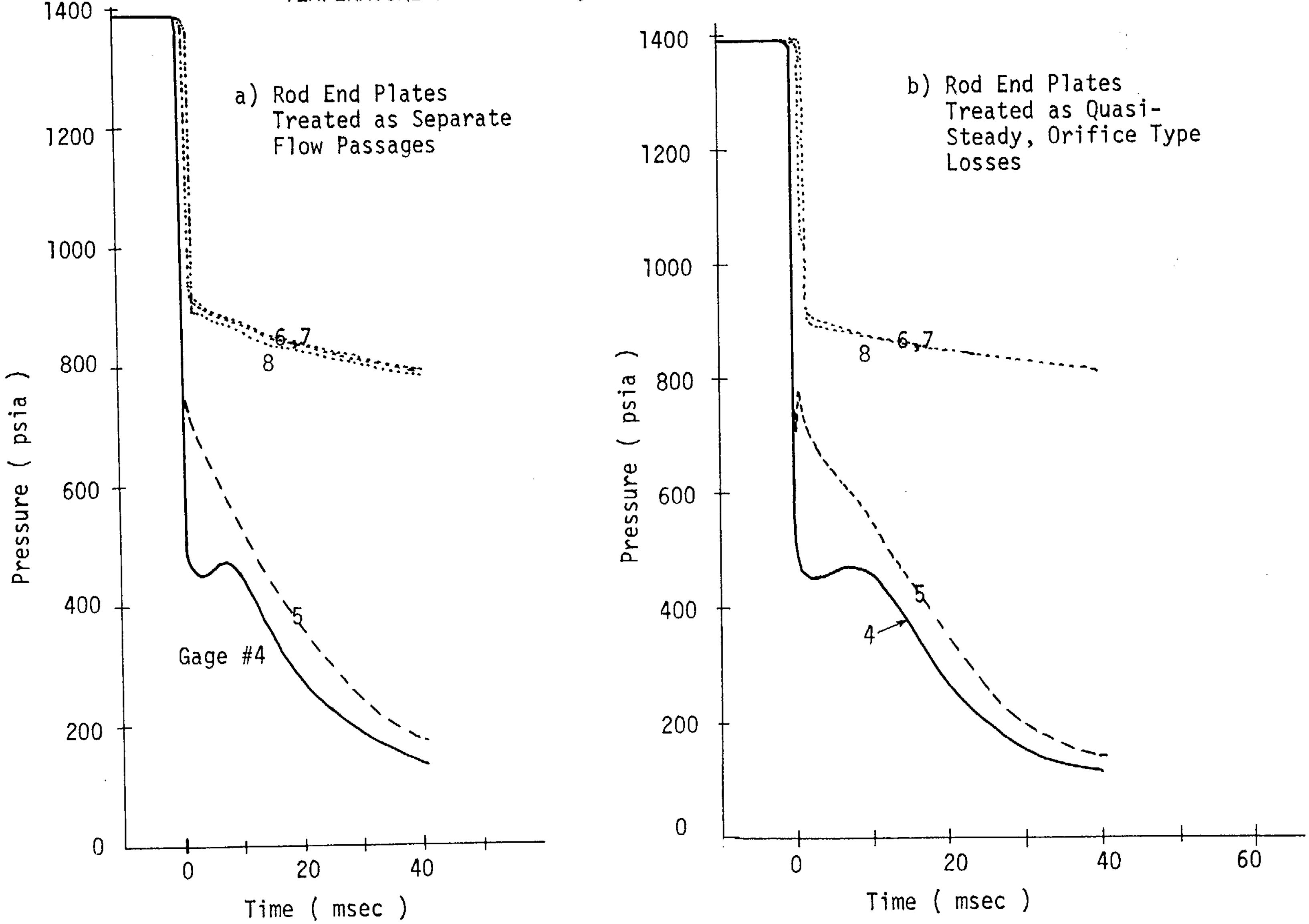

Figure 3-15. IITRI Pipe with Rod Bundle

SECTION 4

VESSEL BLOWDOWN

4.1 SMALL BARE VESSEL: LOFT SEMI-SCALE TEST NO. 522

LOFT Semi-Scale Tests, Phase I, were conducted at the National Reactor Test Station in Idaho by the Phillips Petroleum Company Atomic Energy Division (now part of Idaho Nuclear Corp.) and employed the vessel shown in Figure 4-1. The blowdown pipe fitted with the rupture disk assembly could be placed at either the top or the bottom vessel nozzle. The configuration shown in Figure 4-1 pertains to Test 522 in which the blowdown pipe did not contain a flow restricting orifice; this is referred to as a "100 percent break."

The rupture disk assembly consists of two disks fitted in series, with the space between them initially pressurized with gas so that the assembly seals the high pressure liquid from the atmospheric pressure ambient. To initiate blowdown, the space between the disks is overpressurized (with gas), causing the outer disk to rupture. As the space between the disks is thus decompressed, the inner disk bulges and eventually breaks, thus initiating blowdown. During this series of events (i.e., before the inner disk has started to "leak" the fluid) a decompression pulse of appreciable amplitude is injected into the system. However, its presence and subsequent reflections within the blowdown pipe cannot be simulated by BLODWN-2 code because it is assumed that the break opens linearly in a specified number of milliseconds, t^*. For all LOFT test comparisons, t^* was set equal to 1.1 milliseconds, which is the reported upper bound. The initial pressure was 1272 psig, and the mean water temperature was 445°F. The rupture disks were estimated to have fully cleared the blowdown pipe flow area in 0.7 ± 0.4 milliseconds. A BLODWN-2 representation of the geometry is shown in Figure 4-2.

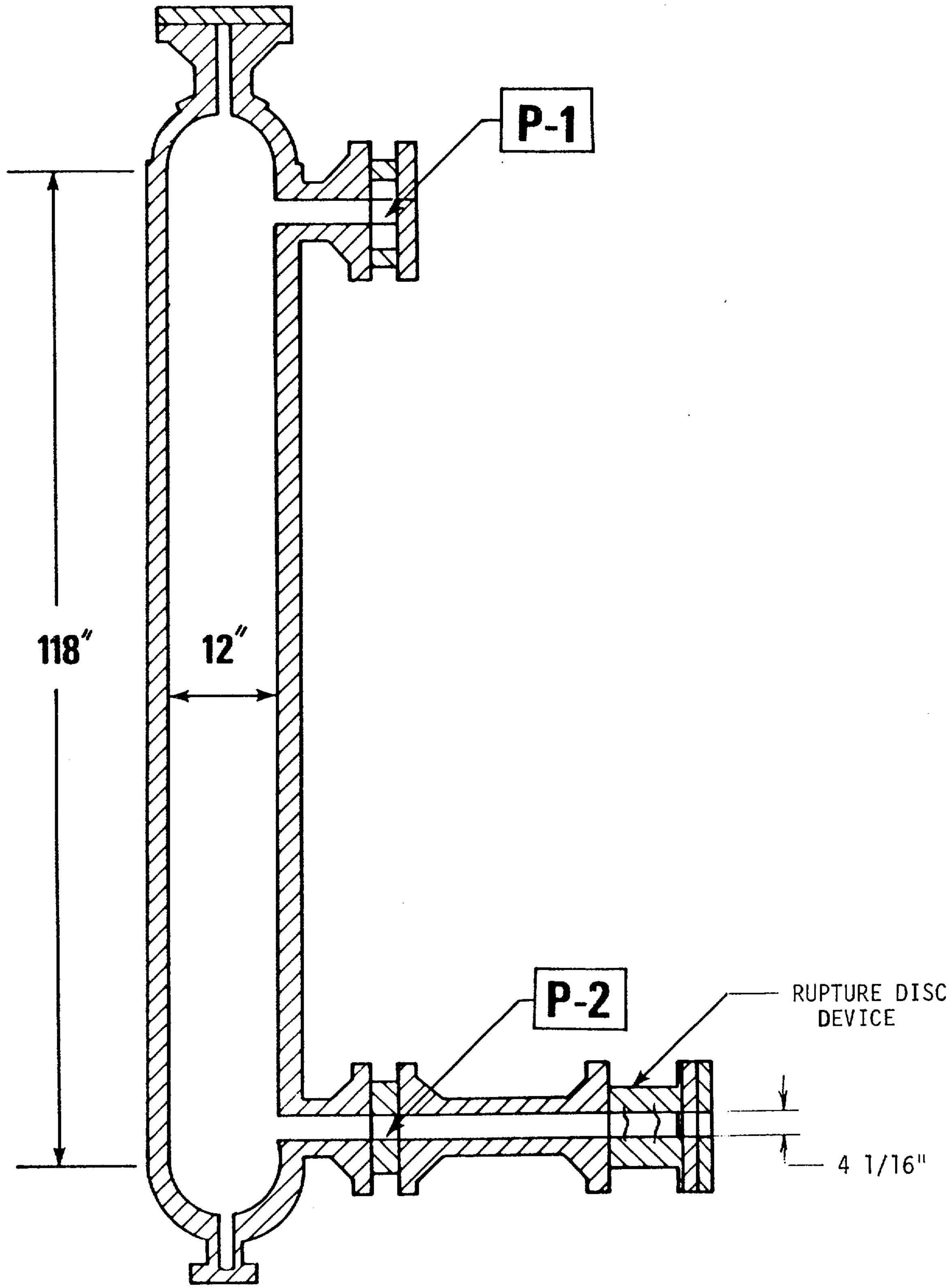

Figure 4-1. High Pressure Flask #1

FINE MESH REPRESENTATION OF GEOMETRY
FOR SHORT TERM BLODWN-2 CALCULATIONS

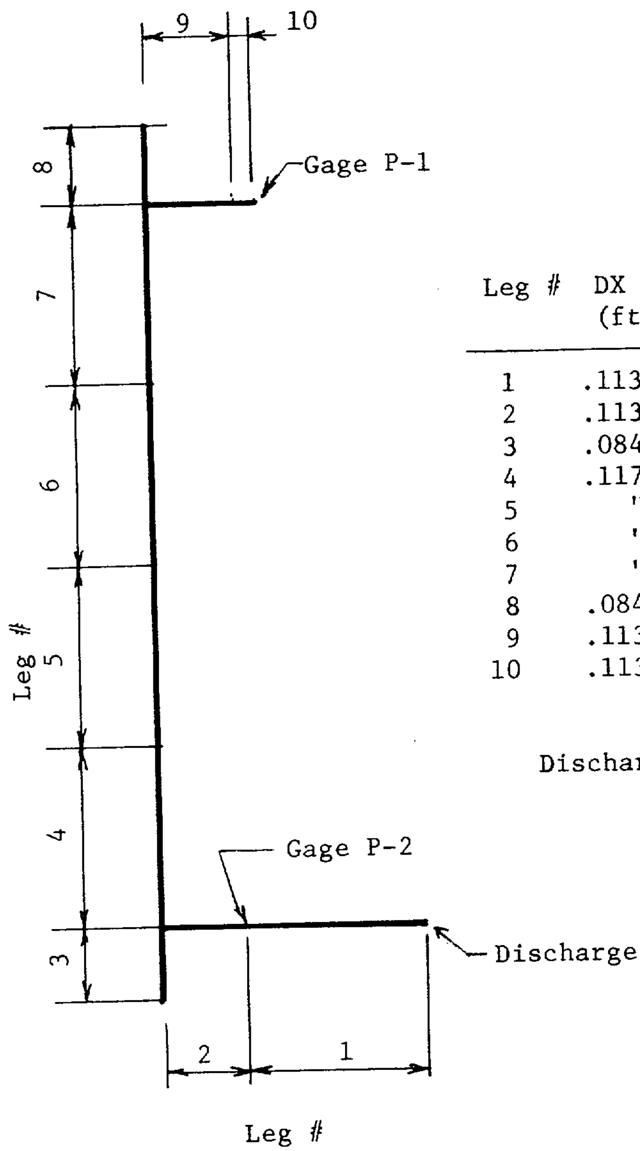

Leg #	DX (ft)	No. of space increments	Flow Area (ft^2)
1	.11384	18	.090
2	.11384	9	.090
3	.08400	8	.785
4	.11790	18	.785
5	"	"	"
6	"	"	"
7	"	"	"
8	.08400	8	.785
9	.11384	9	.090
10	.11384	2	.090

Discharge Flow Area= .090 (ft^2)

Figure 4-2. Semi-Scale LOFT Run No. 522. Fine Mesh Representation of Geometry for Short Term BLODWN-2 Calculations

Three runs were performed. In the first run, the entire system was at uniform temperature, whereas in the second the temperature in the dead-end nozzle was assumed to drop linearly along the nozzle from 445° at the vessel to 300°F at the dead end. This turned out a poor choice because it is more likely that a steep temperature drop occurs only within a few inches at the dead end. Figures 4-3 and 4-4 show comparisons between BLODWN-2 predictions and measurements at gage locations P-2 and P-1, respectively. Note the absence of the pressure undershoot in the blowdown pipe (P-2). The computed pressure at P-1 shows no undershoot for the uniform temperature case, as expected.

The unfortunate choice of the temperature profile in the second run caused the predicted pressure at P-1 to undershoot and oscillate for a while because, during that time, the liquid did not flash anywhere within the dead-end nozzle. A steep temperature drop only at the dead end would have resulted in higher initial (445°F) temperature within most of that nozzle, causing early flashing and thus preventing pressure oscillations. The pressure under-shoot measured at P-1 during this test differs from those recorded in all other tests insofar as it is unusually long. Such condition could be expected to occur only if an air pocket existed at that location.

In the third run, a "coarse mesh" representation (shown in Figure 4-5) was employed to save computer time since the complete blowdown was analyzed. Figure 4-6 shows the comparison for the pressure at location P-2. Coarser mesh leads to prediction of faster decompression, hence a shorter blowdown duration.

4.2 SMALL VESSEL WITH SIMULATED CORE: LOFT SEMI-SCALE TEST NO. 609

This is a "top blowdown" test with a 100 percent break in which a long, small-diameter passage in the vessel simulates a "high inertance" core (refer to Figure 4-7). The purpose of this test was to obtain conditions which would most likely produce the pressure and flow oscillations predicted by the FLASH-1 and SATAN-1 codes. Such oscillations, however, were not observed. A nonuniform initial water temperature profile was introduced by first

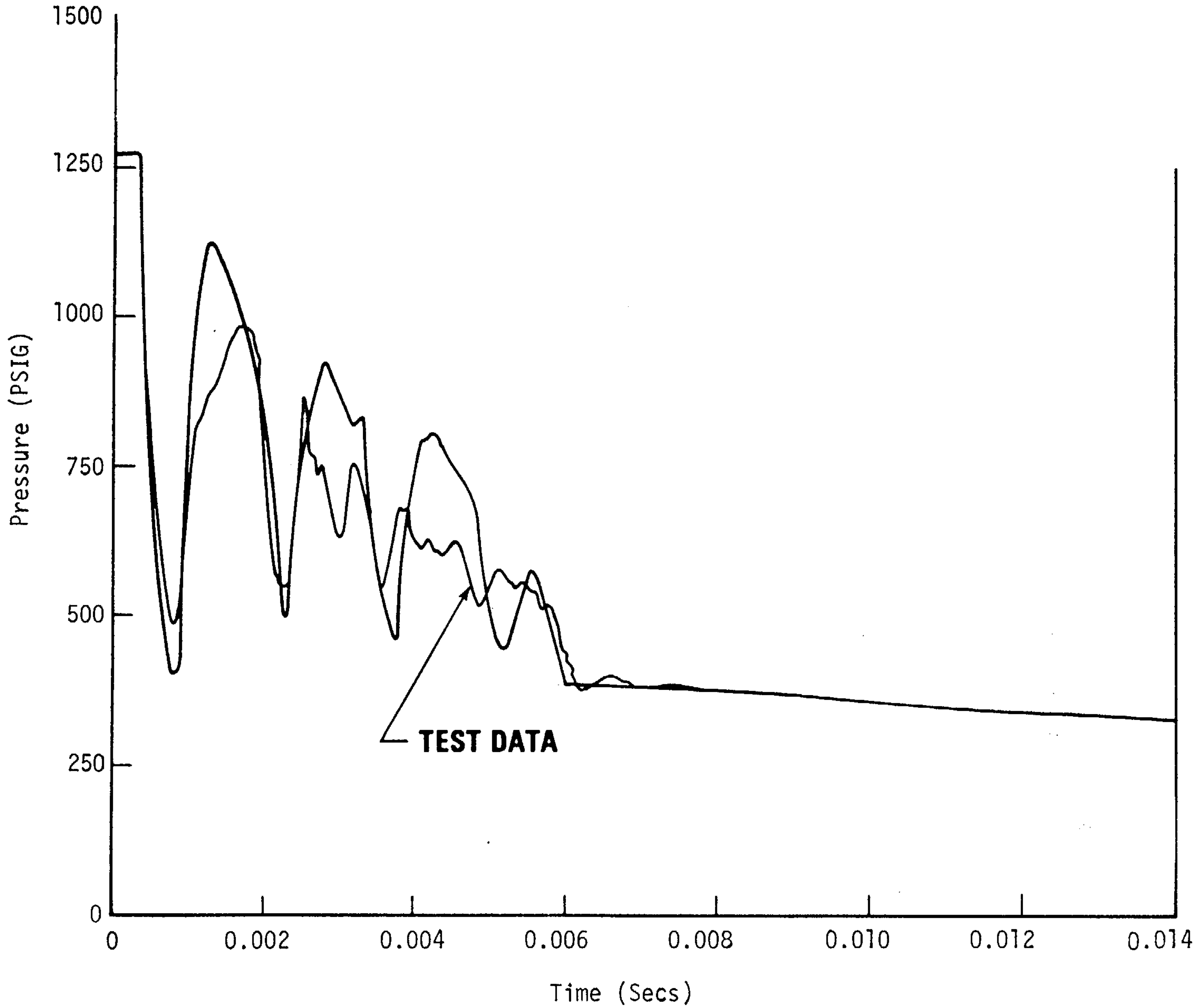

Figure 4-3. BLODWN-2 Prediction for LOFT Semi-Scale Run No. 522 (Pressure in Vessel (P-2))

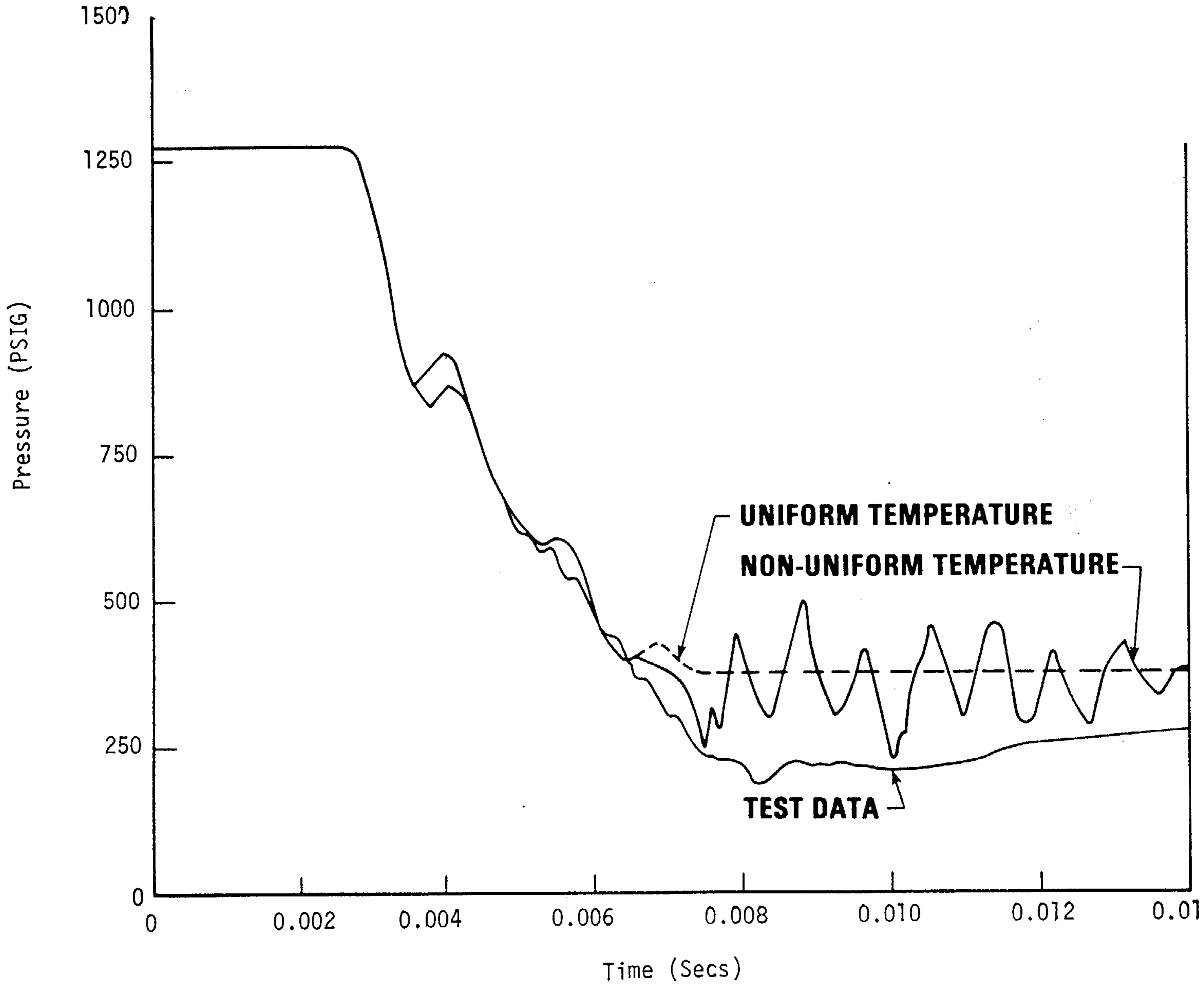

Figure 4-4. BLODWN-2 Results for LOFT Semi-Scale Run No. 522 (Pressure in Vessel (P-1))

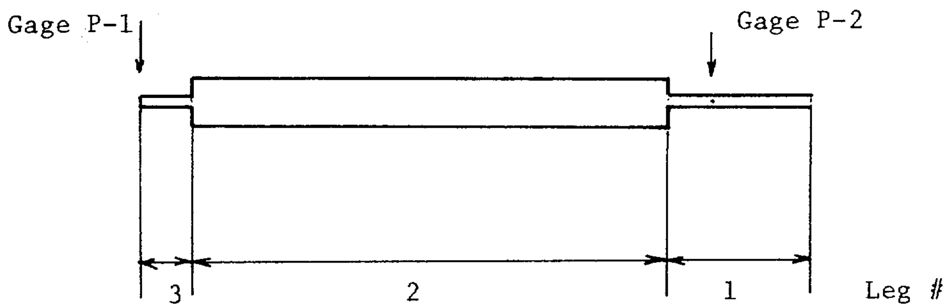

Leg #	DX ft)	No. of space increments	Flow area (ft^2)
1	0.5000	6	0.090
2	1.0354	10	0.785
3	0.5200	2	0.090

Discharge flow area = 0.090 (ft^2)

Figure 4-5. Semi-Scale LOFT Run No. 522. Coarse Mesh Representation of Geometry for Long Term BLODWN-2 Calculations

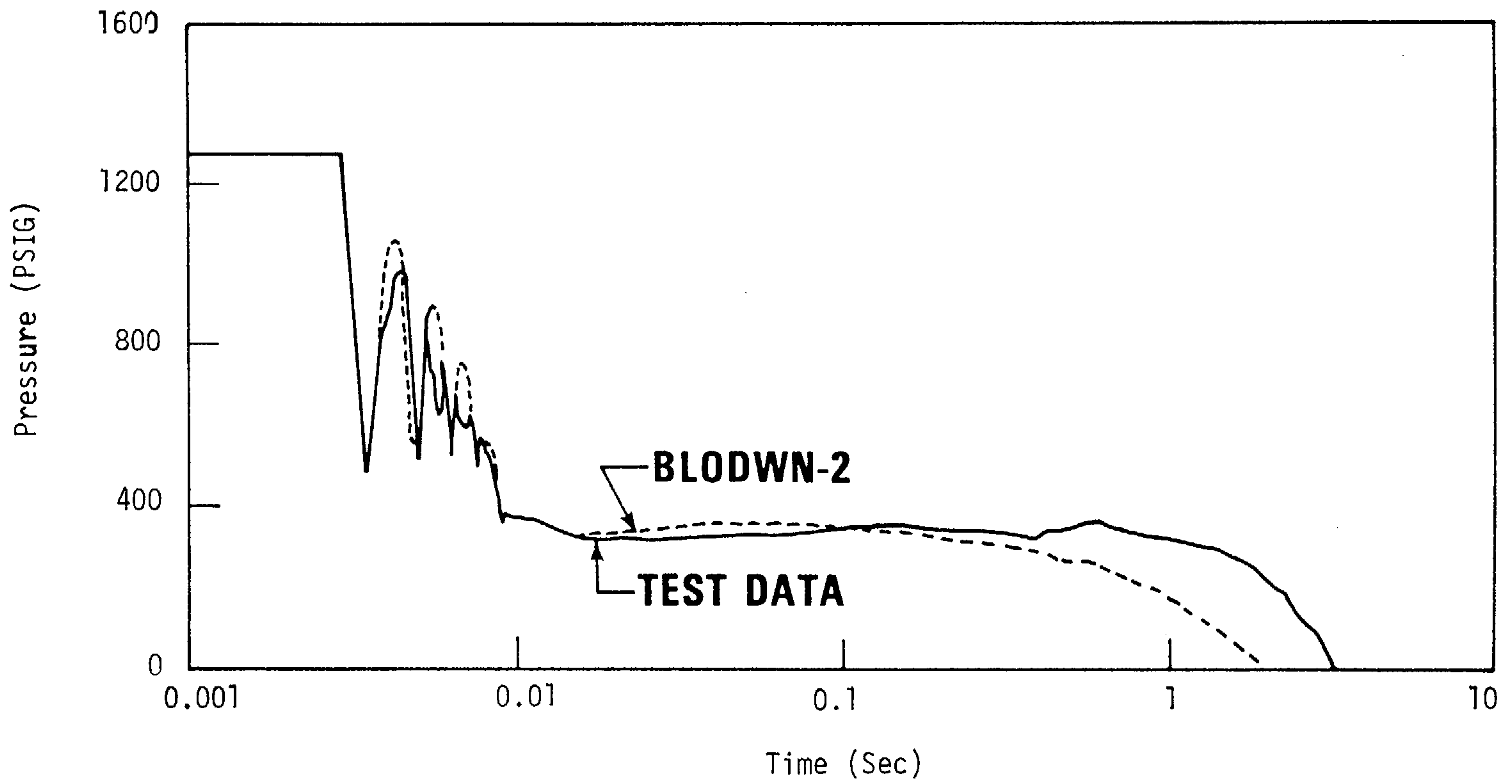

Figure 4-6. Comparison of BLODWN-2 Results with Test Data for 3-Pipe Model of LOFT Run No. 522 (Pressure in Blowdown Nozzle (P-2))

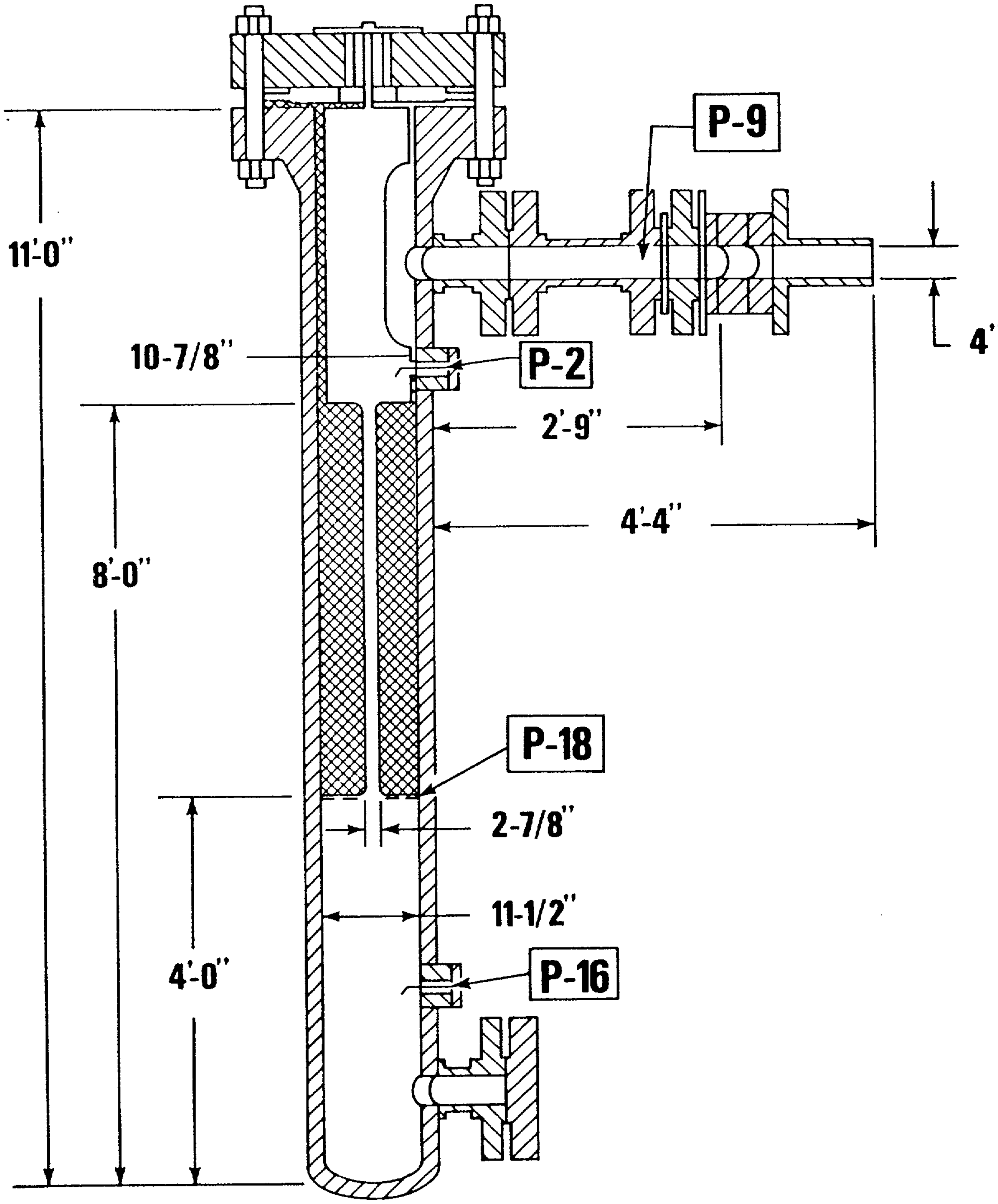

Figure 4-7. Modified Flask with Inertance Core LOFT Run #609

heating up the whole system to approximately 537°F and then introducing a colder water into the bottom plenum. Details of the resulting temperature profile are not known, except that the bottom plenum temperature (presumably at the bottom nozzle) was approximately 490°F. The geometric model and assumed temperature profile for this test are shown in the Appendix.

Comparisons between BLODWN-2 results and pressure measurements at four gage locations are illustrated in Figures 4-8 through 4-11, with the gage locations shown in Figure 4-7. The computer run covered both the subcooled and the transition blowdown regimes. The comparisons are good except for the location P-18 in the saturated regime, which indicates that the initial water temperature was higher than that assumed.

4.3 SMALL VESSEL WITH SIMULATED CORE AND CORE SUPPORT BARREL: LOFT 1/4 - SCALE TEST 711

The test geometry configuration (shown in Figure 4-12) departs markedly from the one-dimensional flow situation. While the flow field above and within the "core" is one-dimensional, its redistribution in the lower plenum and within the annulus formed by the support barrel and the vessel wall will be decidedly multidimensional. The presence of a core was simulated by thickening a portion of the barrel wall.

This test featured a 30 percent break in which the top vessel nozzle was connected to the rupture disk assembly and the restricting orifice. The initial pressure was 2290 psig and plenum temperatures above and below the simulated core were 540°F and 505°F, respectively. Details of temperature distribution within the vessel and (especially) within the annulus are not known. The model of this geometry and the assumed temperature profile are shown in the Appendix.

Figures 4-13 through 4-16 illustrate comparisons between BLODWN-2 results and pressure measurements at the four locations shown in Figure 4-12. The agreement is satisfactory, despite the drastic simplification in the flow pattern forced by the one-dimensional model adopted for this comparison. No doubt the smallness of the test system greatly contributed to make this comparison favorable.

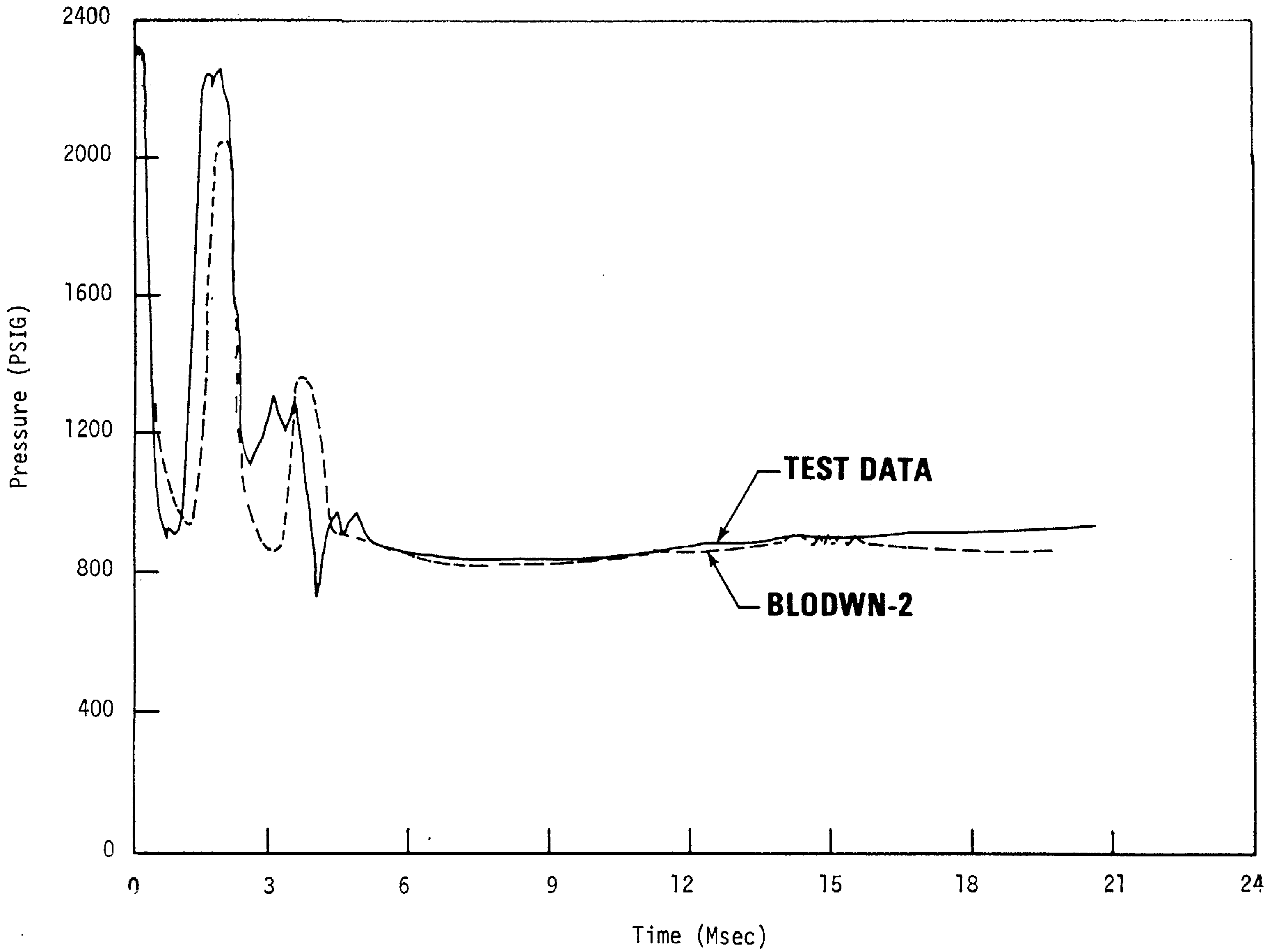

Figure 4-8. BLODWN-2 Results for LOFT "Inertance" Core Test No. 609 (Gage Location (P-9))

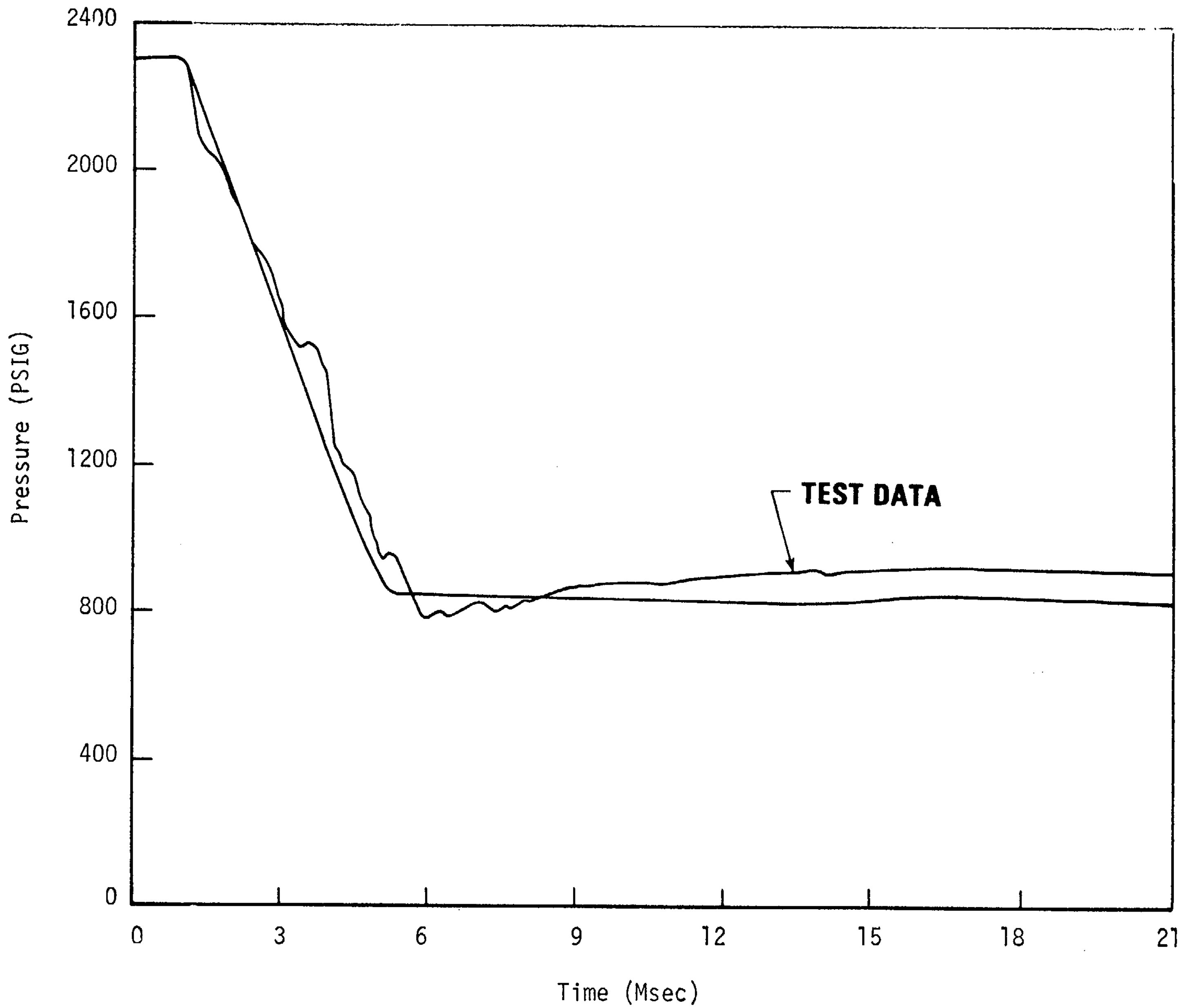

Figure 4-9. BLODWN-2 Results for LOFT Inertance Core Run No. 609 (Pressure Above "Core" (P-2))

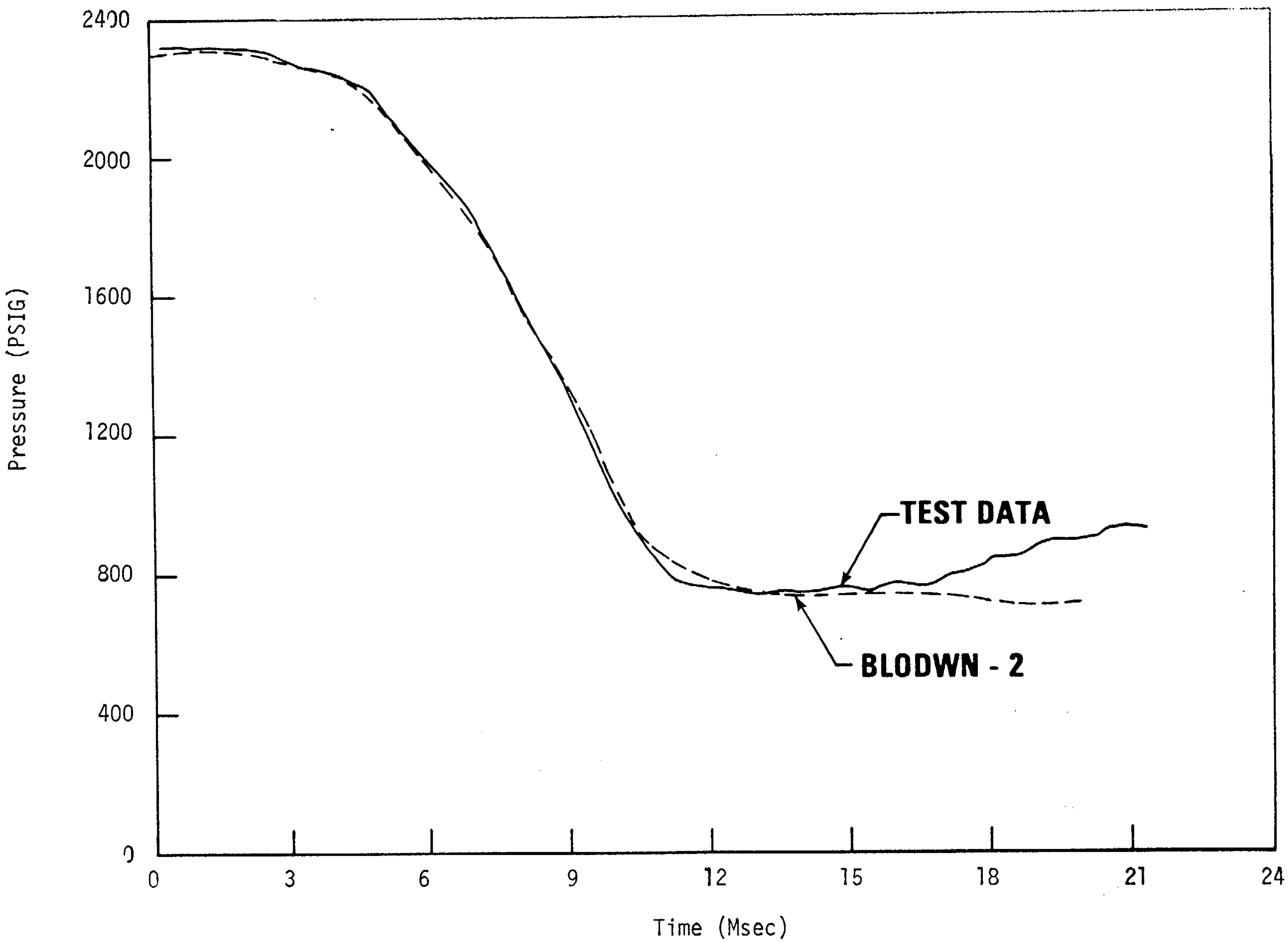

Figure 4-10. BLODWN-2 Results for LOFT "Inertance" Core Test No. 609 (Gage Location (P-18))

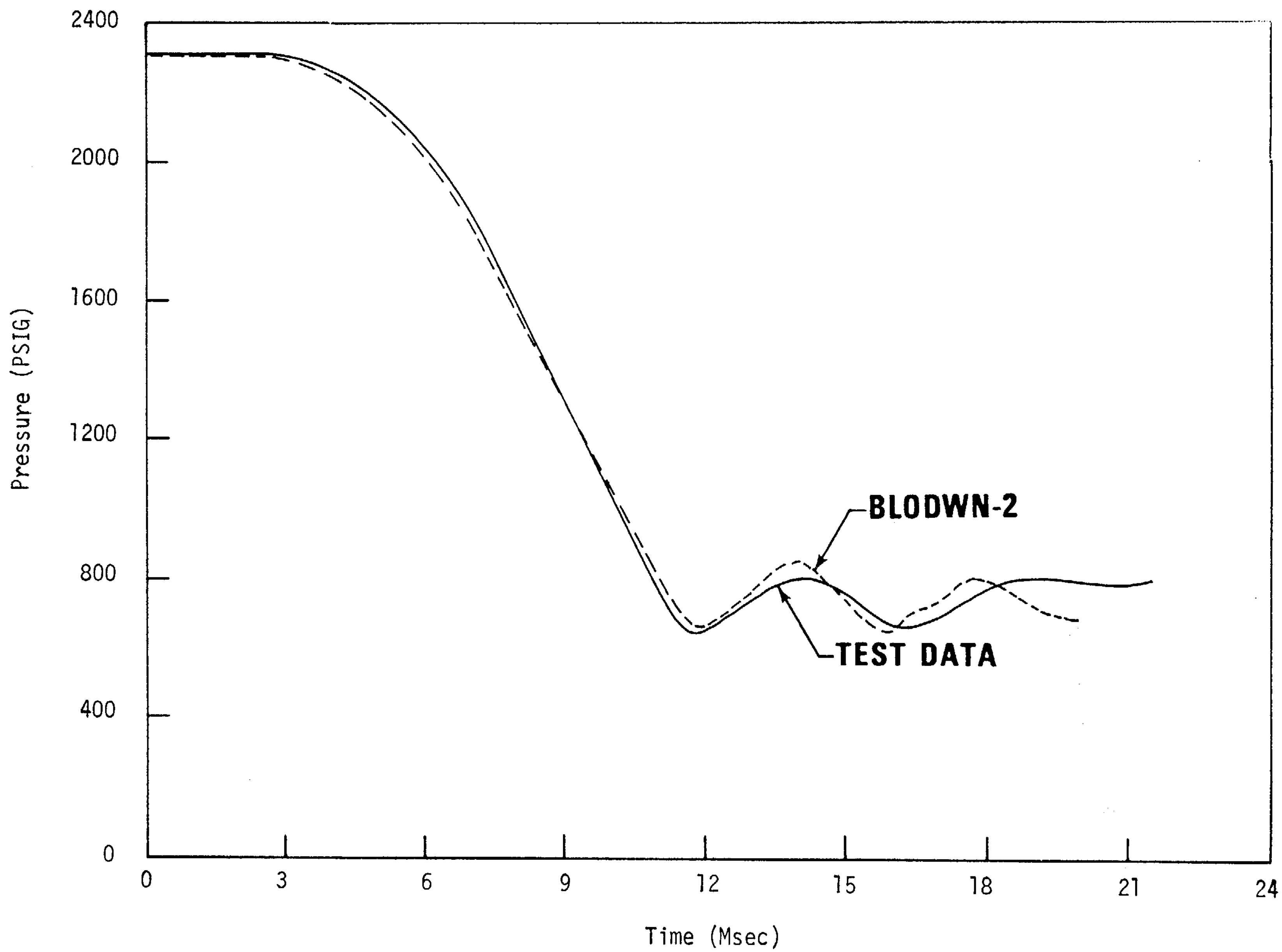

Figure 4-11. BLODWN-2 Results for LOFT "Inertance" Core Test No. 609 (Gage Location (P-16))

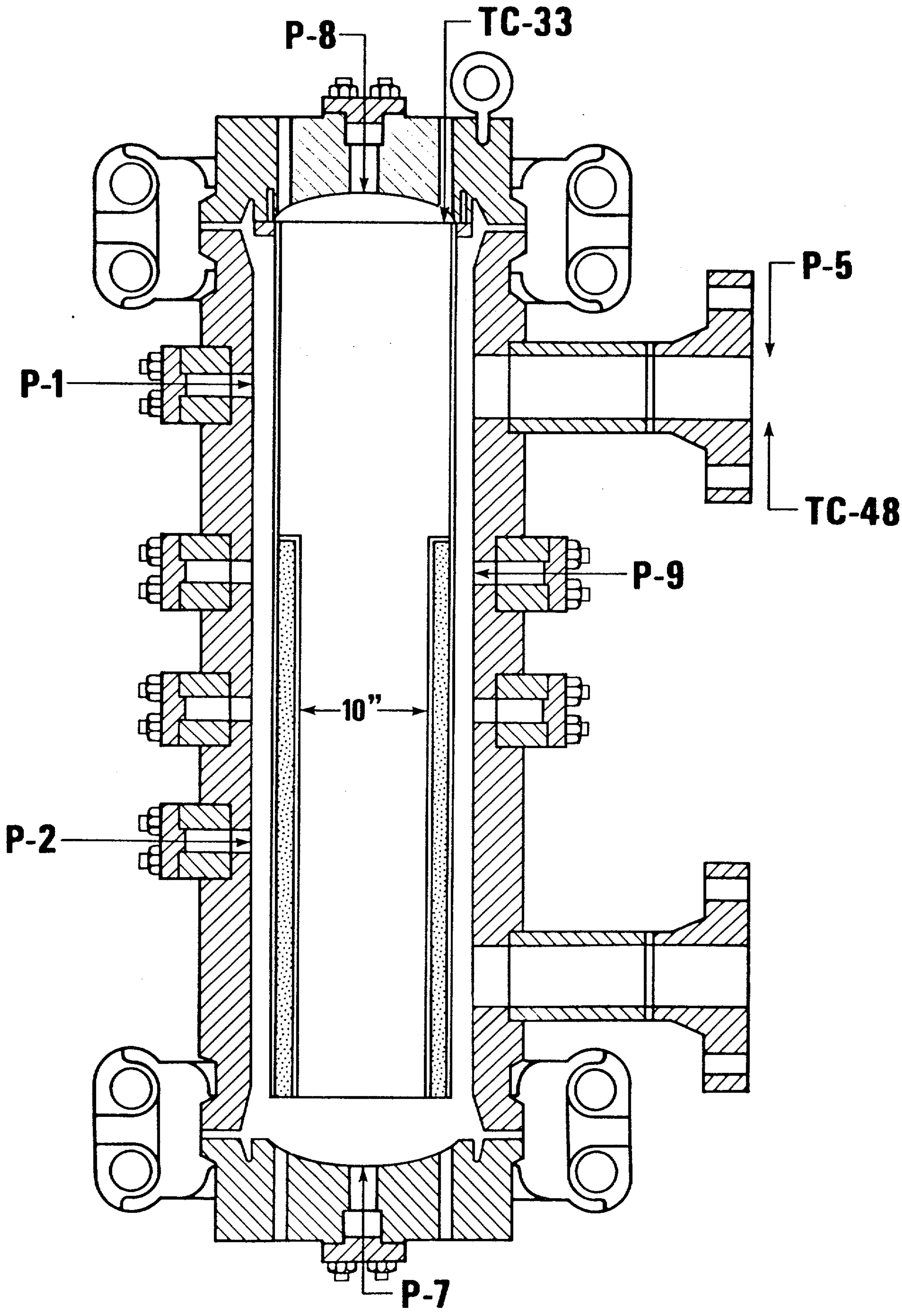

Figure 4-12. LOFT 1/4 Scale "Core Barrel" Test

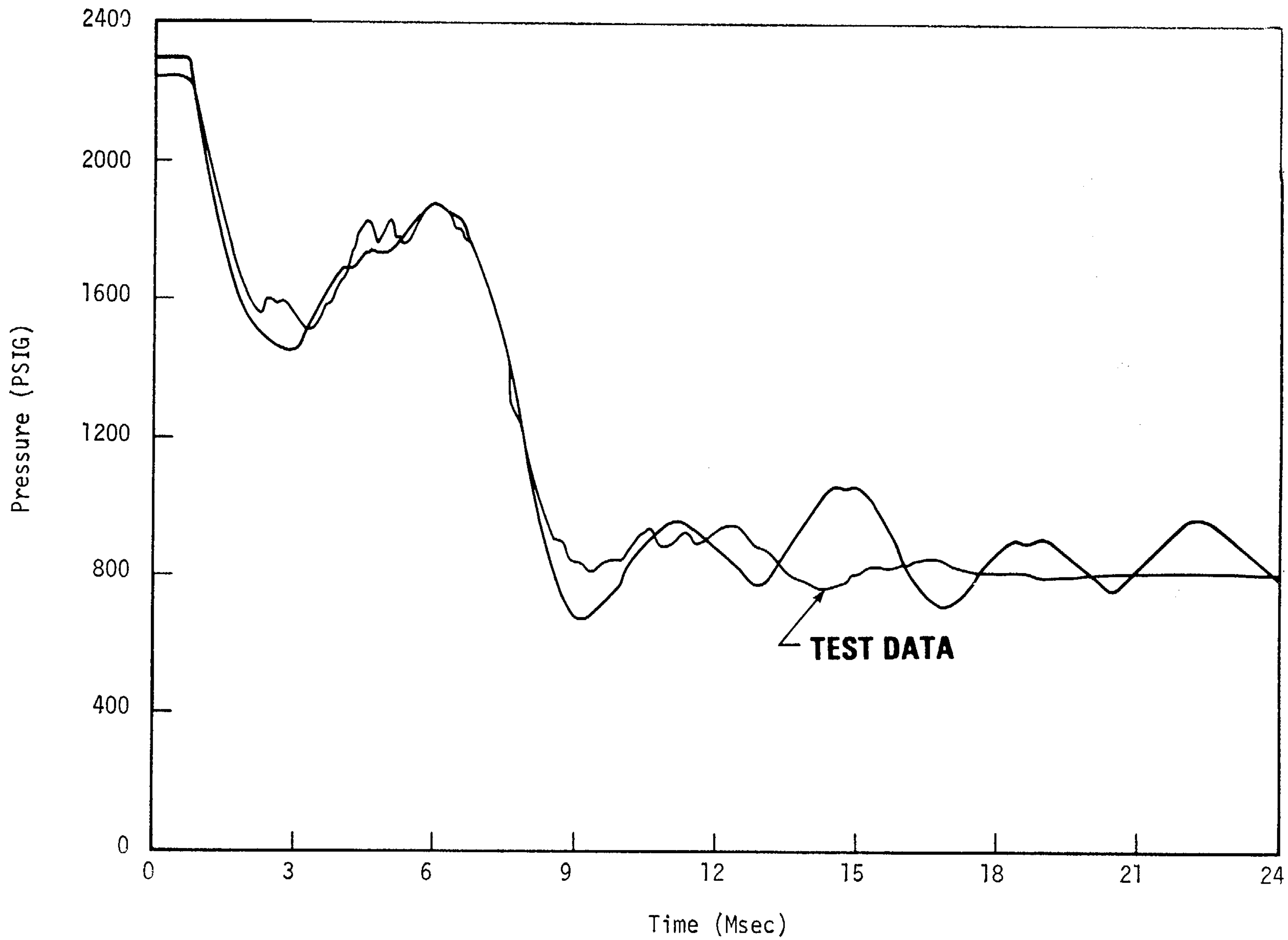

Figure 4-13. BLODWN-2 Results for LOFT "Core Barrel" Run No. 711 (30% Rupture, Location (P-1))

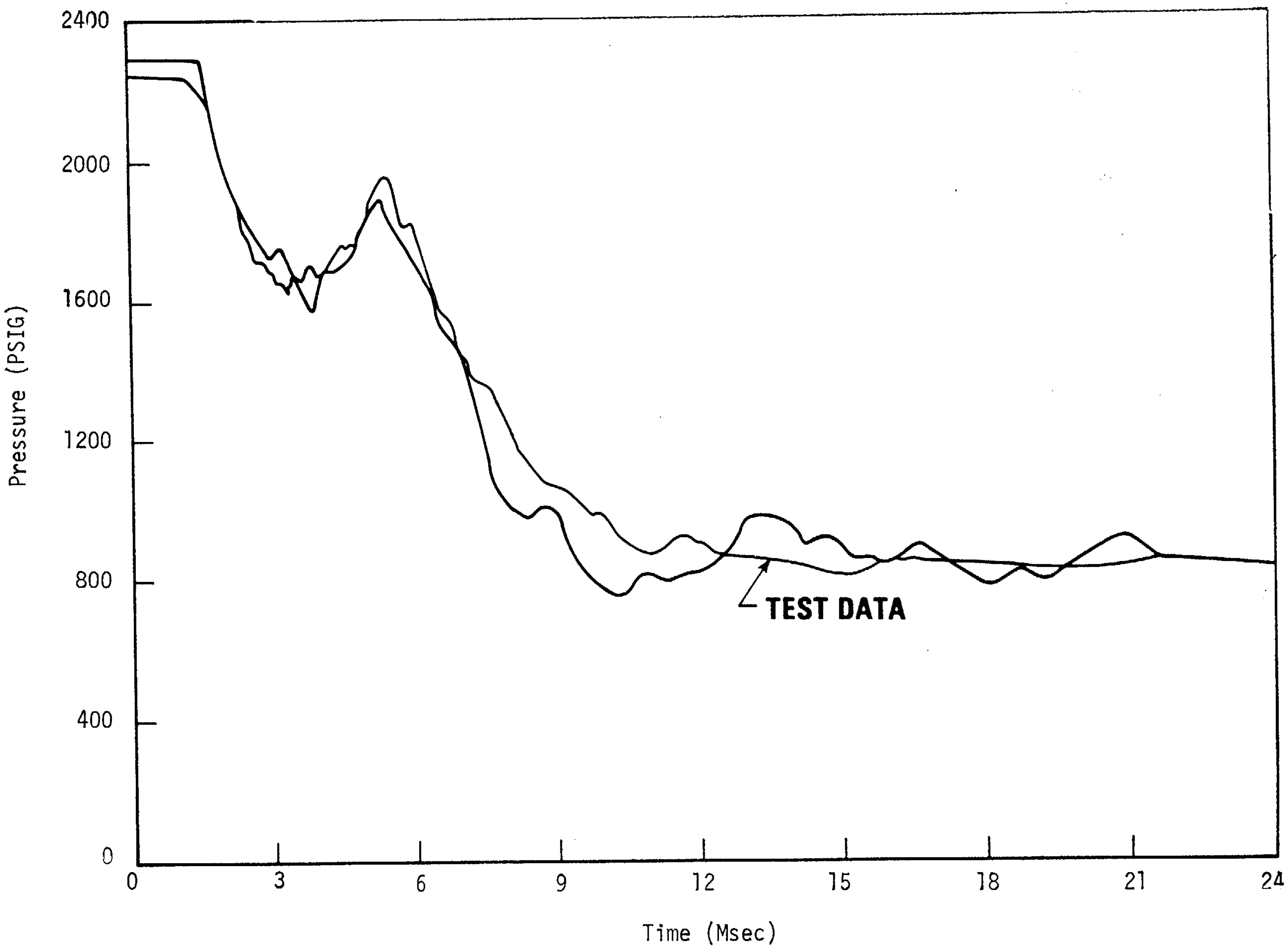

Figure 4-14. BLODWN-2 Results for LOFT "Core Barrel" Run No. 711 (30% Rupture, Location (P-2))

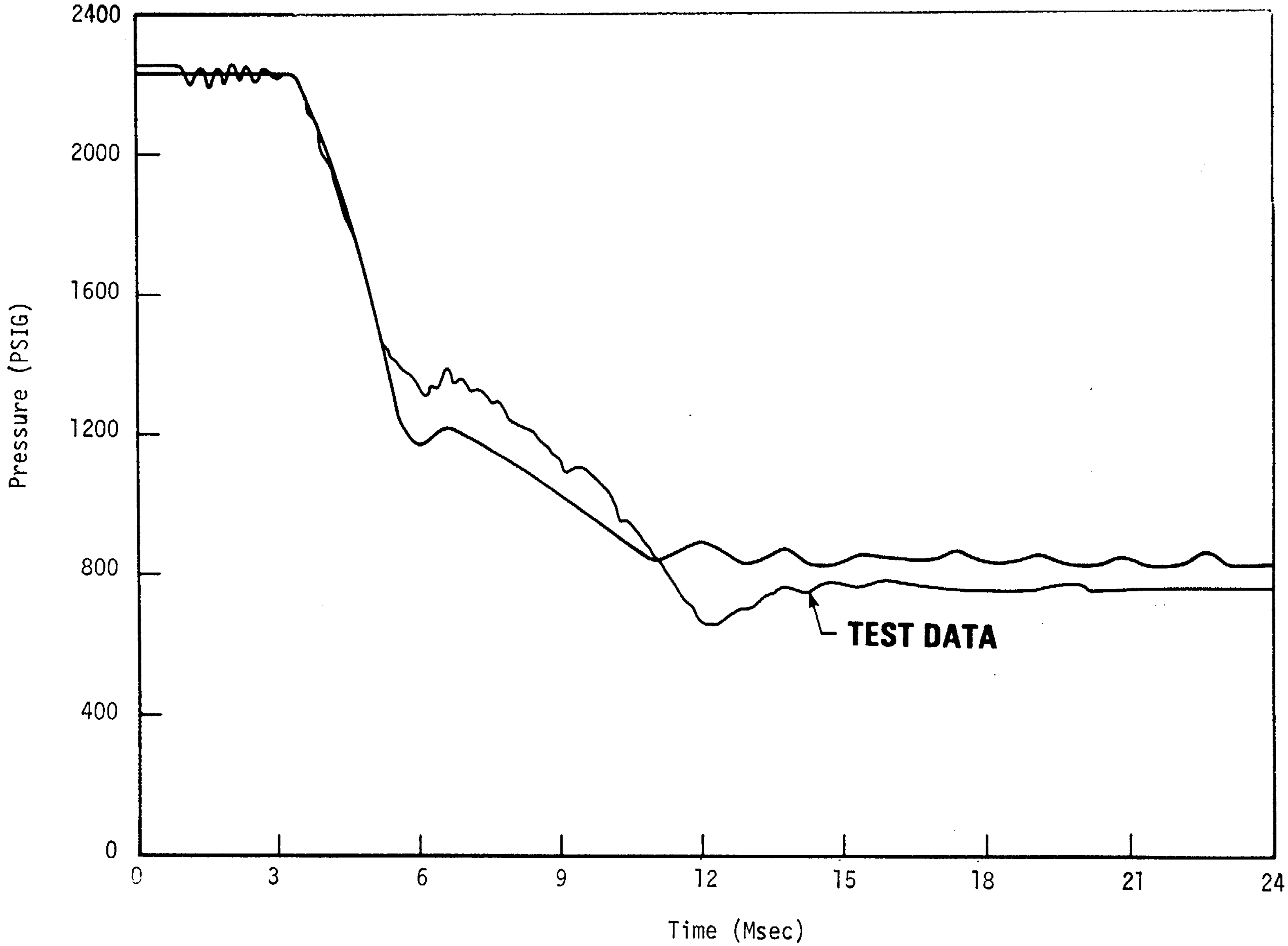

Figure 4-15. BLODWN-2 Results for LOFT "Core Barrel" Run No. 711 (30% Rupture, Location (P-8))

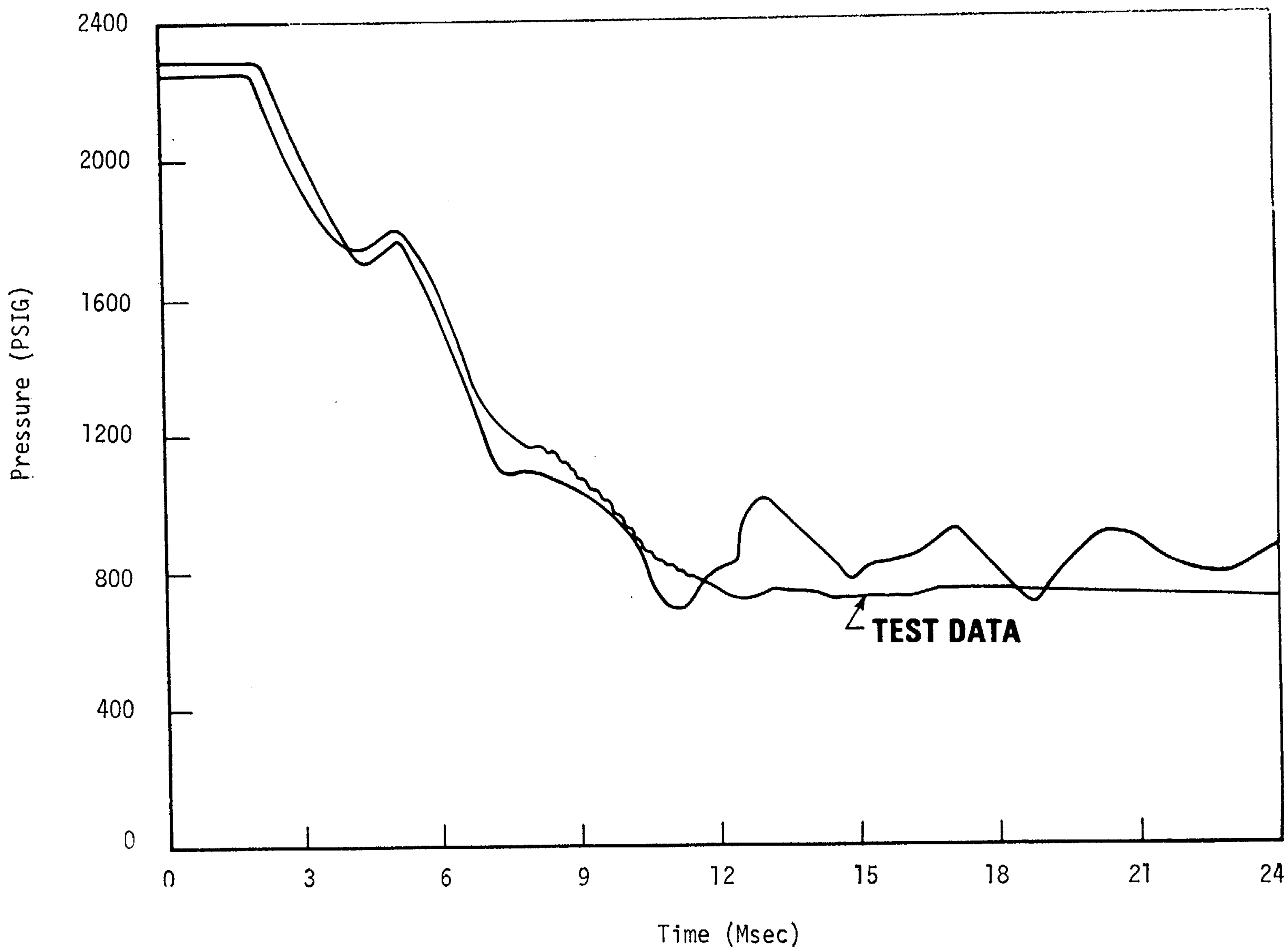

Figure 4-16. BLODWN-2 Results for LOFT "Core Barrel" Run No. 711 (30% Rupture, Location (P-7))

4.4 LARGE VESSEL WITH CORE PLATE: BNWL-CSE TEST NO. B-19B

4.4.1 One-Dimensional Modeling

The Containment Systems Experiments (CSE), conducted by the Battelle-Northwest Laboratory, feature a blowdown vessel appreciably larger than the one used in the LOFT Semi-Scale Tests; in fact, its size approximates the size of the planned Full-Scale LOFT vessel. Figure 4-17 illustrates the CSE vessel in the configuration used for Test No. B-19B in which a thick, perforated plate subdivided the vessel into two regions. Volumes of the upper and the lower regions were approximately 106 ft^3 and 46 ft^3, respectively. The core plate contained 64 holes, with a total flow area of 0.559 ft^2. Just upstream of the rupture disk assembly a 1.689-inch ID orifice provided a flow restriction. The initial pressure and temperature were 2115 psia and 590°F to 603°F, respectively.

BLODWN-2 comparisons were run with three model configurations. The purpose of the first two configurations (MODELS "A" and "B," shown in the Appendix) was to examine the effect of the core plate modeling. In the "A" model, the core plate was considered as a quasi-steady, orifice-type loss in a uniform (large) area passage. In the "B" model, the flow passage through the core plate was treated as a separate flow passage of the smaller flow area (equal to 0.559 ft^2).

The departure from a one-dimensional flow pattern is much more pronounced in the configuration of the "B" model wherein the total flow area is lumped into one thick-walled orifice. The fluid near such a core plate (containing only one large hole) would have a considerable radial component of motion, the motion becoming purely radial for radial locations larger than the orifice radius. When the core plate contains many uniformly-spaced holes the flow at any radial location near the plate is mainly axial, hence acoustic reflections from such a perforated core plate should not be very significant. This would cause the system to respond acoustically as though the core plate were absent. One should bear in mind that BLODWN-2 code is spatially one-dimensional, therefore, the fluid cannot bend to flow into a smaller flow area hole at the end of the passage. However, the axial flow velocity at that end

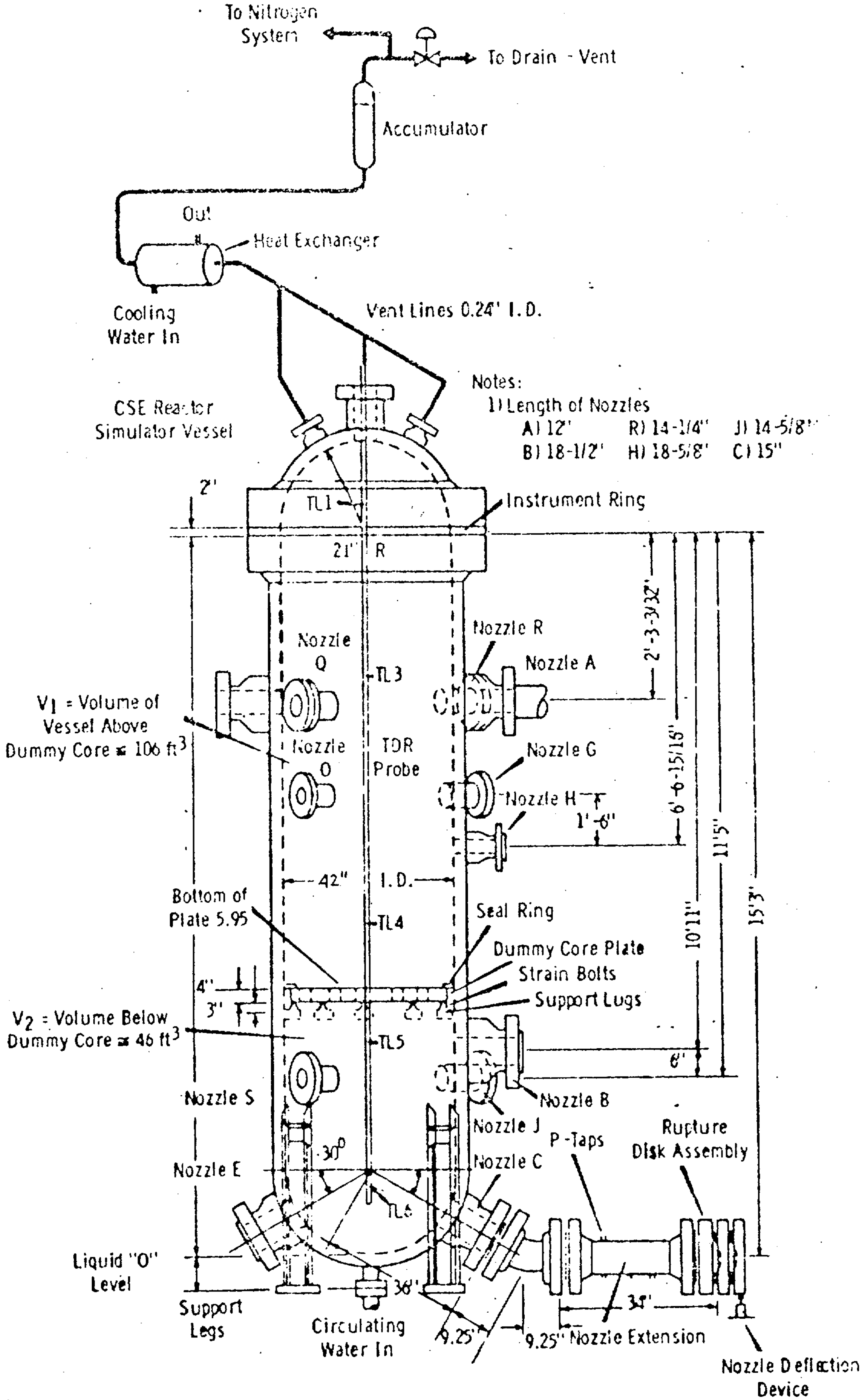

Figure 4-17. CSE Reactor Simulator Vessel with Core Plate Run B-19

adjusts itself to conserve the mass flow, equal to the mass flow into the orifice. This causes computations of wave reflections of excessive magnitudes.

Figure 4-18 shows the comparison between the computed pressures for models "A" and "B" for the location just beneath the core plate. One can see that these computed pressures are, in fact, out of phase. Figure 4-19 shows the comparison between the measured pressure at that location and the computed pressure utilizing the "A" model. The two are in phase, and the computed pressure falls in the middle of the high frequency oscillations caused by the "breathing" mode of the acoustical vibrations of the vessel. This result supports the previously made statement that the core plate representation of the "A" model is more appropriate. Examination of the computed core plate loads will be deferred pending a brief discussion of three-dimensional acoustic pressure fields and the description of the "C" model.

Comparison between the "A" model results and measurement at nozzle "L" is shown in Figure 4-20. The "L" nozzle is a small, 10-inch-long, 1.689" ID nozzle at the same elevation on the vessel as Nozzle A.

4.4.2 Modes of Natural, Acoustic Vibration of Liquid in a Cylindrical Plenum

In the subcooled blowdown regime (i.e., while the system is still filled with liquid which has a very high velocity of sound in comparison with the fluid particle velocity) the Navier-Stokes equations can be simplified and combined to form the following three-dimensional wave equation:

$$\frac{1}{r}\frac{\partial}{\partial r}\left(r\frac{\partial p}{\partial r}\right)+\frac{1}{r^2}\cdot\frac{\partial^2 p}{\partial\theta^2}+\frac{\partial^2 p}{\partial z^2}=\frac{1}{c^2}\cdot\frac{\partial^2 p}{\partial t^2}$$

The solution pertaining to the natural vibration of a plenum of radius R and height ℓ becomes[17]

$$p(r,\theta,z,t)=\begin{matrix}\cos\\ \sin\end{matrix}(m\theta)\cos\left(\frac{\omega_z z}{c}\right)J_m\left(\frac{\omega_r r}{c}\right)e^{-2\pi i\nu t}$$

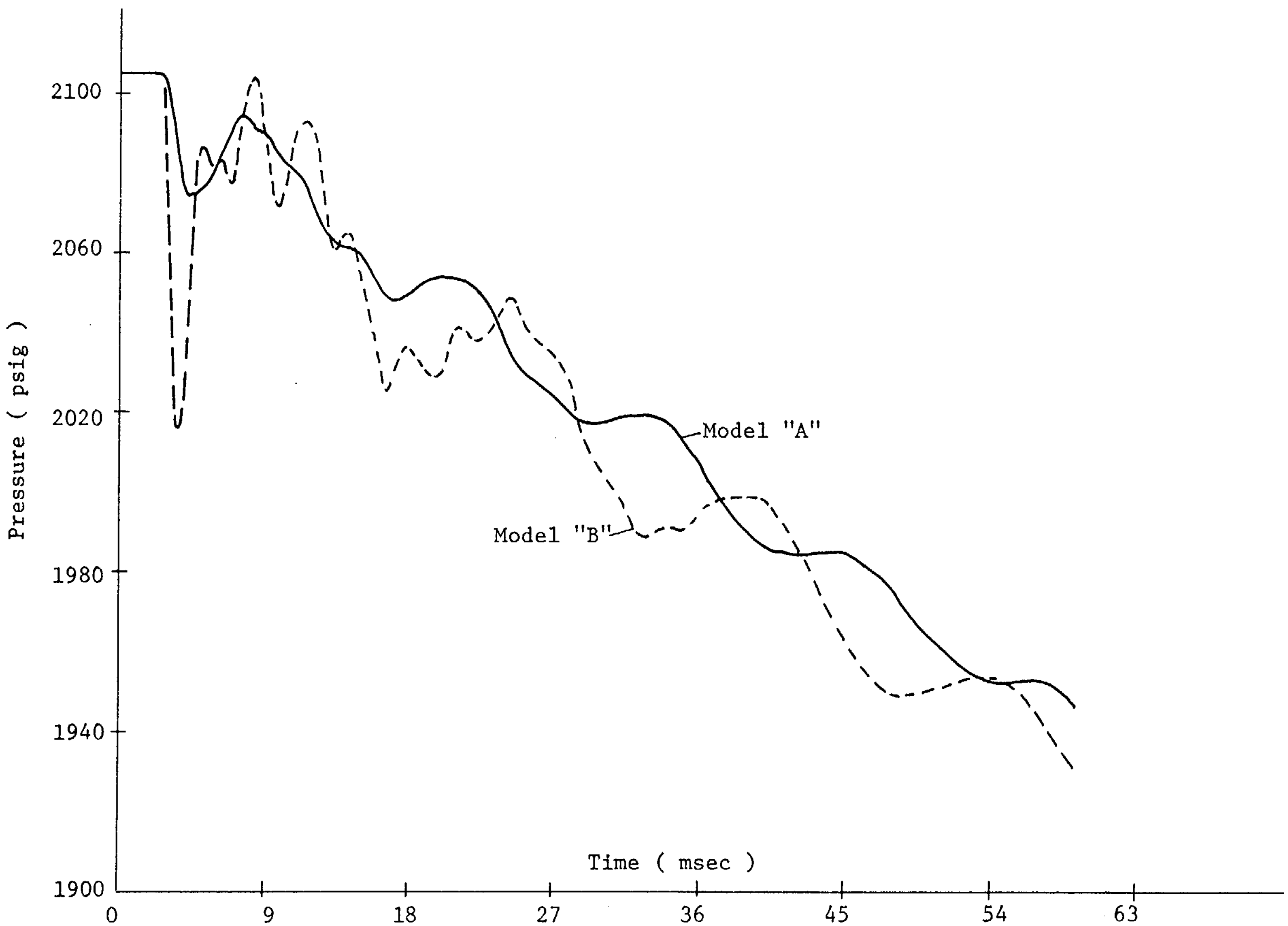

Figure 4-18. CSE B-19B, Pressure at Support Lug No. 7. BLODWN-2 Results: Comparison Between Models "A" and "B"

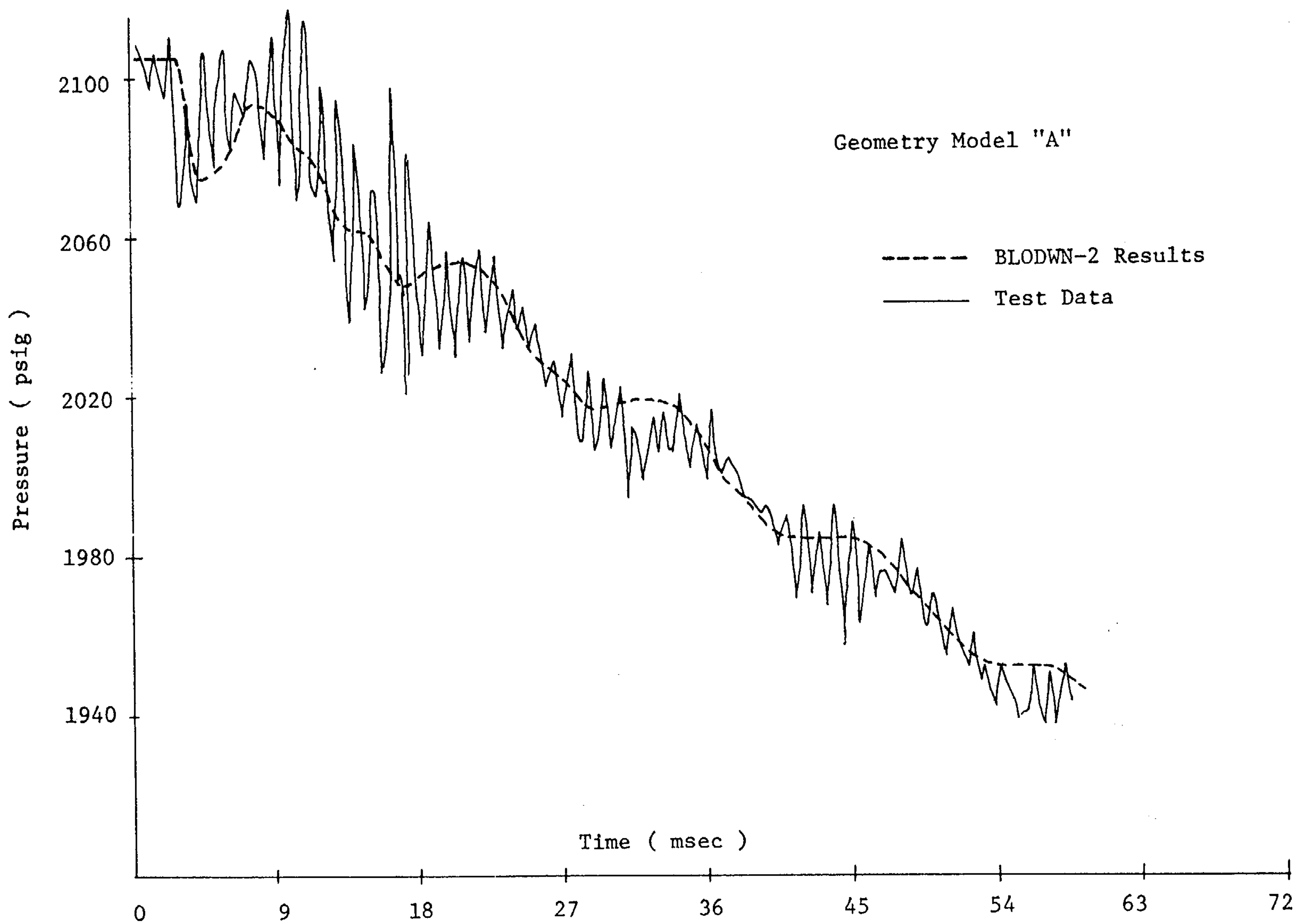

Figure 4-19. CSE B-19 B, Pressure At Support Lug #7

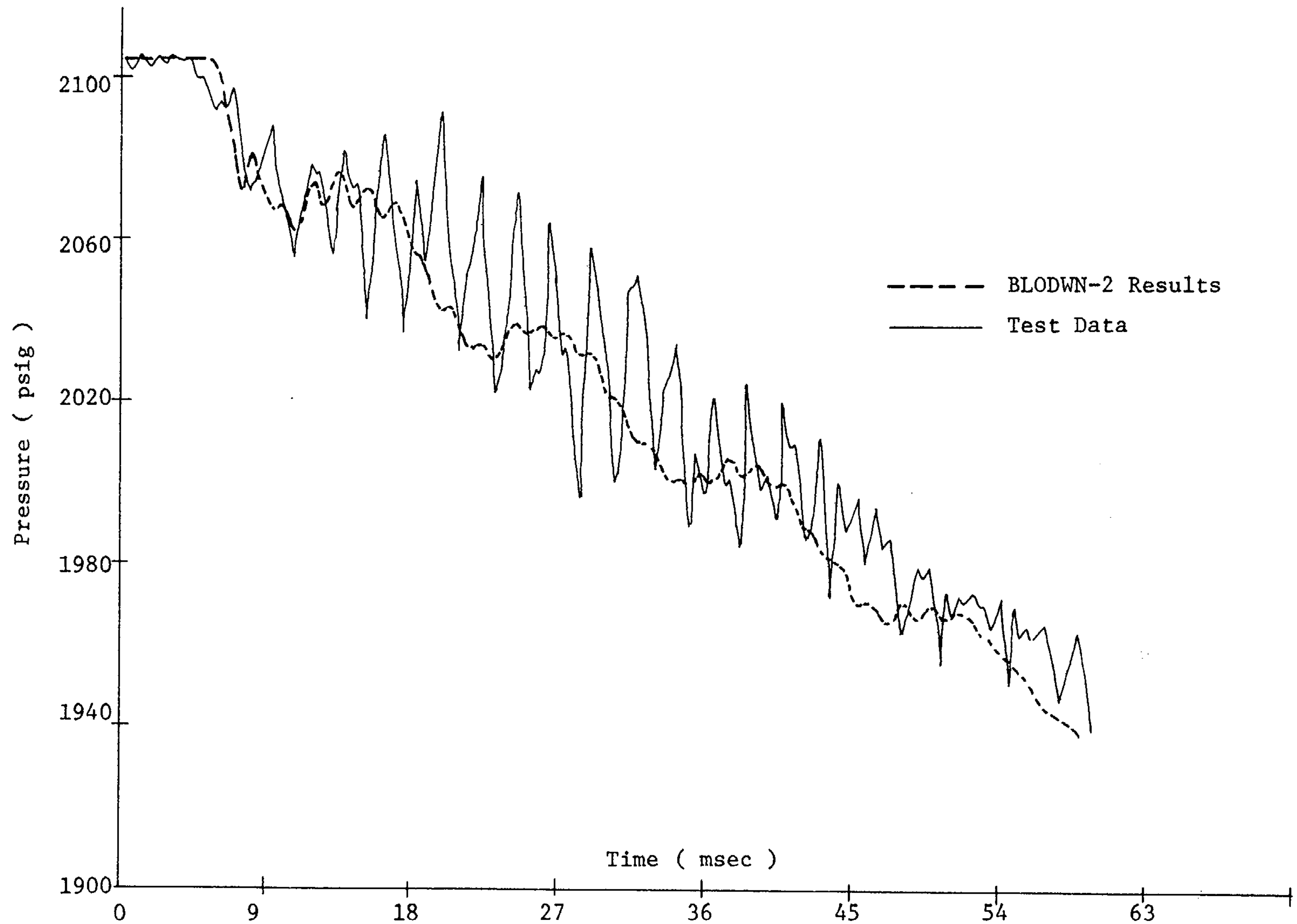

Figure 4-20. CSE B-19B, Pressure At Nozzle "L",Geometry Model "A"

where

ν = natural frequency $= \frac{1}{2\pi}\sqrt{\omega_z^2 + \omega_r^2}$

z = 0 at lower end

c = velocity of sound

$J_m(\ )$ = Bessel function, order m

For the z-component of particle velocity to be zero at both $z = 0$ and $z = \ell$

$$\left(\frac{\partial p}{\partial z}\right)_{\substack{z=0\\ z=\ell}} = 0$$

hence, with the cosine function

$$\omega_z \frac{\ell}{c} = n_z\, \pi (n_z = 0,1,2,3,\ldots)$$

For the r-component of particle velocity to be zero at $r = R$

$$\left(\frac{dJ_m}{dr}\right)_{r=R} = 0$$

$$\therefore\ \omega_r \frac{R}{c} = \pi\alpha_{m,n}$$

where α_{mn} are solutions of $\frac{dJ_m(\pi\alpha)}{d\alpha} = 0$, tabulated on page 399 of Reference 17.

Therefore,

$$\omega_z = \left(\frac{\pi c n_z}{\ell}\right) n_z = 0,1,2,\ldots$$

$$\omega_r = (\pi \alpha_{mn} \frac{c}{R})$$

$$\nu = \frac{c}{2} \sqrt{(\frac{n_z}{\ell})^2 + (\frac{\alpha_{mn}}{R})^2} \quad (c/sec)$$

The significance of the subscripts m, n, and n_z is as follows:

When m = 0, n = 0 acoustic waves are plane waves traveling along the cylinder (z) axis. One-dimensional representation of the above-described models "A" and "B" accounts for such waves only.

When m = 0, n_z = 0 acoustic waves are purely radial, resulting in the largest oscillations at the cylinder axis. The nodal lines (i.e., the locations where the amplitudes of the particle displacement are zero) are circles located at such radii r*, which make

$$J_m (\pi \alpha_{mn} \frac{r^*}{R}) = 0$$

because the particle displacement (not velocity) is proportional to the local pressure. The amplitudes of pressure oscillations have local maxima where local particle velocities are zero; i.e., where

$$\frac{dJ_m}{dr} = 0$$

Now, since

$$\frac{dJ_m(x)}{dx} = -J_{m+1}(x)$$

the local maxima of pressure amplitudes in the n_z = 0 case occur at such radii, r**, where

$$J_{m+1}(\pi \alpha_{mn} \frac{r^{**}}{R}) = 0$$

Hence, for any value of m, the cylinder axis is a location of the local maxima of pressure oscillations.

The subscript n indicates how many circular nodal lines are present, while the subscript m designates the number of diametral nodal lines.

The case $n = 0$, $n_z = 0$ describes the waves which travel close to the curved walls and have little motion near the cylinder axis. These are referred to as "ϕ-waves." Pressure gages located near the cylinder axis will detect very small amounts of oscillation having the frequency of the ϕ-waves. Pressure gages located in the nozzles around the vessel wall circumference will, on the other hand, sense the ϕ-wave frequencies rather strongly.

In the case of blowdown of a system composed of various geometry regions connected in series and/or in parallel, a number of natural modes of vibration are excited in each region, each mode making a different contribution to the local amplitude of pressure oscillation. In general, the lowest modes are the largest contributors except when the boundary condition between two adjacent regions may force one particular mode to be more prominent.

The amplitudes of the natural vibration mode oscillations decay unless re-excited by phenomena occurring at the region boundaries.

4.4.3 Multidimensional Acoustic Vibration of CSE Vessel Fluid

Let $\ell = 16$ ft (representing the empty vessel), $R = 1.75$ ft, $c \approx 2500$ ft/sec. The natural frequencies of various vibrational modes are found from

$$\nu = \frac{c}{2}\sqrt{\left(\frac{n_z}{\ell}\right)^2 + \left(\frac{\alpha_{mn}}{R}\right)^2} \text{ cycles/sec}$$

where $\alpha_{00} = 0$, $\alpha_{01} = 1.2197$, $\alpha_{02} = 2.2331$, $\alpha_{10} = 0.5861$, $\alpha_{11} = 1.6970$, $\alpha_{12} = 2.7140$, etc.

Hence, the longitudinal, plane wave fundamental frequency becomes

$$(\nu)_{\substack{m=0\\ n=0\\ n_z=0}} = 78.2 \text{ c/sec}$$

and the higher plane wave mode $(\nu)_{\substack{m=0\\ n=0\\ n_z=2}} = 156.2$ c/sec

The breathing mode (radial wave) frequencies become

$$(\nu)_{\substack{m=0\\ n=1\\ n_z=0}} = 871.2 \qquad (\nu)_{\substack{m=0\\ n=1\\ n_z=2}} = 885.1 \text{ c/sec}$$

$$(\nu)_{\substack{m=0\\ n=2\\ n_z=0}} = 1595.1 \qquad (\nu)_{\substack{m=0\\ n=2\\ n_z=1}} = 1602.7 \text{ c/sec}$$

The circumferential mode (ϕ-wave)

$$(\nu)_{\substack{m=1\\ n=0\\ n_z=0}} = 418.6 \qquad (\nu)_{\substack{m=1\\ n=0\\ n_z=2}} = 446.8 \text{ c/sec}$$

$$(\nu)_{m=2,\ n=0,\ n_z=0} = 694.4 \qquad (\nu)_{m=2,\ n=0,\ n_z=2} = 711.8 \text{ c/sec}$$

$$(\nu)_{m=3,\ n=0,\ n_z=0} = 955.2 \qquad (\nu)_{m=3,\ n=0,\ n_z=2} = 856.8 \text{ c/sec}$$

The mixed, circumferential plus radial frequencies are

$$(\nu)_{m=1,\ n=1,\ n_z=0} = 1212.1 \qquad (\nu)_{m=1,\ n=1,\ n_z=2} = 1222.2 \text{ c/sec}$$

$$(\nu)_{m=2,\ n=1,\ n_z=0} = 1524.7 \qquad (\nu)_{m=2,\ n=1,\ n_z=2} = 1532.7 \text{ c/sec}$$

The above results show that, for the chosen $\ell \simeq 16$ ft, the value of the index n_z plays a very minor part in the range of frequencies of interest.

The frequencies of the measured pressure oscillation were (refer to Figures 4-19 and 4-20):

1. Near support lug No. 7 (6 in. below the core plate)
   Fundamental $\nu \simeq 71$ c/sec
   High frequency component $\nu \simeq 950$ c/sec

2. Inside Nozzle L:
   High frequency component $\nu \simeq 450$ c/sec

It can be seen that the measured low frequency component at the core plate support lug corresponds in magnitude to the component $\nu(m=0,\ n=0,\ n_z=1)$ frequency.

The measured high frequency component at the core plate support lug is bounded by $\nu(m=0,\ n=1)$ and $\nu(m=1,\ n=1)$, with the component $\nu(m=3,\ n=0)$ being very close to the measurement. The first of these three is the axially symmetric r-wave; the second is the axially asymmetric r-wave (i.e., the mixed r and ϕ-wave); and the third is the pure ϕ-wave. The effect of the ϕ-wave should be significant because the core plate support lug is located very close to the vessel wall.

As far as the "L" nozzle is concerned, its own natural acoustic vibration frequency is that of an organ pipe closed at one end and "blown" at the other:

$$\nu_n^L = \frac{c}{4\ell_L'} n_L \quad (n_L = 1,\ 3,\ 5,\ 7,\ .\ .\ .)$$

where $\ell_L' = \ell_L + 0.8\ \sqrt{A} = 0.833 + 0.8\ \sqrt{0.015} = 0.931$ ft

$$\therefore\ \nu^L = 671.3,\ 2014,\ .\ .\ .\text{c/sec}$$

All of these are above the measured high frequency component of 450 c/sec. The measurement is within the computed $\nu(m=1,\ n=0)$ belonging to the vessel ϕ-wave. This is not unexpected since the strength of the ϕ-wave is large near the vessel wall, thus driving the nozzle which now acts as an organ pipe in forced vibration. The high frequency component of the computed (Model A) pressure for Nozzle L has the frequency approaching the $\nu^L \simeq 670$ c/sec computed above for the organ pipe fundamental.

An attempt was made to synthesize a three-dimensional piping network simulation of the CSE vessel (shown in Figure 4-21) in order to compute the above-described local pressure oscillations. The network consists of one-dimensional flow passages interconnected at various branch points. Both the upper and the lower plenums are represented by one central vertical passage,

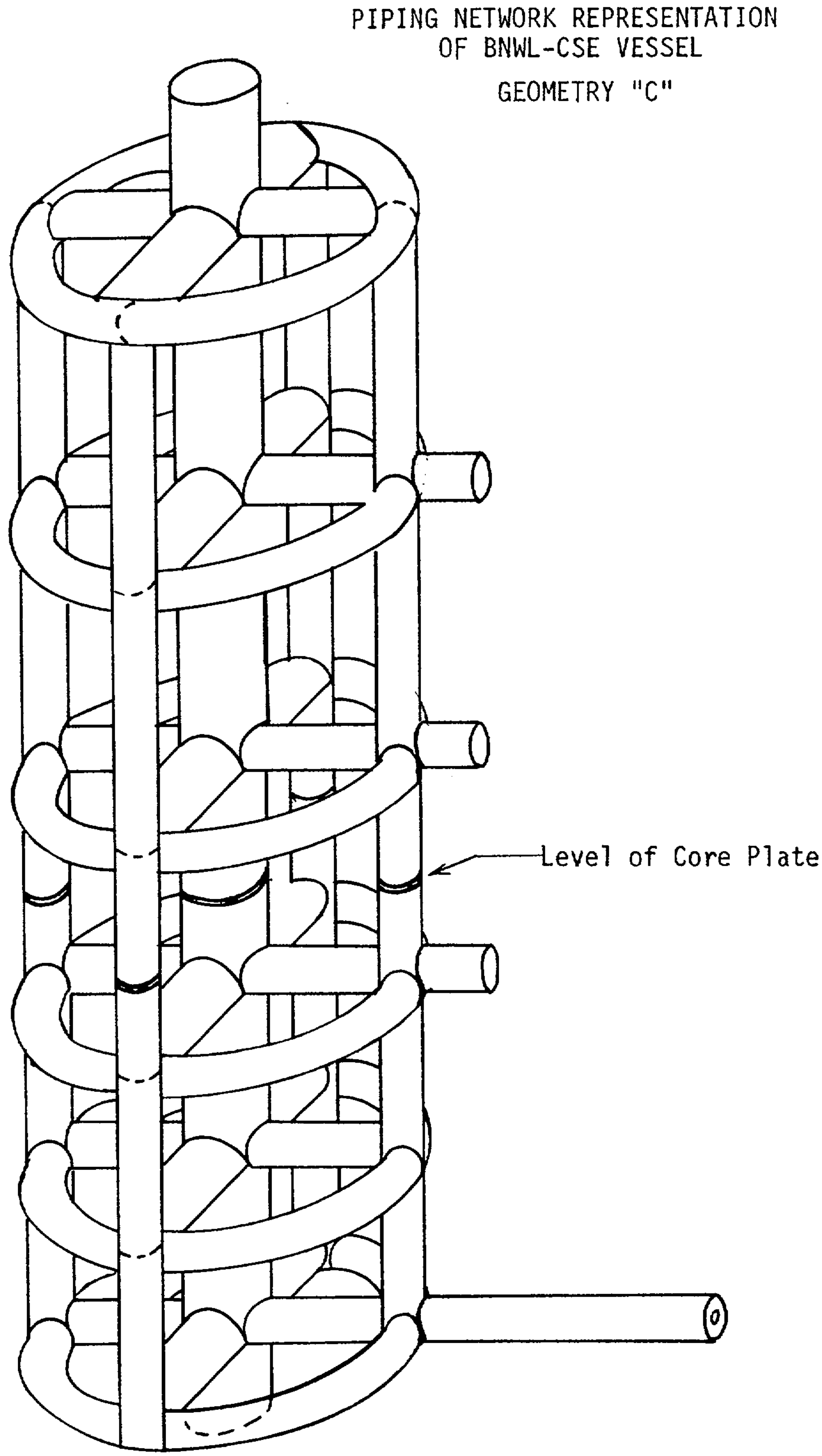

Figure 4-21. Piping Network Representation of BNWL-CSE Vessel Geometry "C"

four vertical passages at the periphery, and three "wheels" -- each being composed of four circumferential and four radial passages. Lengths of these passages conserve the important patch lengths for the sonic wave in axial, radial, and circumferential directions. The cross section area was distributed in such a manner as to conserve the volumes of the upper and the lower plenums. The core plate was modeled as a quasi-steady orifice loss without the reduction of the flow passage area. This piping network representation was designated as Model "C."

Figures 4-22 and 4-23 illustrate comparisons between the Model "C" BLODWN-2 results and the test data. Although in this case the computed pressures show more "structure," the latter bears no relationship to the anticipated frequencies of the radial and/or circumferential waves. The frequencies of the oscillations in Figures 4-22 and 4-23 are about 200 c/sec and 166 c/sec, respectively. Therefore, the piping network of Figure 4-21 failed to reproduce the true three-dimensional effects.

There still remains, however, the question whether the measured fine structure in Figure 4-22 does indeed represent the pressure fluctuations -- or something else. Consider the measured sharp spike at about one millisecond after initiation of blowdown. The rarefaction wave generated at the rupture could not have reached that particular transducer in such a short time. On the other hand, the whole vessel will have felt a mechanical vibration or at least a jolt caused by the first discharge through the rupture. Consequently, the pressure transducer, being attached by a bracket to the core plate support lug, could have been set into an oscillatory motion, causing it to record the reported high frequency "structure." This question will have to be resolved in future tests.

4.4.4 Core Plate Loads During Blowdown

Let us now consider a steady-state flow of fluid through a horizontal pipe containing an orifice at its midplane. Figure 4-24 illustrates the flow regime, velocity, and pressure profiles in the vicinity of the orifice plate. Contraction of fluid, jet formation and creation of eddies make the flow and pressure fields multidimensional. The axial pressure profile shows that the

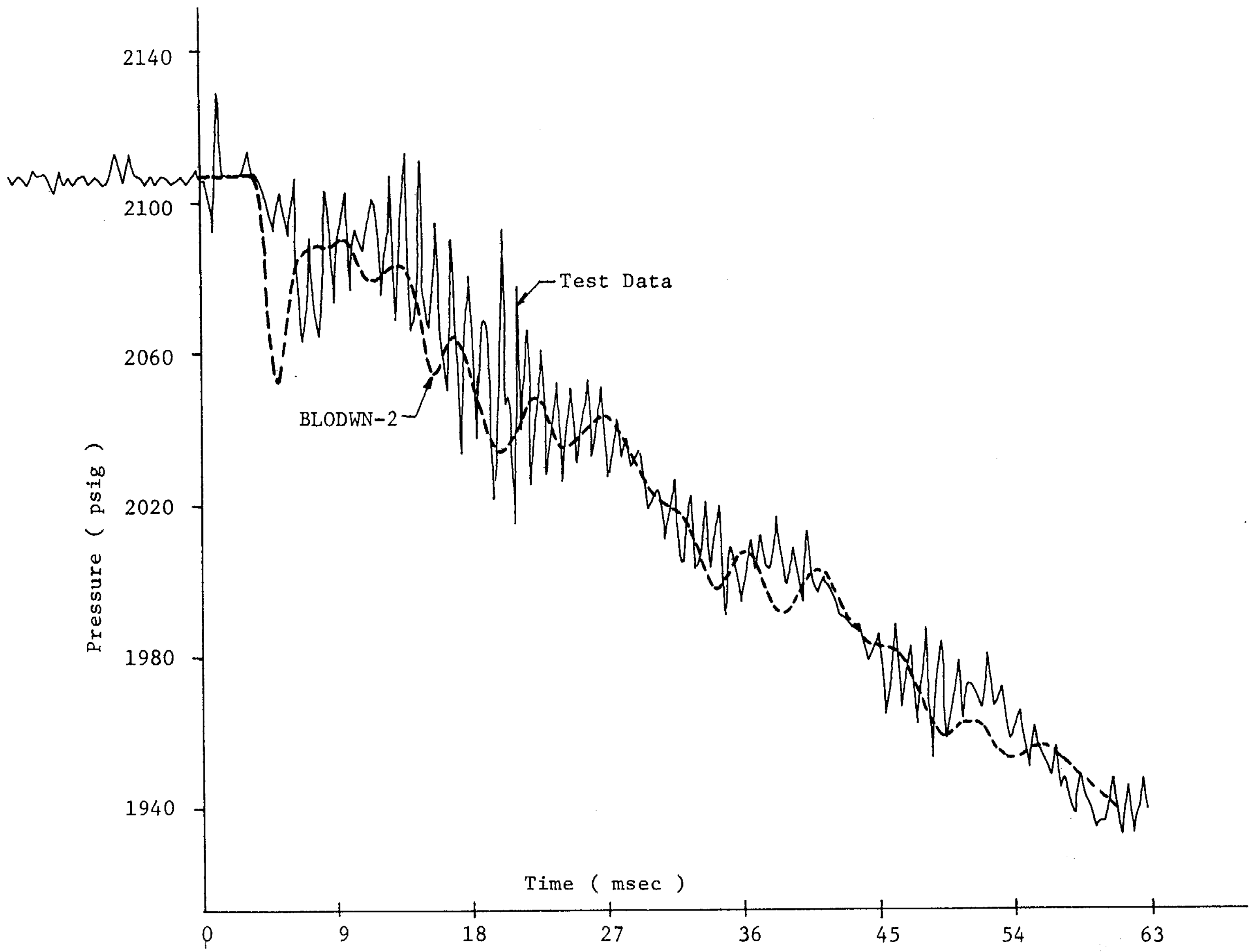

Figure 4-22. CSE Blowdown Run No. B-19B, Pressure at Core Plate Support Lug 7, Piping Network Model "C"

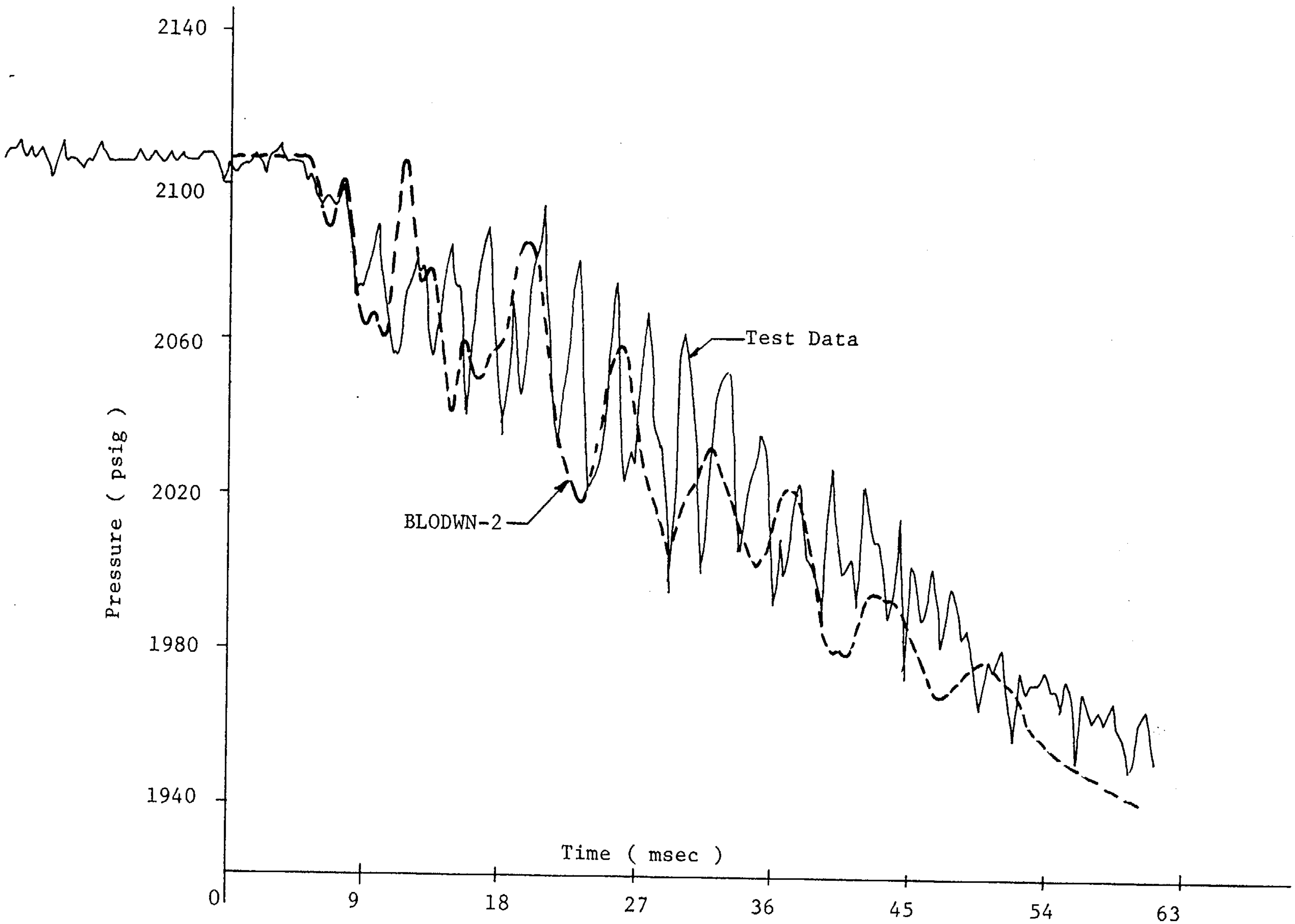

Figure 4-23. CSE Blowdown Run No. B-19B, Pressure At Nozzle "L", Piping Network Model "C"

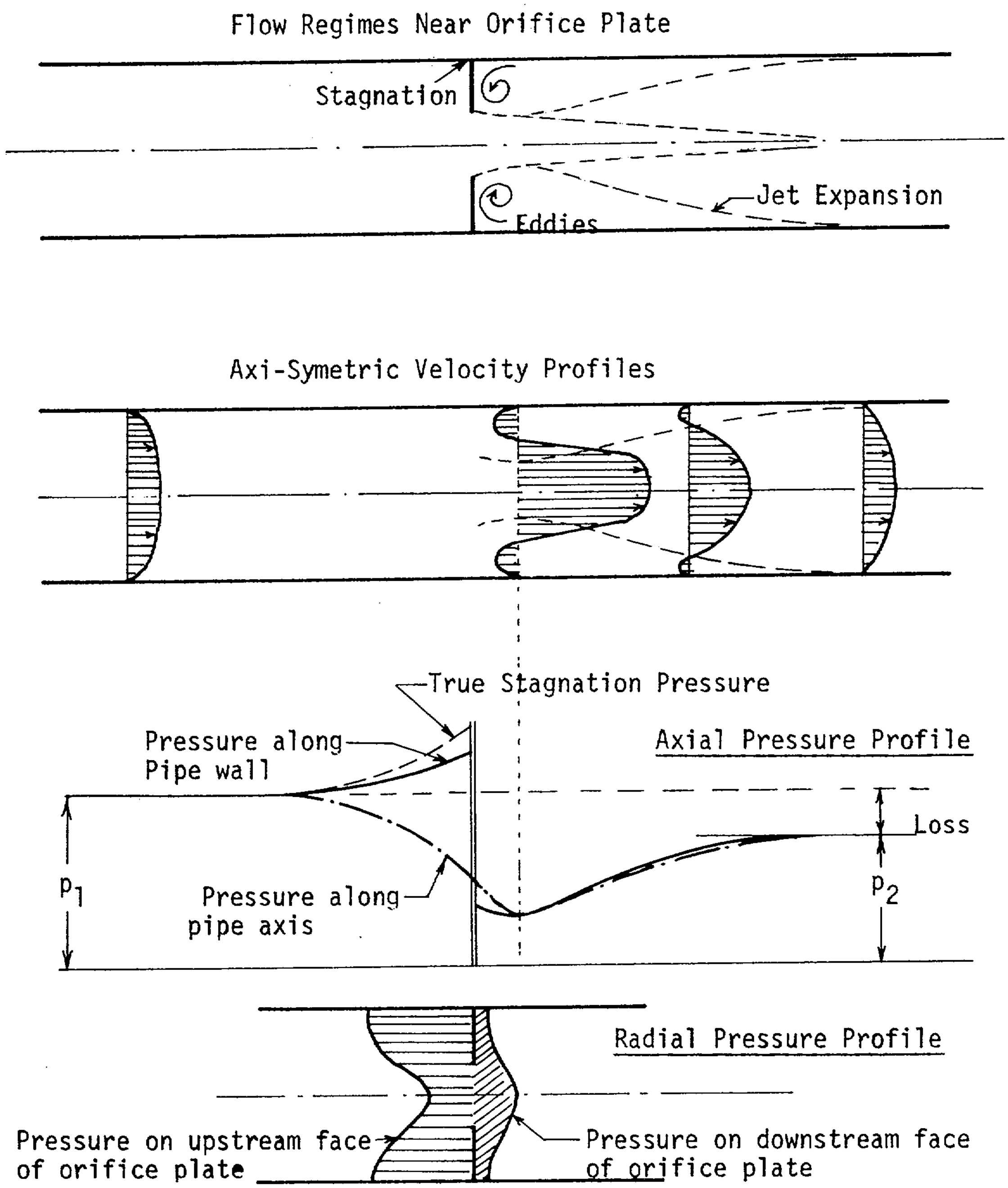

Figure 4-24. Flow Regimes, Velocity, and Pressure Distribution at Pipe Orifice

pressure acting on the upstream face of the orifice, near the pipe wall, is higher than the fluid pressure a few pipe diameters further upstream, p_1, and somewhat lower than the stagnation pressure. Along the pipe axis, the fluid pressure first drops from p_1 to some low pressure at the vena contracta just downstream of the orifice plate, and then recovers to p_2 a few diameters downstream. The pressure p_2 is lower than p_1 by the amount referred to as the "orifice (minor) loss" caused by the dissipation of kinetic energy in eddies and friction. One-dimensional fluid analyses employ the orifice loss expressed in terms of the dynamic hea of the flow through the orifice aperture. This head is used to compute the downstream pressure p_2 when the instantaneous values of the upstream pressure, p_1, and the mean velocity are known.

The hydraulic loading on the orifice plate can be found by integrating, over the orifice plate, the local differences of pressure acting on the upstream and the downstream faces of the orifice. This integrated pressure differential load F is higher than $F_o = (A_p - A_o) x (p_1 - p_2)$, where A_p and A_o are the pipe and the orifice aperture areas, respectively (see the radial pressure profile in Figure 4-24).

Therefore, in one-dimensional analysis a correction term ΔF must be added to F_o, where ΔF is unually expressed in terms of the dynamic head.

Hence,

$$F = (A_p - A_o) \cdot \{(p_1 - p_2) + C_F \cdot \rho \frac{u_o/u_o/}{2g_c}\}$$

where the constant C_F can either be obtained from measurements of the actual orifice plate load, or from the comparison of the one-dimensional and multi-dimensional hydraulic analyses when the latter is available.

In the case of a perforated orifice plate, one can always define the portion of the orifice plate surrounding any given hole and identify it with a single orifice located in a single flow channel (or "pipe"), thus allowing the above-described calculation procedure for the hydraulic load.

The perforated "core" plate in the CSE vessel is mounted on a number of lugs located along its circumference. The plate is attached to the lugs by bolts provided with strain gages to allow measurement of axial load transmitted at each lug. The measured load, in the case of transients, includes the structural dynamic response of the elastically-mounted core plate when subjected to the transient hydraulic load. In such a case, the strain gage reading should be calibrated for both the steady as well as cyclic loading over the spectrum of the expected frequencies. Calibration was performed only for the steady loads, and the dynamic structural response was analytically computed by BNWL in order to deduce the hydraulic load history.

Figure 4-25 shows such hydraulic loads deduced from measurement at three support lugs (identified in the figure) for Test B-19B. Apart from some sharp spikes which were recorded before and during blowdown (hence are attributed to electronic problems associated with the data sampling), the traces pertaining to the period prior to blowdown exhibit a noise level of the maximum amplitude of about 3 psi of the equivalent hydraulic load. The mean hydraulic loading history illustrated in the following three figures was obtained by taking the mean of the reported measurements of Figure 4-25, in which the sharp spikes were disregarded. It contains, therefore, the above-mentioned uncertainty of $\pm$ 3 psi.

Figures 4-26, 4-27 and 4-28 illustrate the comparisons between the predicted and measured "pressure difference" responsible for the core plate loading, for the geometric representations of Models "A," "B," and "C," respectively. In these figures the thin dashed line represents the computed p_1-p_2 (refer to Figure 4-24) while the thick solid line represents the computed total Δp which contains the correction embodied in ΔF discussed above. The measurement-deduced Δp is shown by the dot-dash line.

Referring first to Figure 4-26, which pertains to the "A" model in which the core plate was treated as a quasi-steady, orifice type loss, it can be seen that:

1. The predicted and the measured loads are in phase, indicating the validity of the "A" model; and

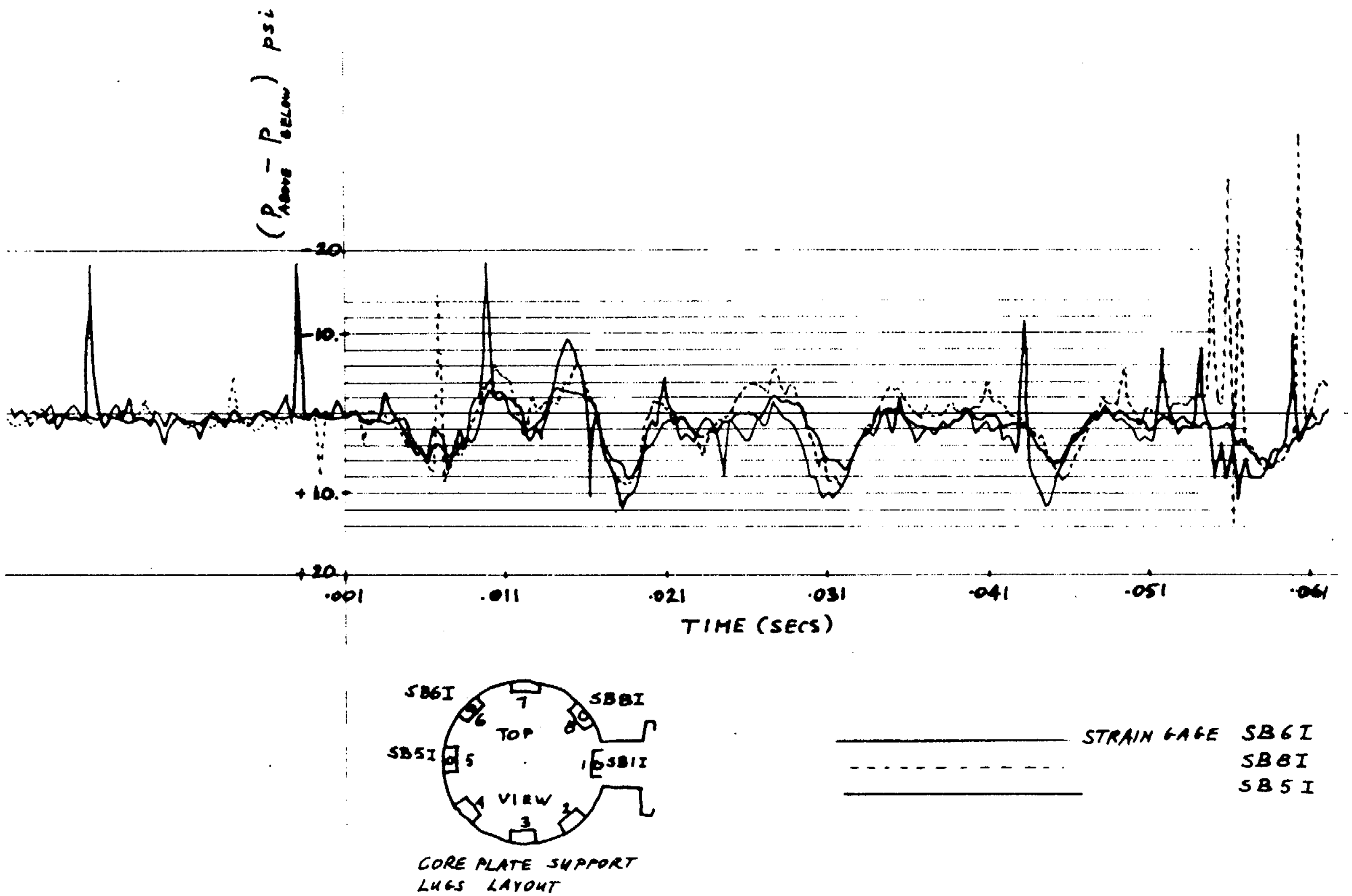

Figure 4-25. CSE B-19B Pressure Difference Across Core Plate Deduced from Strain Measurements At Support Lugs

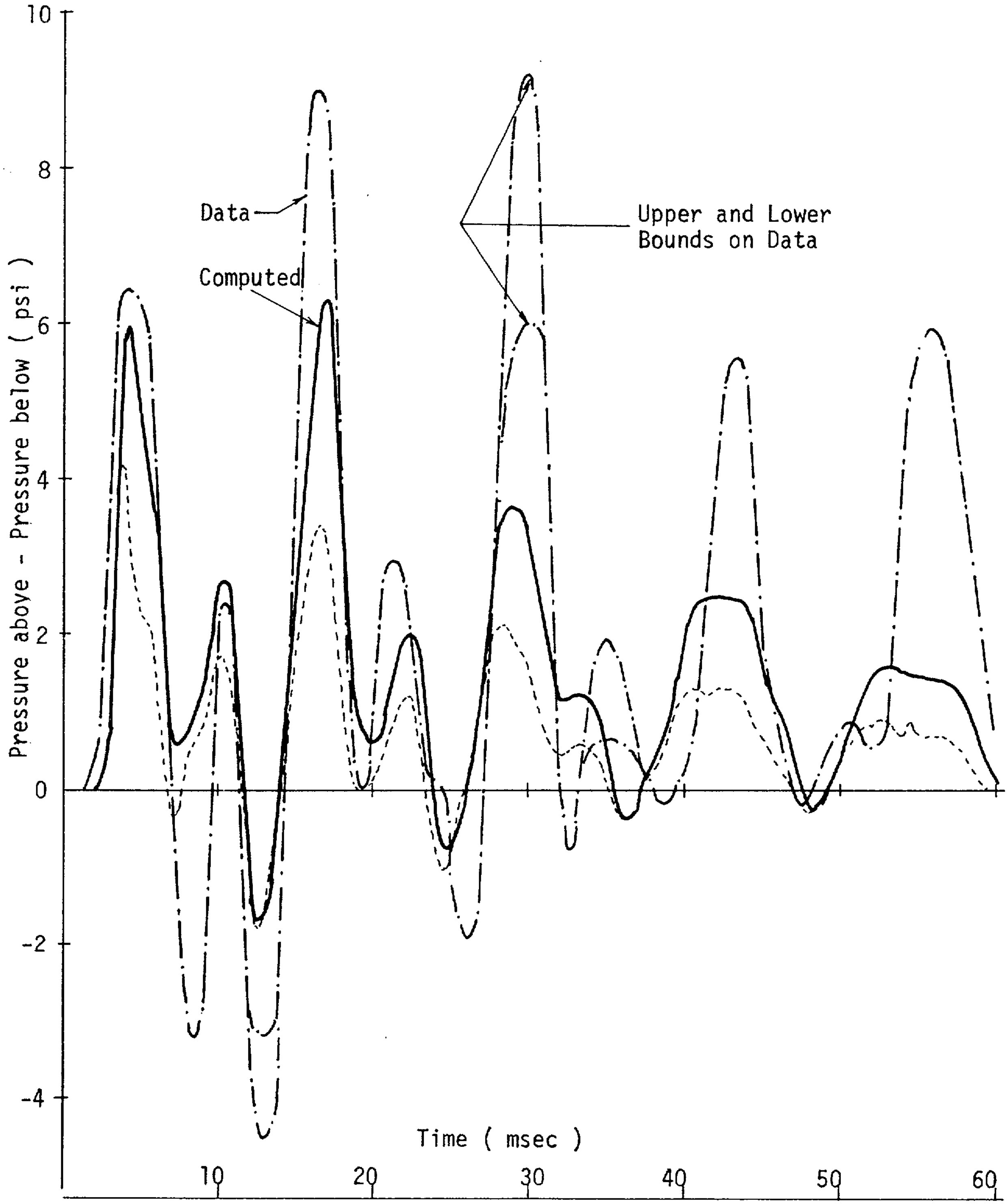

Figure 4-26. BNWL (CSE) B-19b Test Comparison Between Measured and Computed Pressure Difference Across The Core Plate; Model "A"

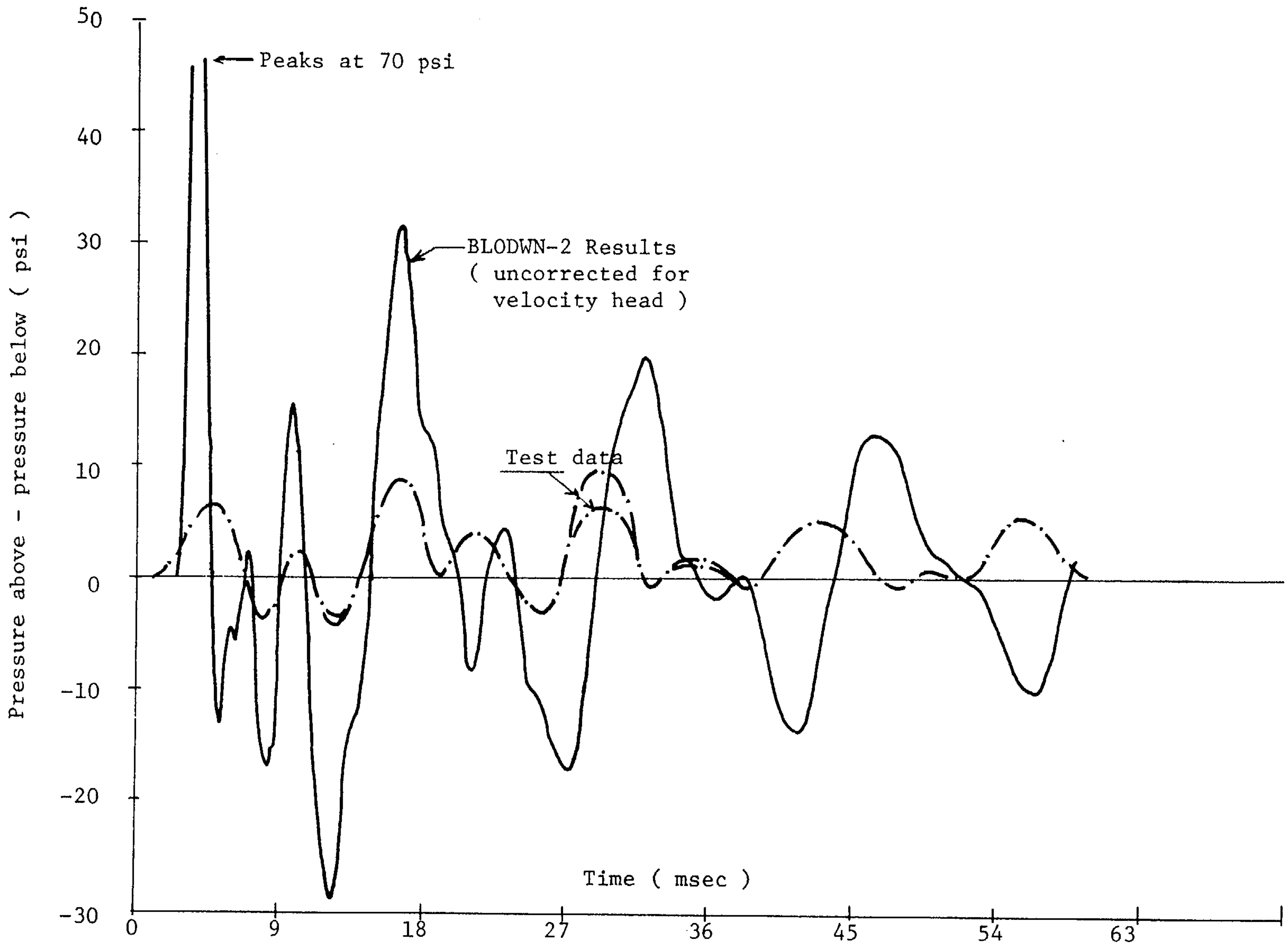

Figure 4-27. BNWL (CSE) B-19B Test Comparison Between Measured and Computed Pressure Difference Across the Core Plate; Model "B"

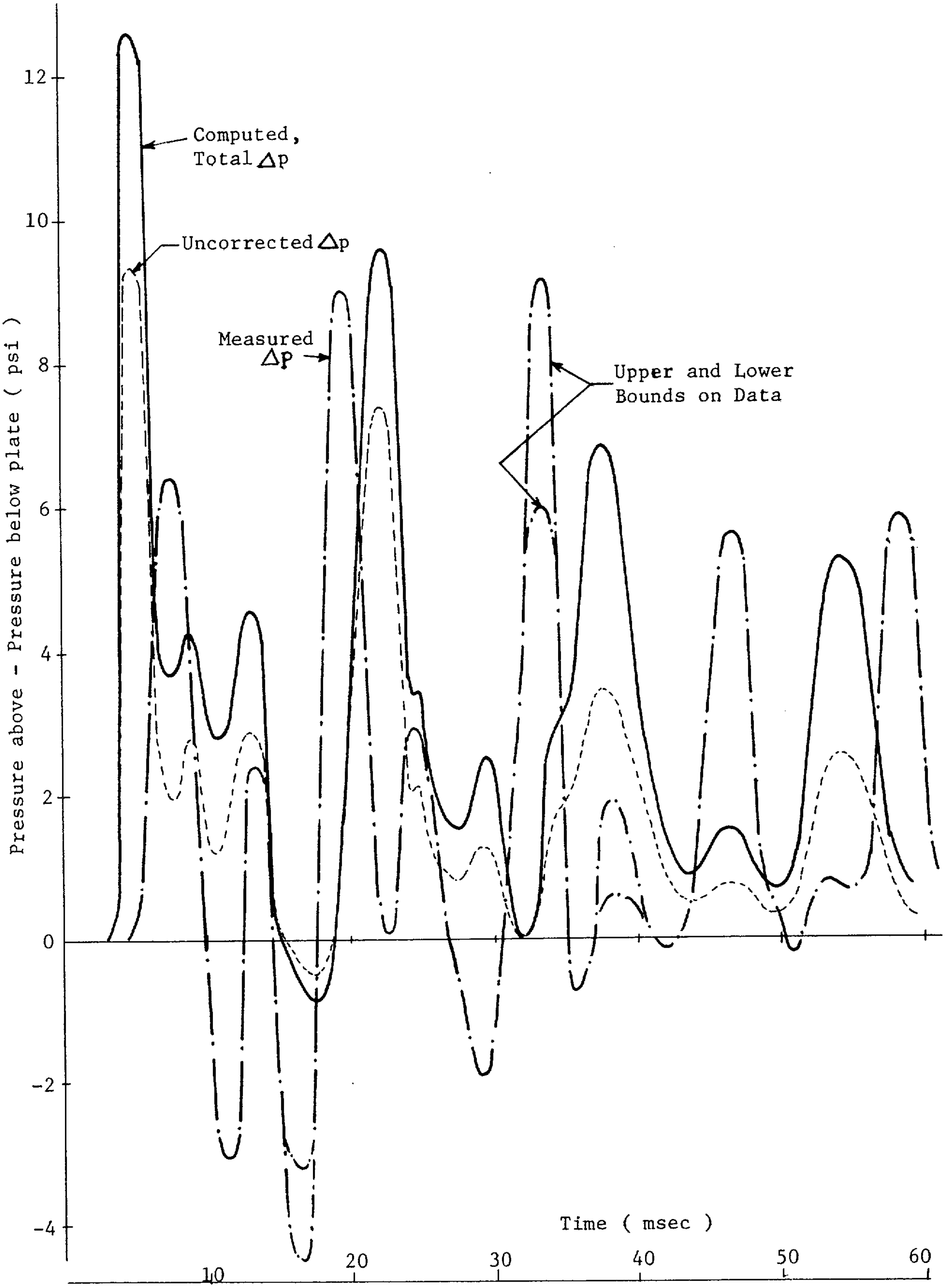

Figure 4-28. CSE Blowdown Run # B-19B Pressure Difference Across Core Plate Piping Network Model "C"

2. While the first two cycles agree within the above-stated uncertainty, the predicted Δp for subsequent cycles diminishes at a much faster rate than shown in the measurements.

The "B" model prediction of Δp (shown in Figure 4-27) in which the orifice plate was treated as a separate passage of the smaller flow area resulted in:

1. Mismatching of the phases of the predicted and the measured oscillations; and
2. Gross overestimate of the hydraulic loads, especially in the first few cycles. Because of this fact, only the predicted $(p_1 - p_2)$ is shown since the correction term makes the matter even worse.

Figure 4-28 illustrates the comparison between the predicted and the measured core plate Δp pertaining to the Model "C," in which gross three-dimensional effects were simulated by an equivalent piping network. The core plate treatment was as per model "A" except that the Δp constituted the arithmetic mean of Δp's pertaining to each of five vertical legs. This comparison shows that:

1. The longer acoustic paths associated with the equivalent pipes cause longer periods of oscillations which, in turn, increase the degree of phase mismatch at later times; and
2. Amplitudes of the predicted p oscillations do not drop off as steeply as in the "A" model. The first positive peak is somewhat overestimated, while the subsequent positive peaks are satisfactory. The negative peak was underestimated.

In the above predictions, factor C_F in the correction term was set equal to 1.5, resulting, for this particular test, in

$$\Delta p \simeq \Delta p_{code} + 1000\, G/G/$$

where G is the mass velocity ($lbs/sec/ft^2$) at (not through) the core plate.

From the above three comparisons it appears that the core plate loads are best predicted by the piping network Model "C." More such comparisons involving other test conditions will be needed to both gain confidence in measurement and to finalize the best geometric representation with one-dimensional models.

SECTION 5

PRIMARY COOLANT LOOP BLOWDOWN

5.1 GENERAL

The loop geometry adds considerable complexity to the hydraulic flow circuit. In addition to the vessel and the blowdown nozzle, it contains the pump, heat exchanger, pressurizer and associated piping with tees, elbows and a control valve. Figure 5-1 illustrates the LOFT 1/4-Scale Loop and the locations of pressure transducers p-1, p-2, etc. The pressurizer with its connecting pipe is shown simplified. In reality, the pressurizer is composed of two vessels connected in series, attached to a 1-inch pipe which, in turn, connects to the main loop both before the heat exchanger inlet and before the control valve. One section of this pipe is wrapped with heating elements. The geometric model, sizes and other input information for the BLODWN-2 analysis are shown in the Appendix.

One of the important unknowns in modeling the loop for analysis of the early blowdown is the representation of the pump. The most one can hope to obtain from the pump manufacturers are the homologous curves described in the WHAM program documentation.[16] Such curves, which are also utilized by the BLODWN-2 code, describe the steady-state pump behavior under the normal and abnormal pump operating regimes in which either the fluid velocity or the pump speed, or both, can be higher or lower than nominal (or even reversed). How the pump behaves during the passage of acoustic waves, (i.e., what fractions of the wave are transmitted and reflected) is not known. The LOFT 1/4-scale loop is not the ideal test configuration for obtaining data on pump transients; however, much could be learned by proper instrumentation of the existing loop. Available information on the LOFT 1/4-Scale Loop pump consisted only of the head/flow curve in the normal operating regime. This information was used to define the appropriate homologous curves wherein the characteristics in the abnormal operation regimes were necessarily guessed.

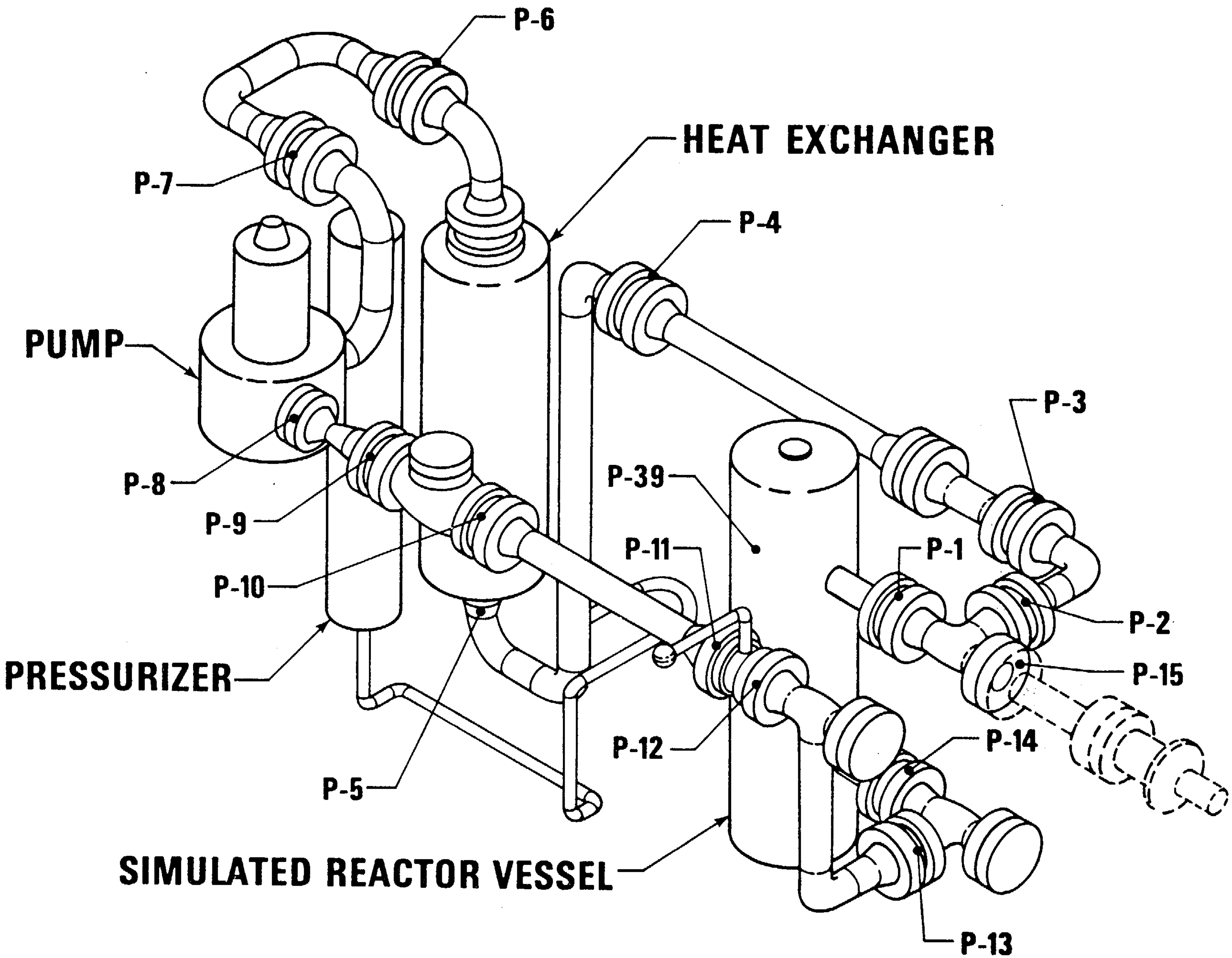

Figure 5-1. LOFT 1/4-Scale Loop (Locations of Pressure Gages)

5.2 LOFT 1/4-SCALE LOOP, 30 PERCENT BREAK; SUBCOOLED AND TRANSITION BLOWDOWN REGIMES

The BLODWN-2 analysis was performed with a 47-leg representation in which the initial temperature of water was assumed to be 585°F, spatially uniform. The pump inlet and outlet pressures were assumed to be 2316 psia and 2357 psia, respectively, with the initial pressure distribution specified on the basis of the computed pressure drops for the various loop elements. The largest pressure drop occurs at the flow control valve; its magnitude is such that for the known flow rate of 327 gpm the pressures at the pump's inlet and outlet match the pump operating characteristics. The flow passage through the pump was assumed to have an area of 0.0045 ft^2, based on Phillips Petroleum Company's input information for WHAM program calculations. This was their estimate of the effective area seen by an acoustic wave passing through the pump.[18] The blowdown pipe, containing a 30 percent orifice and the rupture disk assembly, was attached to the simulated reactor vessel outlet.

Comparison between BLODWN-2 results and the reported measurements[19] for the Test 809 are illustrated in Figures 5-2 through 5-5. As previously discussed, the sequential breaking of the rupture disks with the resulting initial pressure disturbance cannot be reproduced by BLODWN-2. This leads to some mismatch between the measured and the computed pressure histories, although this mismatch is within the probable error of the measurement. The BLODWN-2 prediction of a pressure disturbance at 18 msec, shown in Figures 5-2 and 5-3 and which is larger than the measured pressure disturbance, was caused by the pump. The assumed flow area past the pump impeller was apparently too small, leading to excessive reflection of the acoustic waves. Figure 5-5 shows the comparison between the computed and the measured pressure histories for Tests 809 and 813. The latter test was a duplicate run. The difference in the measured levels of the pressure plateau after 24 msec can be attributed either to the difference in the initial temperature of the liquid at that location between the two runs, or to the pressure transducer drift, or both.

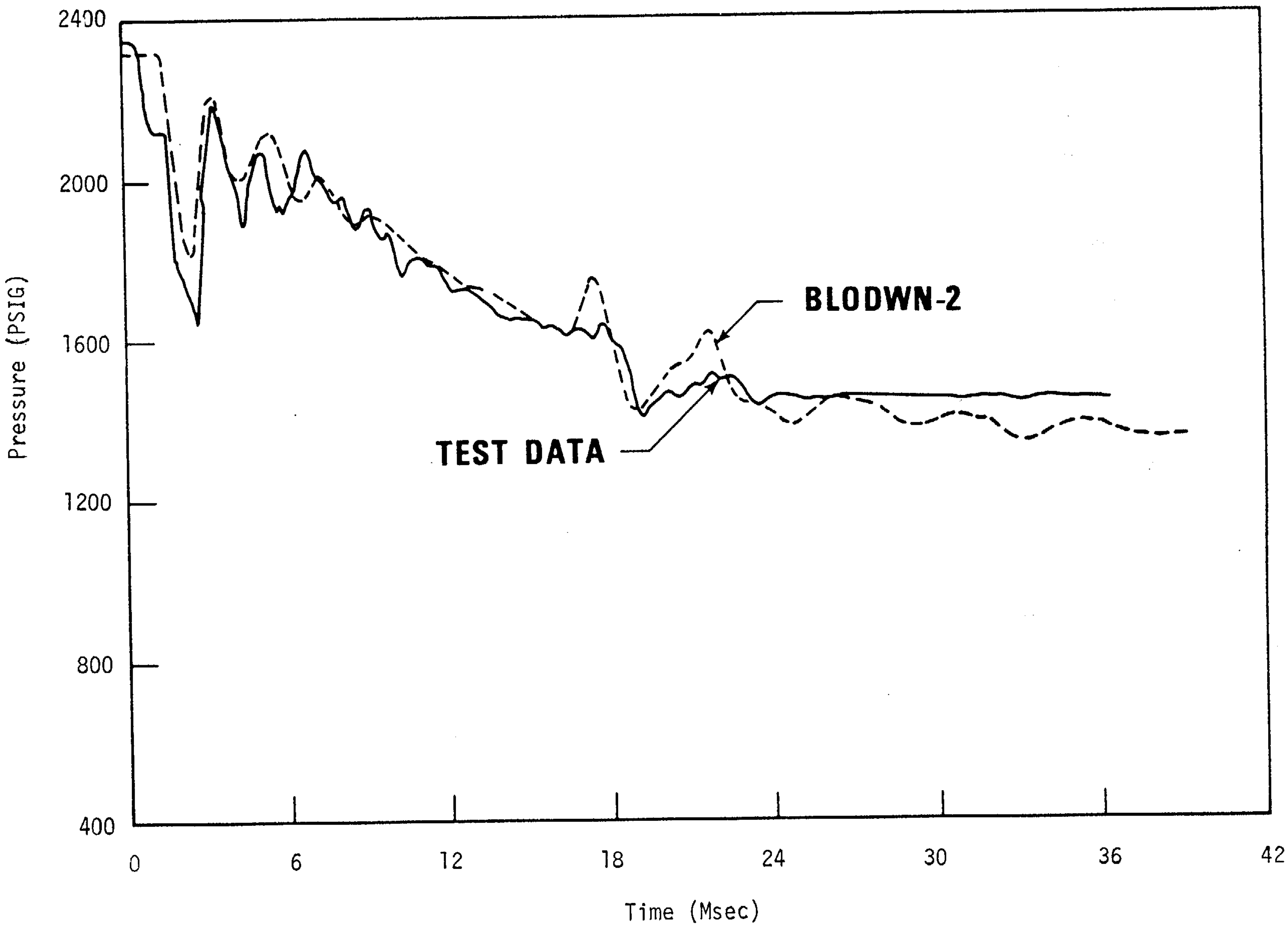

Figure 5-2. BLODWN-2 Results for LOFT 1/4 Scale Loop, Test No. 809 (30% Rupture, Gage Location (P-1))

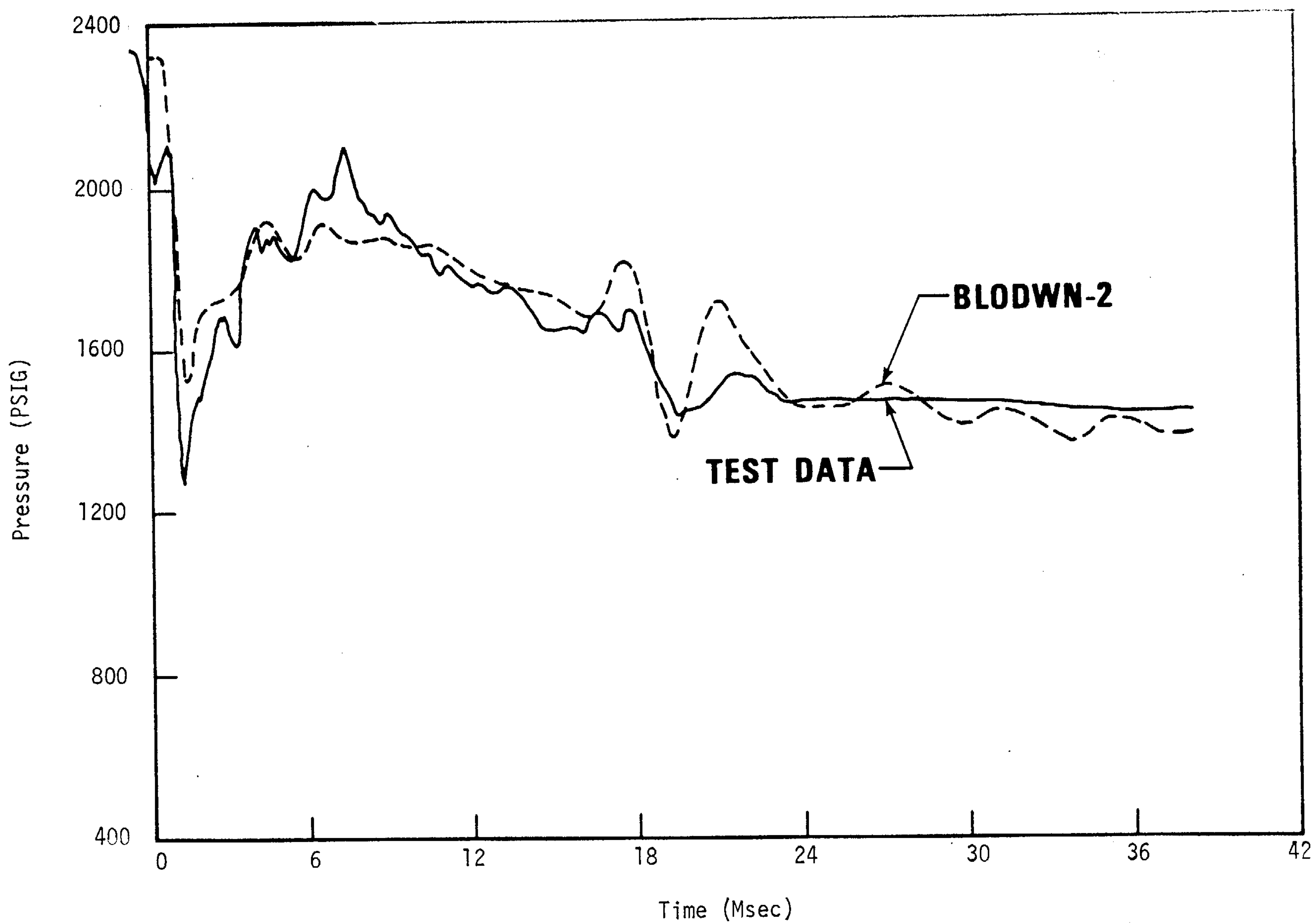

Figure 5-3. BLODWN-2 Results for LOFT 1/4 Scale Loop, Test No. 809 (30% Rupture, Gage Location (P-15))

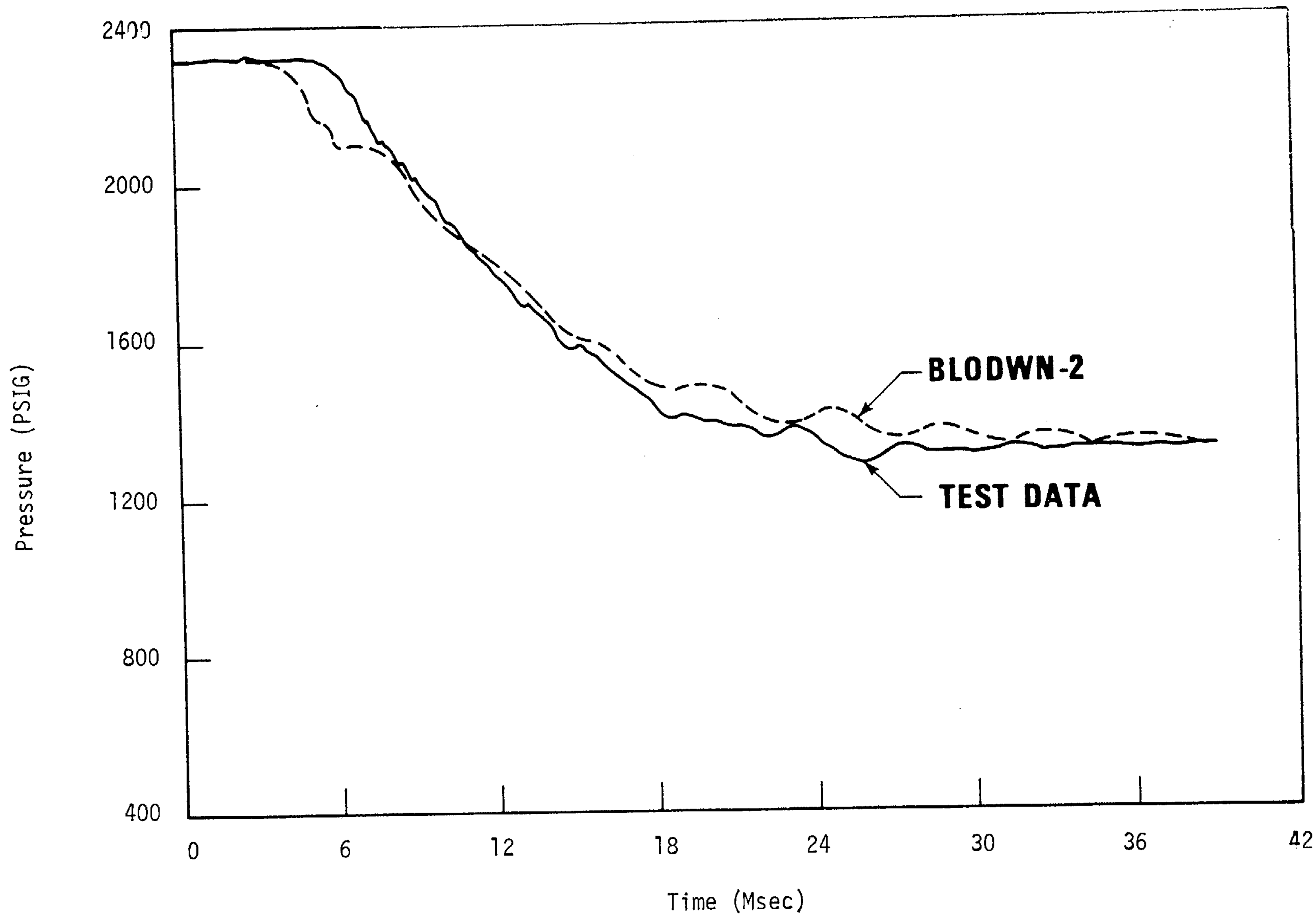

Figure 5-4. BLODWN-2 Results for LOFT 1/4 Scale Loop, Test No. 809 (30% Rupture Gage Location (P-14))

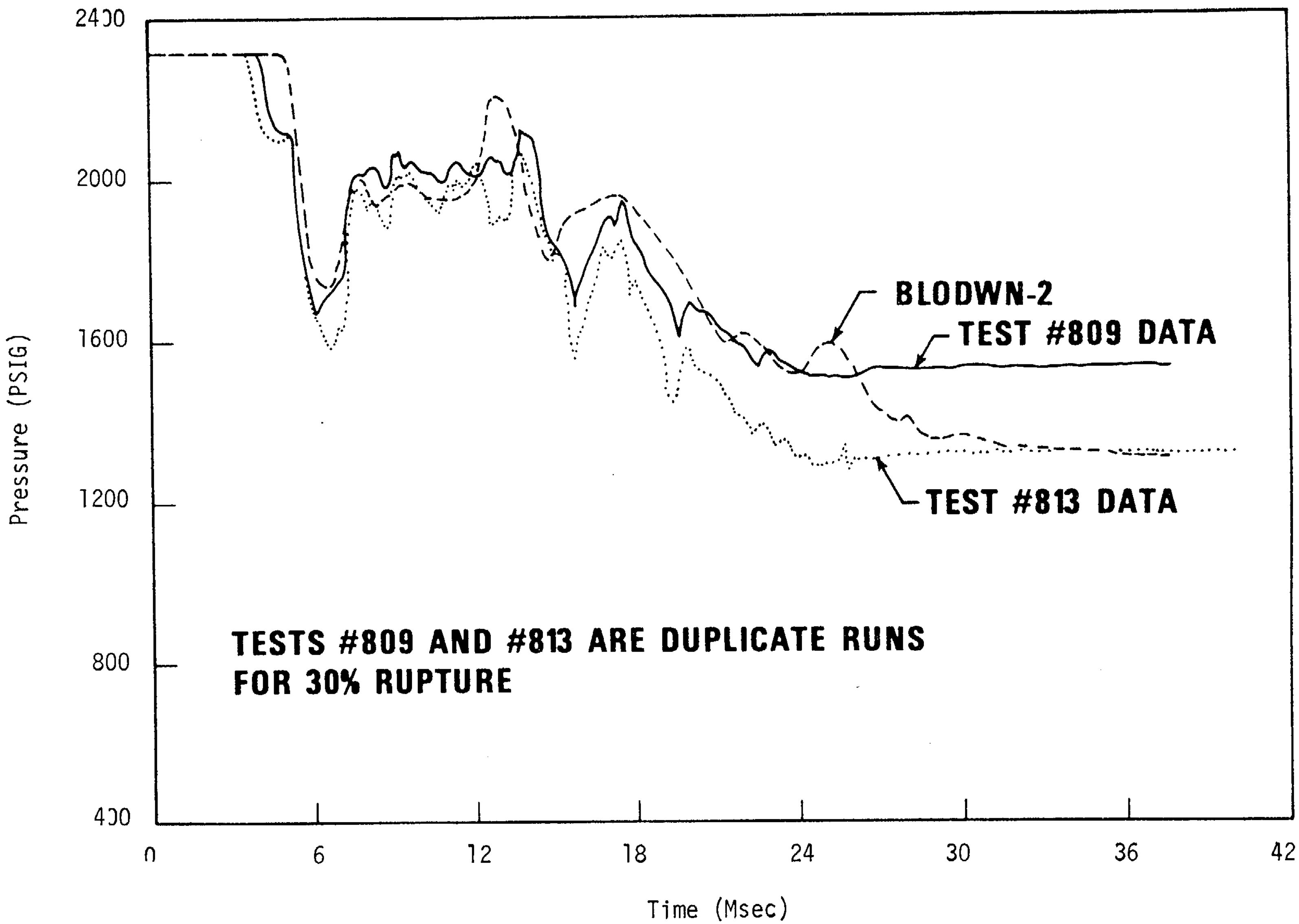

Figure 5-5. BLODWN-2 Results for LOFT 1/4 Scale Loop, Tests Nos. 809 and 813 (Gage Location (P-4))

5.3 LOFT 1/4-SCALE LOOP, 100 PERCENT BREAK; TEST NO. 814

Initial test conditions are P_{vessel} = 2300 psig, T_{vessel} = 584°F, flow rate = 325 gpm. Figures 5-6, 5-7 and 5-8 show comparisons between the measured and computed pressure histories at three locations during the subcooled and the transition regimes. The problem of the sequential breaking of the rupture disks is now more severe. Nevertheless, the agreement between the BLODWN-2 results and the measurement is still satisfactory.

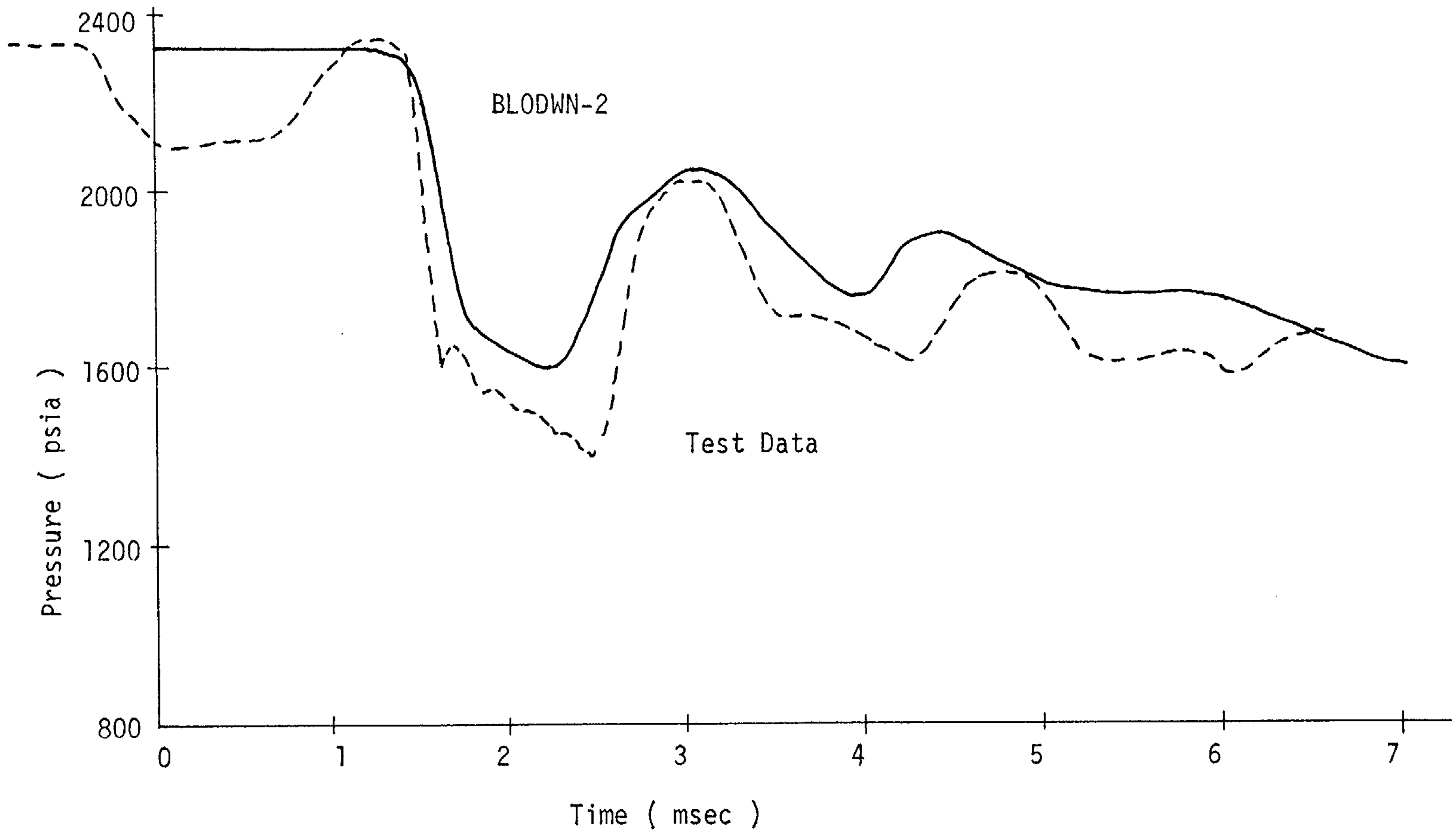

Figure 5-6. Comparison Between BLODWN-2 Results and Test Data LOFT 1/4-Scale Loop, 100% Break, Test No. 814 Gage Location P-1

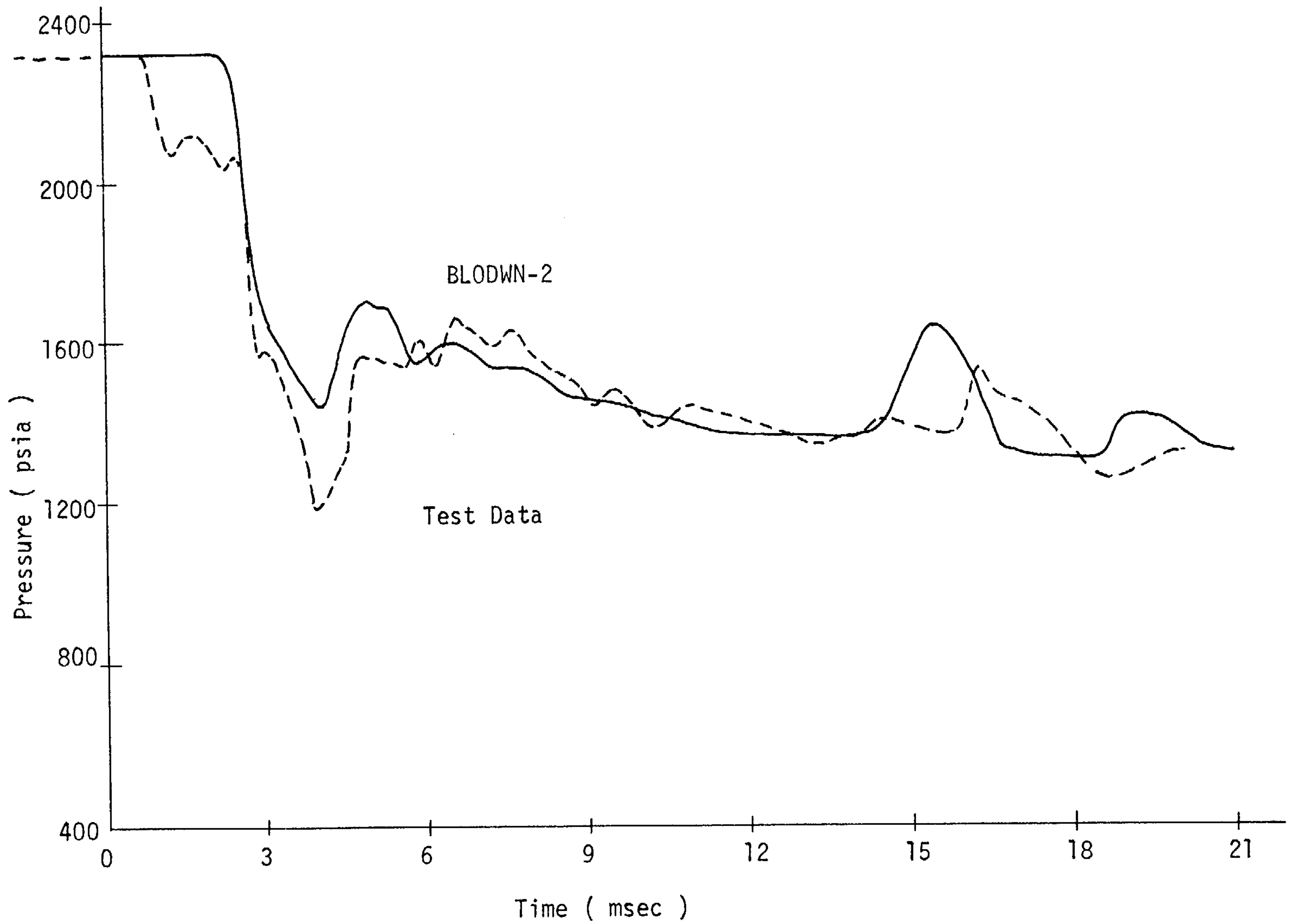

Figure 5-7. Comparison Between BLODWN-2 Results and Test Data LOFT 1/4-Scale Loop, 100% Break, Test No. 814 Gage Location P-3A

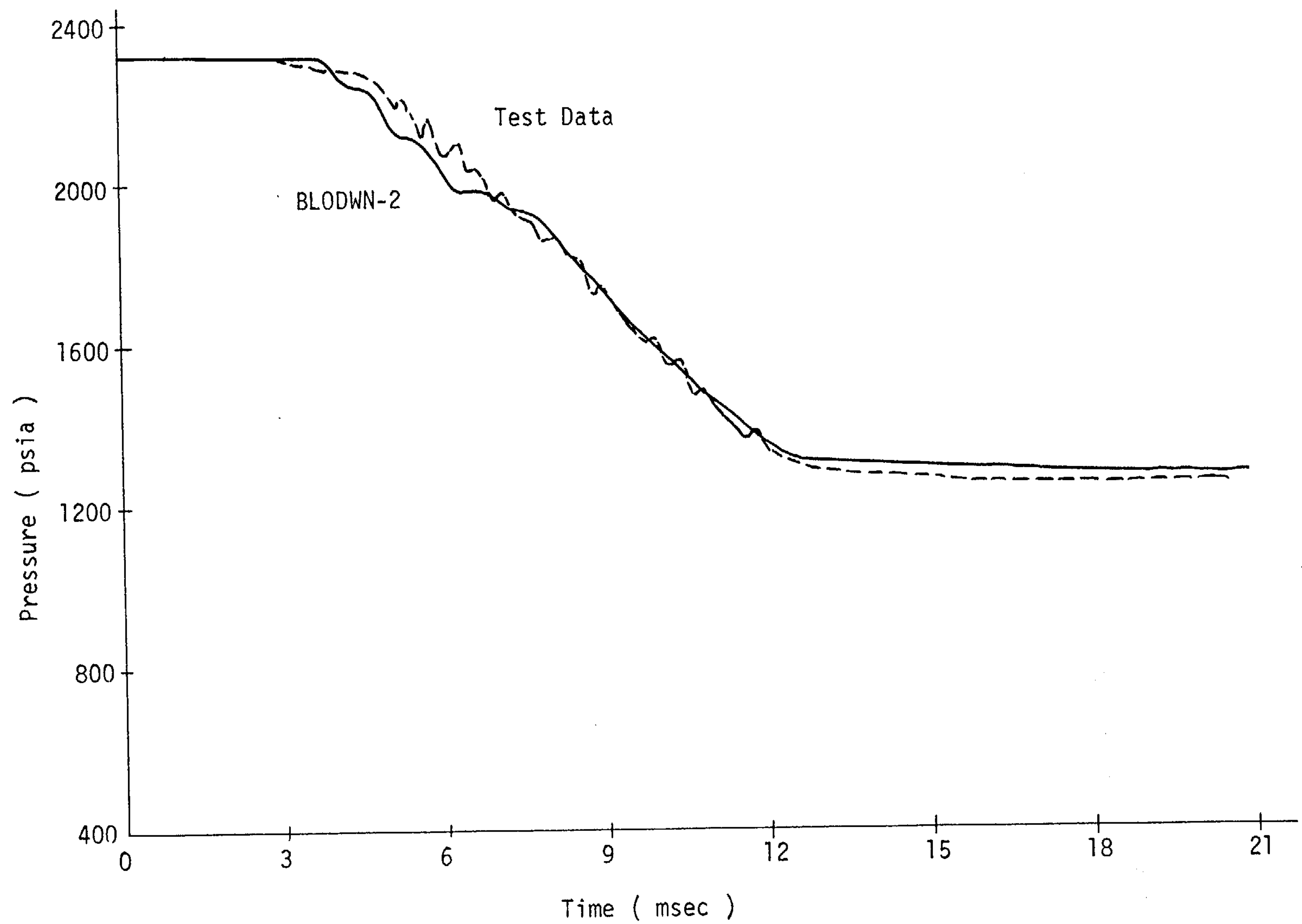

Figure 5-8. Comparison Between BLODWN-2 Results and Test Data LOFT 1/4-Scale Loop, 100% Break, Test No. 814 Gage Location P-14

SECTION 6

HIGHLY SIMPLIFIED REPRESENTATION OF A PWR: COMPARISON OF BLODWN-2 RESULTS WITH IITRI CALCULATION RESULTS

The purpose of this section is to compare the calculation results of two methods of characteristics. In the first method, employed by Gallagher in Reference 20, diagrams of the characteristics in the pressure-velocity and space-time planes were constructed to obtain plots of the local pressure-time histories. This is a well known method, long used in the field of gas-dynamics. The second method is that of the fixed time-space mesh employed in the BLODWN-2 code. The latter "finds" by interpolation where the characteristics come from, in order to meet after the elapse of the specified time increment.

The geometry in this case pertains to a highly simplified hydraulic representation of a pressurized water reactor as utilized in Reference 20 and illustrated in Figure 6-1. The fluid within the annulus around the thermal shield is represented by a channel 20 feet long and 16.2 ft^2 in cross section. The bottom plenum, the core, and the top plenum are represented by channels 10, 10, and 30 feet in length, respectively, and 162, 40.5, and 162 ft^2 in area, respectively. The initial temperature distribution divides the reactor into three temperature zones as shown in Figure 6-1.

The break, 5.4 ft^2 in area, was assumed to occur at the reactor inlet nozzle: instantaneously in Reference 20, and with 1 msec duration in the BLODWN-2 calculation. This caused abrupt pressure changes in IITRI calculations whereas in the BLODWN-2 calculations the pressure changes are gradual. Figures 6-2 and 6-3 show the IITRI and BLODWN-2-computed pressure histories, respectively, for three locations within the annular region. The locations are lettered and indicated in Figure 6-1. The scales are somewhat different but a careful comparison will lead one to conclude that the two methods virtually agree in their predictions. The same conclusion is reached after

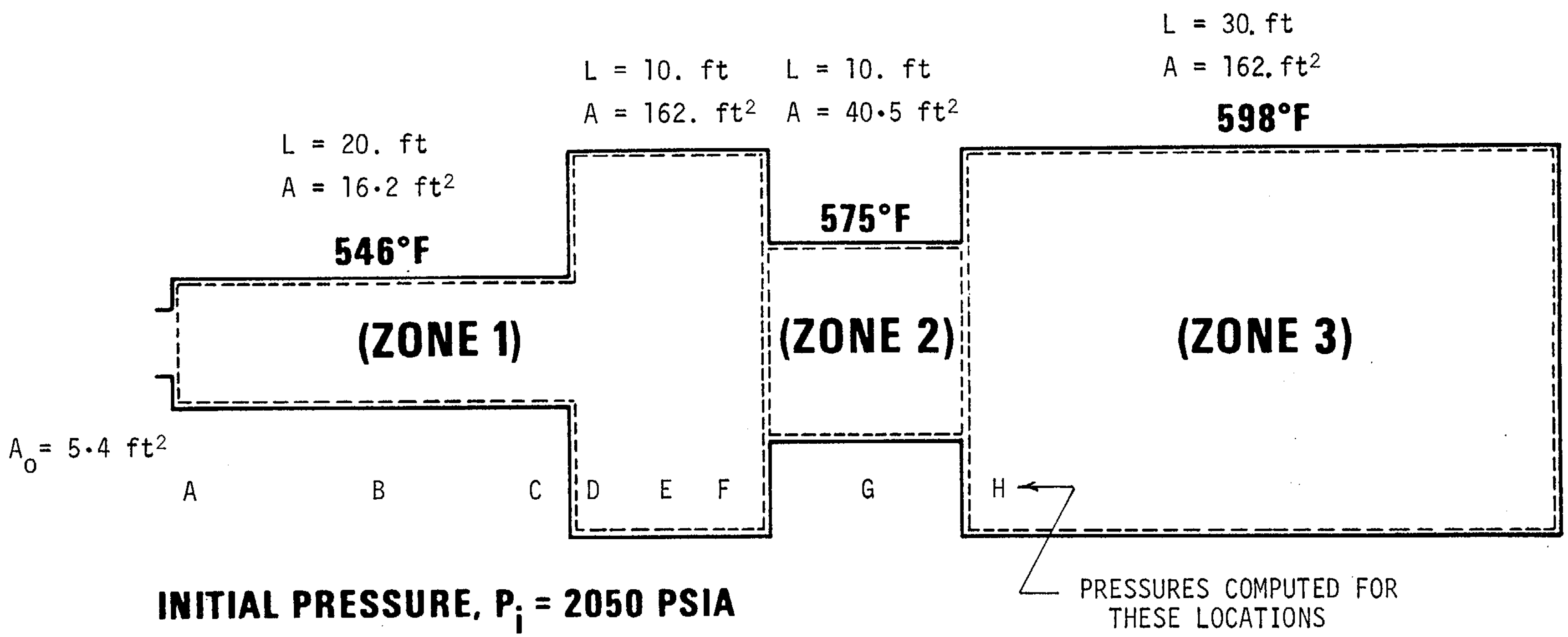

Figure 6-1. Idealized Reactor Geometry and Initial Conditions - Case 2

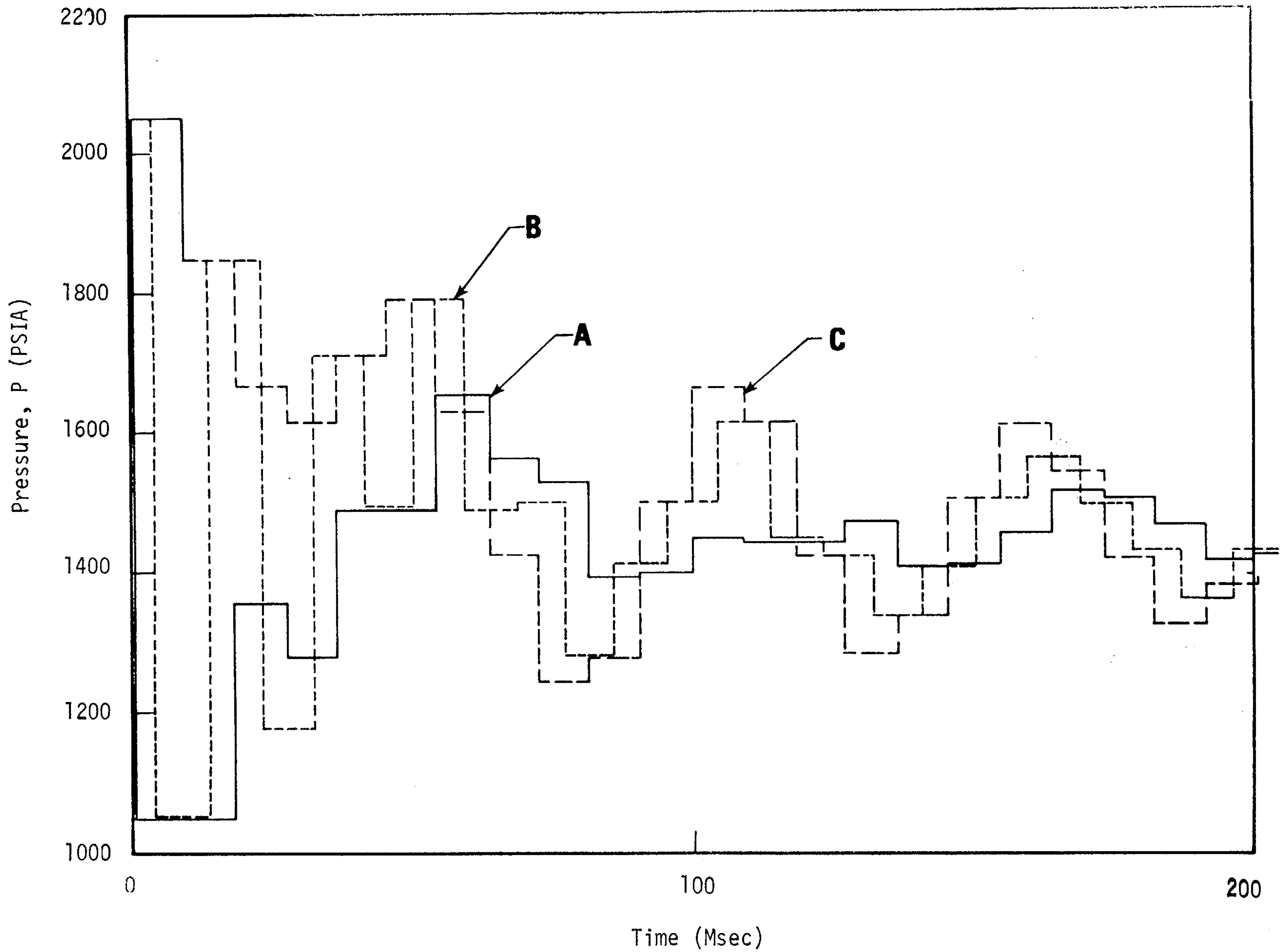

Figure 6-2. Pressure Histories In Annular Region - Case 2
(IITRI Calculation Results)

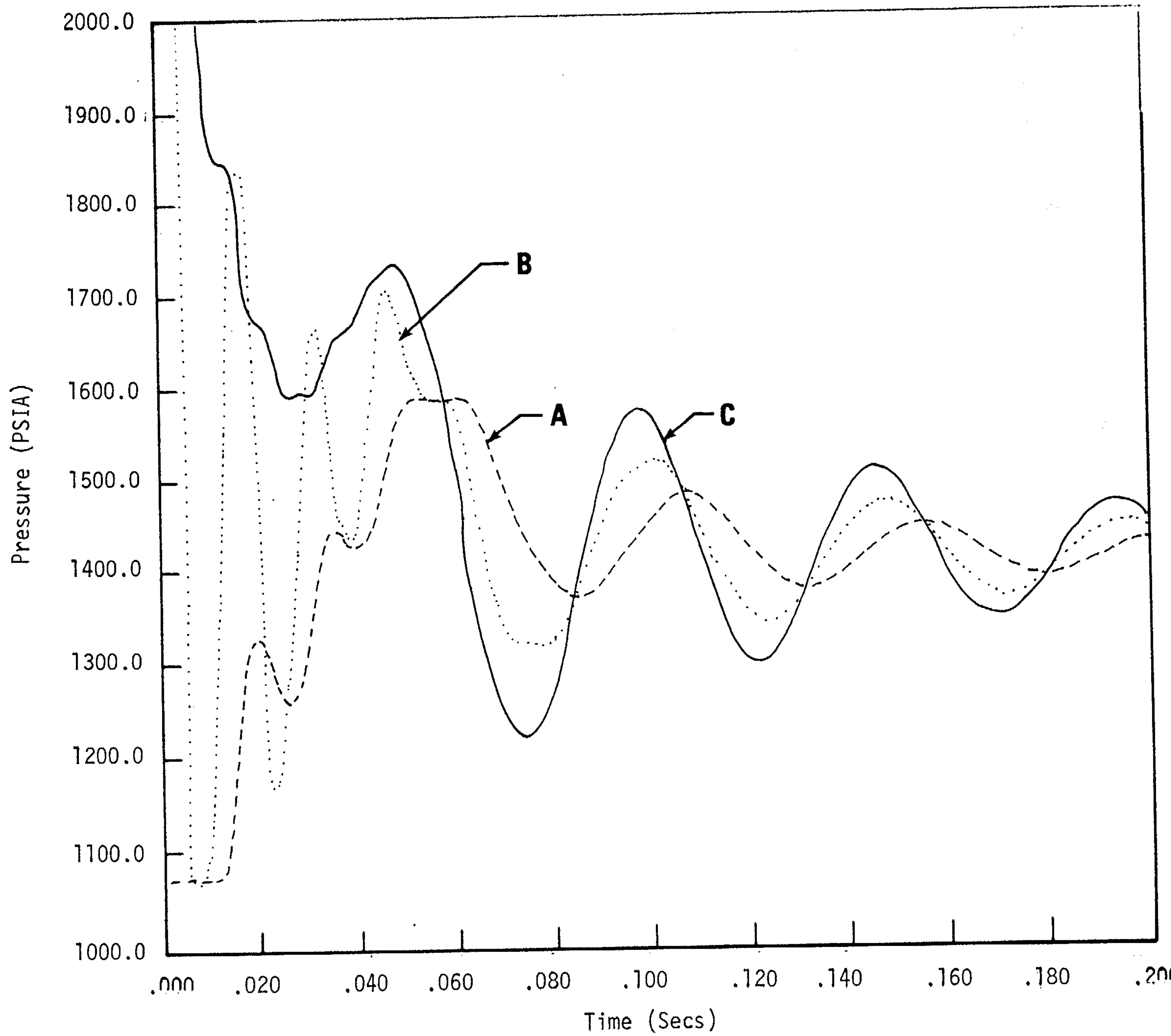

Figure 6-3. BLODWN-2 Results for Annulus Pressures (IITRI Model of PWR, Case 2)

comparing Figures 6-4 and 6-5, and Figures 6-6 and 6-7, which pertain to the IITRI AND BLODWN-2-computed pressure histories in the lower plenum and the core regions, respectively. In the case of BLODWN-2 calculations the contraction and the expansion losses at the area changes were accounted for, causing some damping of the pressure oscillations. This is most evident in the comparison of Figures 6-8 and 6-9, which pertain to the IITRI and BLODWN-2 computed pressure differentials across the reactor core. Both show the largest peak to be about 250 psi, caused by the passage of the first rarefaction wave. Other BLODWN-2 calculations in which the reactor geometry was represented in a much more complex fashion indicated that the peak pressure differential across the core is appreciably smaller.

The above-presented agreement between the BLODWN-2 and IITRI calculations pertaining to the simple geometry raises the confidence in the BLODWN-2 results obtained with a much more complex geometry, whereas the latter precludes the use of the characteristic mesh employed in IITRI calculations.

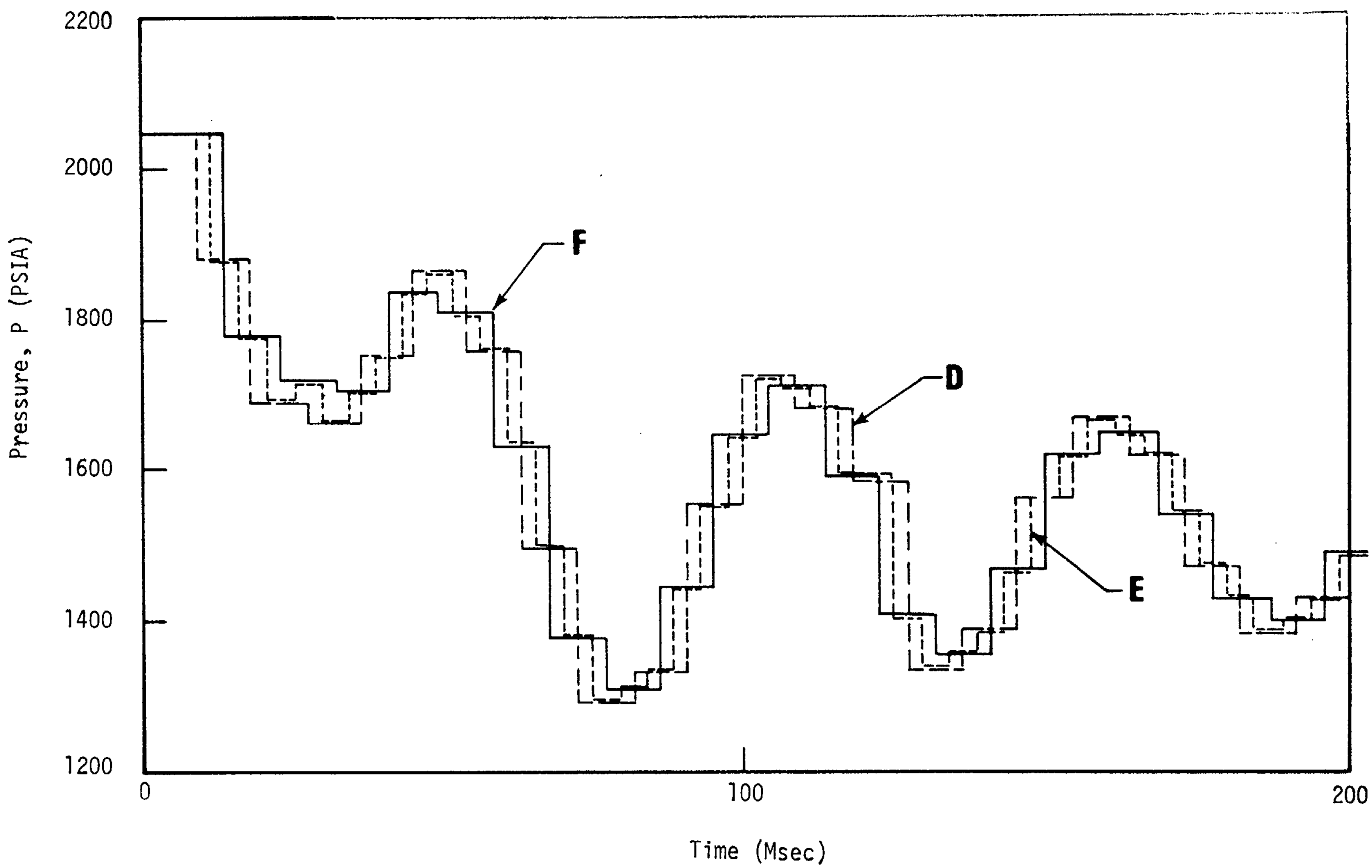

Figure 6-4. Pressure Histories in Lower Plenum - Case 2
(IITRI Calculation Results)

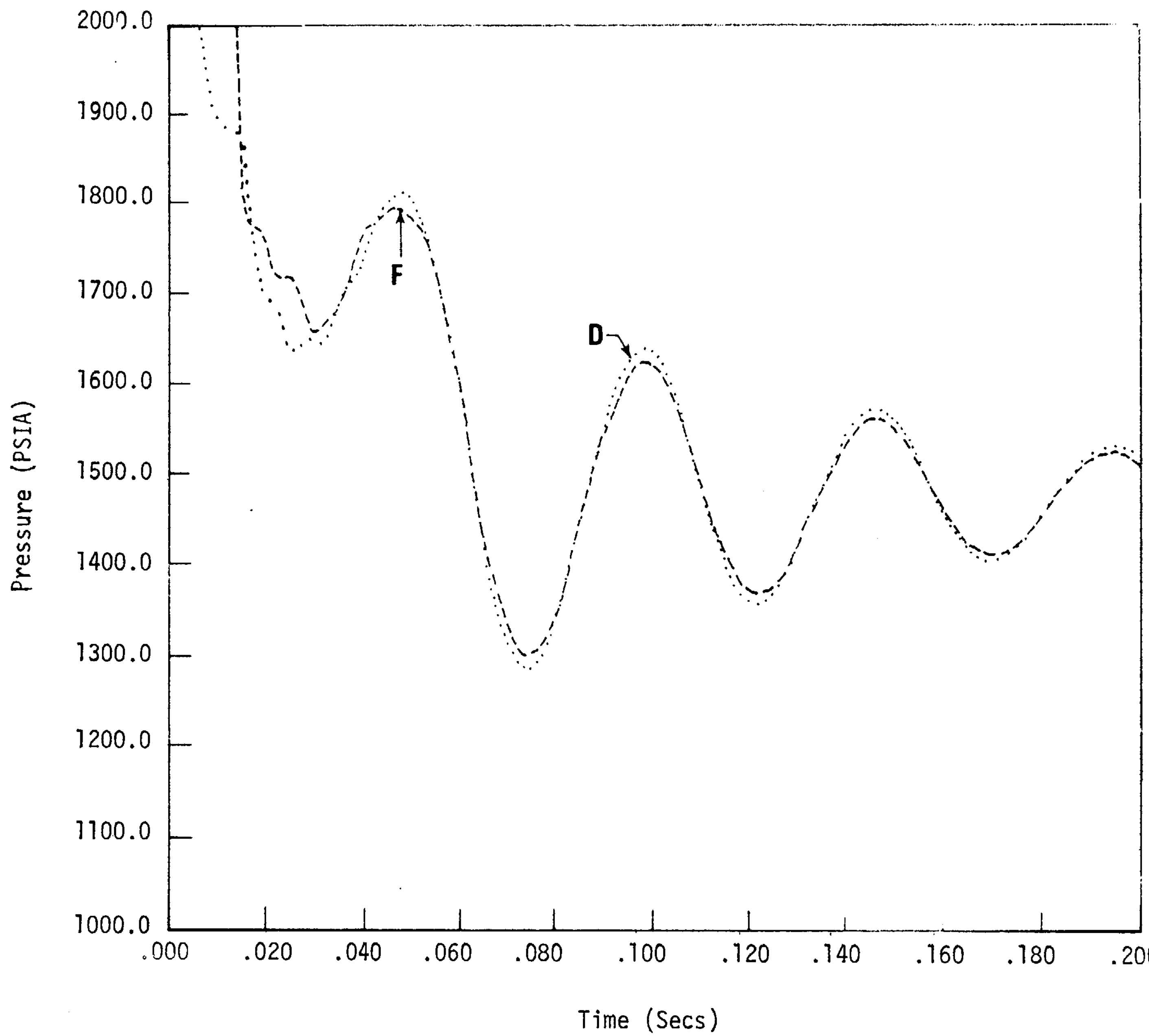

Figure 6-5. BLODWN-2 Results for Lower Plenum Pressures (IITRI Model of PWR, Case 2)

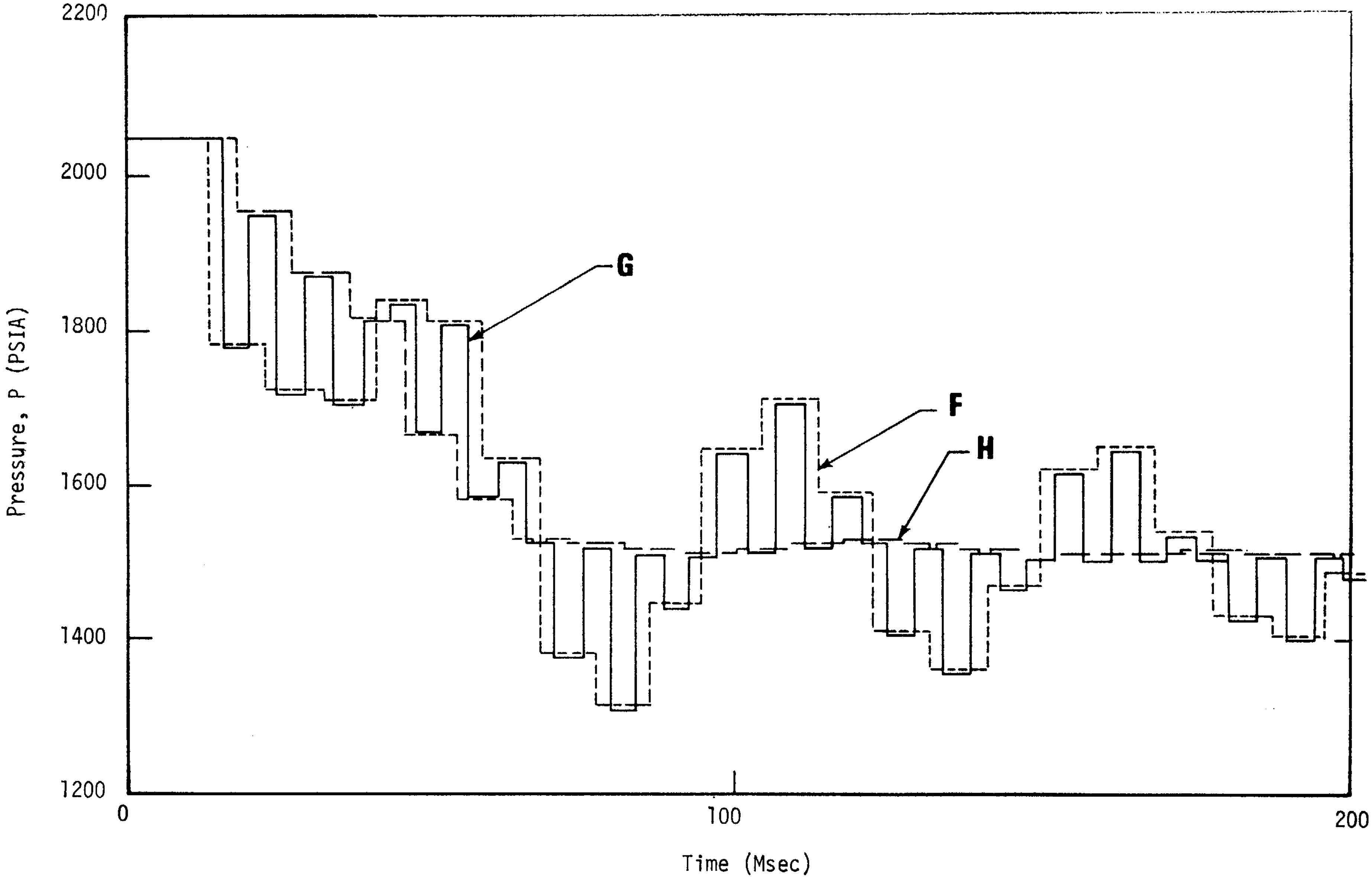

Figure 6-6. Pressure History In Core Region - Case 2
(IITRI Calculation Results)

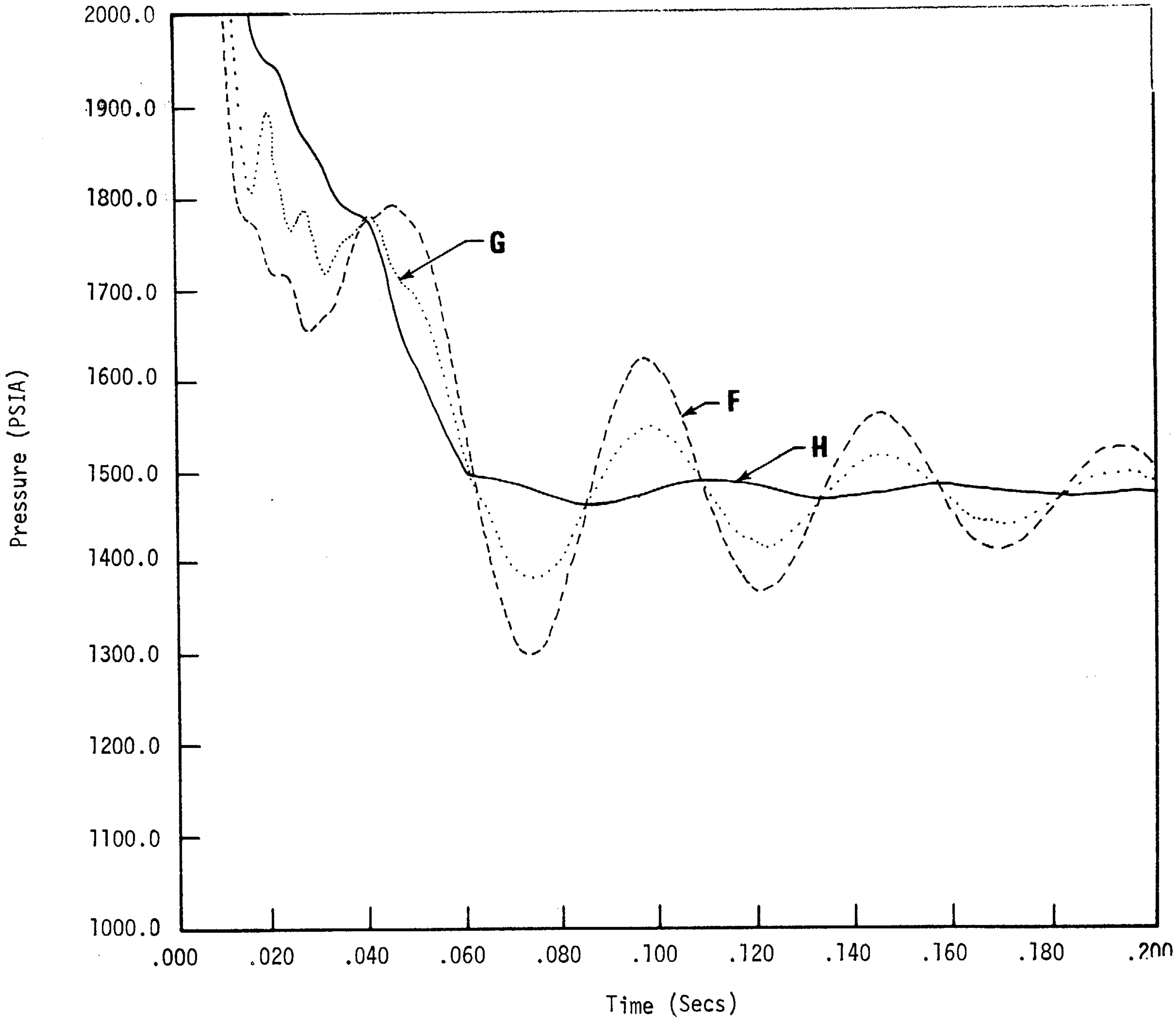

Figure 6-7. BLODWN-2 Results for Core Pressures IITRI Model of PWR, Case 2

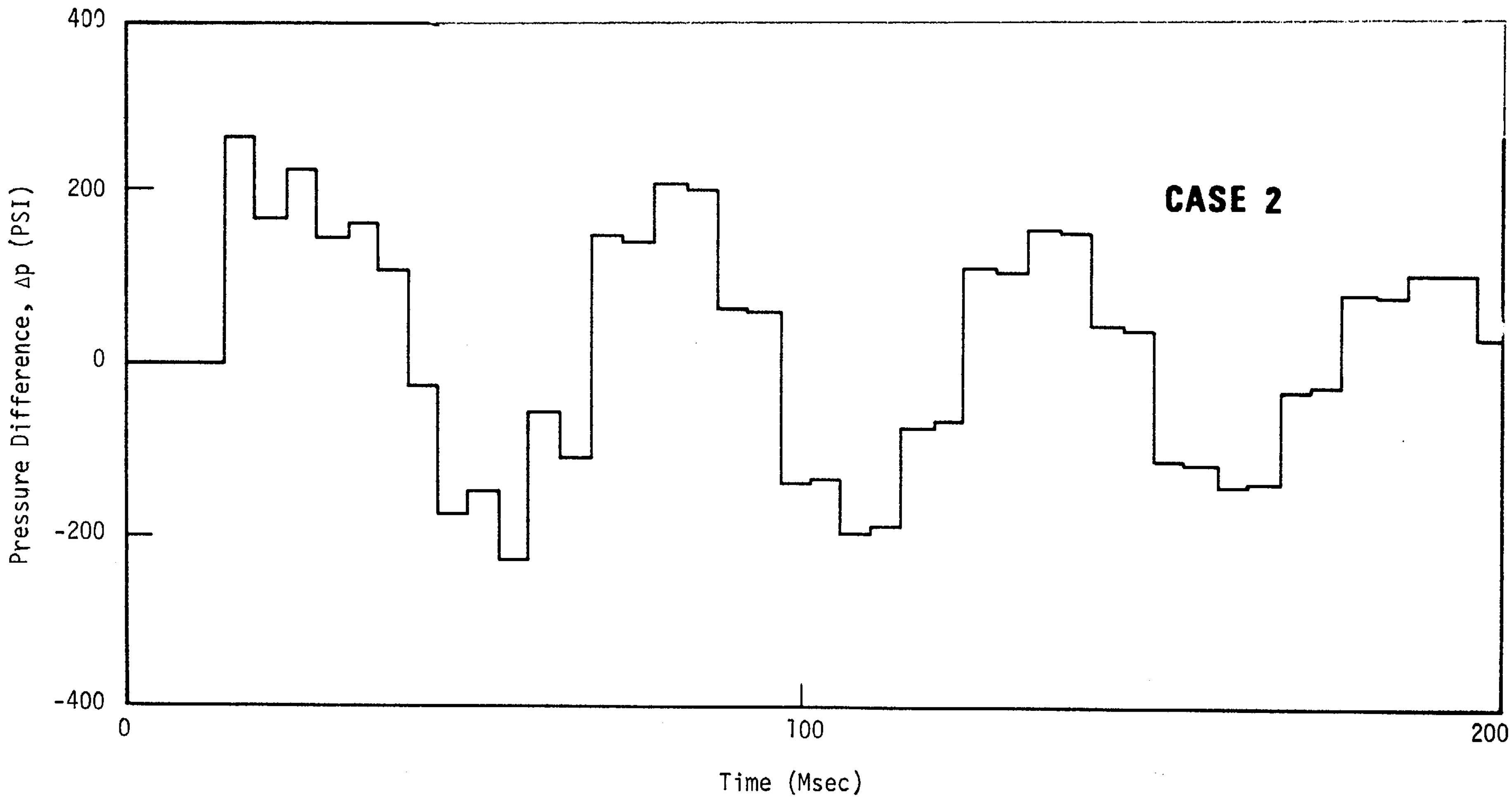

Figure 6-8. Core Load - Case 2, IITRI Calculation Results

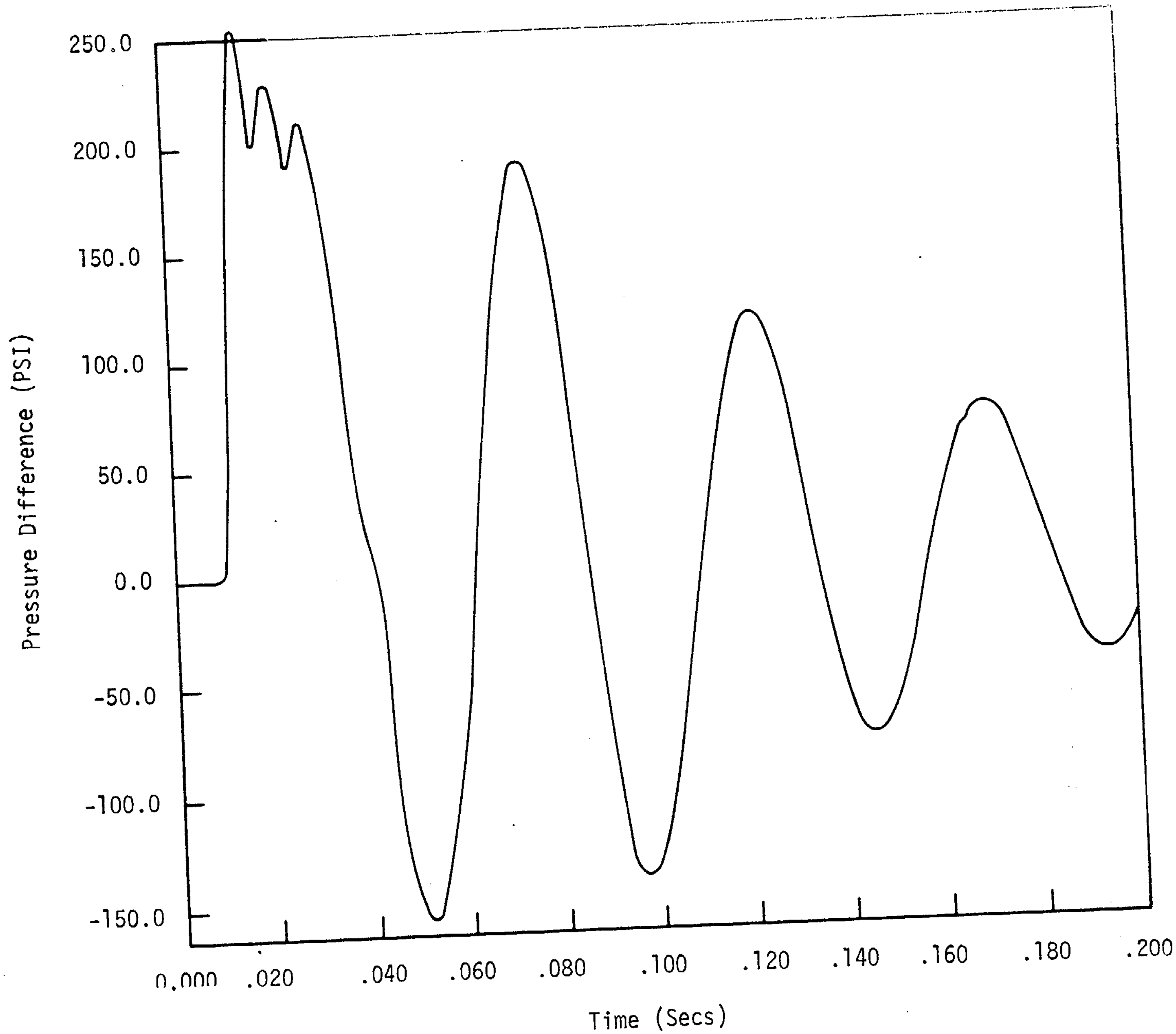

Figure 6-9. BLODWN-2 Results for Pressure Difference Across the Core (IITRI Model of PWR, Case 2)

SECTION 7

CONCLUSIONS

1. The initial temperature distribution of the compressed liquid was found to affect the blowdown history very strongly. It also appears, both from measurements and from calculations, that steep temperature gradients occur at dead-ends of pipes and nozzles and that these gradients are mainly responsible for the observed pressure undershoots. The blowdown models, which include nucleation delays and heat transfer at the growing vapor bubbles, predict strong undershoots everywhere in the system, contrary to most reported observations. The thermal equilibrium assumption, in connection with the modeling of the velocity of sound and the method of characteristics described in Section 2 and incorporated in the BLODWN-2 code, gives satisfactory agreements with most test data examined to date.

2. The ability to accept a large number of spatial increments and to consider multiple flow branches enables the one-dimensional BLODWN-2 code to cope with the hydraulic systems composed of hydraulic passages arranged in complex networks, providing the flow in each of these hydraulic passages does not significantly depart from a one-dimensional (axial) pattern.

3. Representation of three-dimensional hydraulic passages by an equivalent piping network has not yet reached the status of development and acceptance associated with the finite-element theory in structural analysis--although the two have a lot in common. Some general rules concerning the placement of "pipes" (at the antinodes, in order to obtain similar natural frequencies of acoustic vibration) are known and were employed. The desired effects, however, were not obtained, indicating that this particular topic merits additional investigation.

Empty plenums, such as occurred in CSE test B-19B, are the most difficult to model. The annular region around the thermal shield, however, is more or less two-dimensional, and is therefore easier to model. Future CSE tests, in which various reactor internals will be introduced, will provide a valuable "proving ground" for the analytic modeling techniques, provided that the accuracy and reliability of their instrumentation has been thoroughly verified. More calculations and tests with the empty CSE vessel will have to be performed and valid modeling methods found before introducing other complicating effects.

4. In the two-phase blowdown regime, the BLODWN-2 code considers the fluid to be a homogeneous mixture of liquid and vapor. Early in the saturated blowdown regime most test data and comparisons with calculations indicate that a great deal of homogeneity does indeed exist. When most of the severe hydraulic transients have died out, allowing the buoyancy forces to begin separating the vapor from the liquid, the homogeneity ceases to exist, thus invalidating many of the assumptions incorporated in BLODWN-2. As stated in the Introduction to this report, the BLODWN-2 program should not be used in this quasi-steady portion of the saturated blowdown regime--not only because of the run-time economy problems, but also because of the problem of non-homogeneity.

5. Flow restrictions in the form of perforated plates or grids should be modeled as the location where quasi-steady hydraulic losses occur, without the reduction of the channel flow area. Lumping all the holes into one equivalent orifice causes excessive reflections of the acoustic waves, hence significant overestimates of the hydraulic loading of such perforated plates.

6. In view of the satisfactory predictions of the measured pressure histories for a variety of system geometries and test conditions, the use of the BLODWN-2 code for prediction of the reactor primary coolant loop's hydraulic transients during the subcooled, transition, and early saturated blowdown regimes is considered justified. As of now, the one-dimensional modeling of certain complex flow passages and plenums

inside the reactor is still a matter of the intuition and experience of the analyst. More work is needed in obtaining data on blowdown of larger three-dimensional systems and in modeling them with the equivalent piping networks in order to establish whether such an approach is quite satisfactory, and to obtain general ground rules for the synthesis of such networks. The alternative is to extend the analysis into two or three dimensions. As far as the overall philosophy of blowdown computation is concerned, and considering all phases of blowdown, the approach described in the Introduction is, at this stage, the most suitable and all-encompassing.

SECTION 8

REFERENCES

1. Preliminary LOFT Semi-Scale Blowdown Test Data Package, Used in Blowdown Symposium at National Reactor Test Station (July 1966).

2. E. V. Gallagher, "Coolant Decompression Experiments and Analysis: Studies of Reactor Containment," IITRI-578 p. 21-6, Progress Report for May 1969 through June 1963.

3. R. T. Allemann, et. al., "Coolant Blowdown Studies," BNWL Quarterly Progress Report No. BNWL-885, October 1968.

4. B. O. Borgartz, T. P. O'Brien, N. J. M. Rees, A. V. Smith, "Experimental Studies of Water Depressurization Through Simple Pipe Systems," CREST Meeting at Battelle Institute, Frankfurt, Germany, 10-13, June, 1969.

5. A. R. Edwards, "One-Dimensional Two-Phase Transient Flow Calculations," CREST Meeting at Battelle Institute, Frankfurt, Germany, 10-13, June, 1969.

6. S. Fabic, "BLODWN-2: WAPD Computer Program for Calculation of Fluid Pressure, Flow and Density Transients During a Loss-of-Coolant Accident," ANS Transactions Vol. 12, No. 1, p. 358, June 1969.

7. A. N. Nahavandi, "The Loss-of-Coolant Accident Analysis in Pressurized Water Reactors," Nucl. Sci. & Eng. Vol. 36, No. 2, p. 159 (May 1969).

8. H. Goulding, "An Analytical-Experimental Comparison of the Initial Transient Response of High Enthalpy Water During Decompression," ANS Transactions, 1968, Annual Meeting, Toronto.

9. E. V. Gallagher, "Water Decompression Experiments and Analysis for Blowdown of Nuclear Reactor," IITRI-578, p. 21-39 (1969). Final Report on Task No. 3 of PA 31, Contract No. AT(11-1) 578.

   Also personal communication with E. V. Gallagher.

10. A. Ralston and H. S. Wilf, Mathematical Methods for Digital Computers, Wiley & Sons, January 1964.

11. N. I. Semenov, S. I. Kosterin, "Results of Studying the Speed of Sound in Moving Gas-Liquid Systems," Teploenergetika, 1964, Vol 11, No. 6, pp. 46-51.

12. R. E. Henry, "A Study of One- and Two-Component, Two-Phase Critical Flows at Low Qualities," ANL-7430, March 1968.

13. R. E. Henry, H. K. Fauske, "Propagation of Pressure Waves in Two-Phase Mixtures and the Dependency on Flow Regimes," ANS Transactions, Vol. 11, No. 1, p. 364 (1968).

14. R. E. Henry, "Critical Flow of Steam-Water Mixtures," ANS Transactions, Vol. 12, No. 1, p. 353 (1969).

15. F. R. Zaloudek, "The Critical Flow of Hot Water Through Short Tubes," Hanford A. P. P. Report No. HW-77594, May 1963.

16. S. Fabic, "Computer Program WHAM for Calculation of Pressure, Velocity, and Force Transients in Liquid-Filled Piping Newworks," Kaiser Engineers Report No. 67-49-R, November 1967.

17. P. M. Morse, Vibration and Sound, McGraw-Hill, 2nd ed., 1948.

18. G. H. Hanson, "Subcooled-Blowdown: LOFT-Quarter-Scale Experimental Procedures and Calculated Transients using the WHAM-Code," ANS paper, Seattle, Wash., June 18, 1969.

19. H. W. Heiselmann, "Summary Results of Semiscale Blowdown Tests (Single Loop without Core)," Idaho Nuclear Corp. Quarterly Technical Report, LOFT Program Office, April 1 through June 30, 1969, IDO-17303.

20. E. V. Gallagher, "Calculation of Some Blowdown Forces on Internals of a Pressurized Water Reactor Vessel," Letter Report No. IITRI-578, p. 21-37 of January 5, 1968 (from IIT Res. Inst. to USAEC Div. of Reactor Dev. & Technology).

APPENDIX A

Flow Area = .04524 (ft^2), Discharge flow area = .03936 (ft^2) due to partial blockage by glass

Leg #	1	2	3	4	5	6	7
DX (ft)	.13375	.14421	.15737	.15167	.15167	.13079	.12750
No.of space increments	8	19	19	12	13	19	3

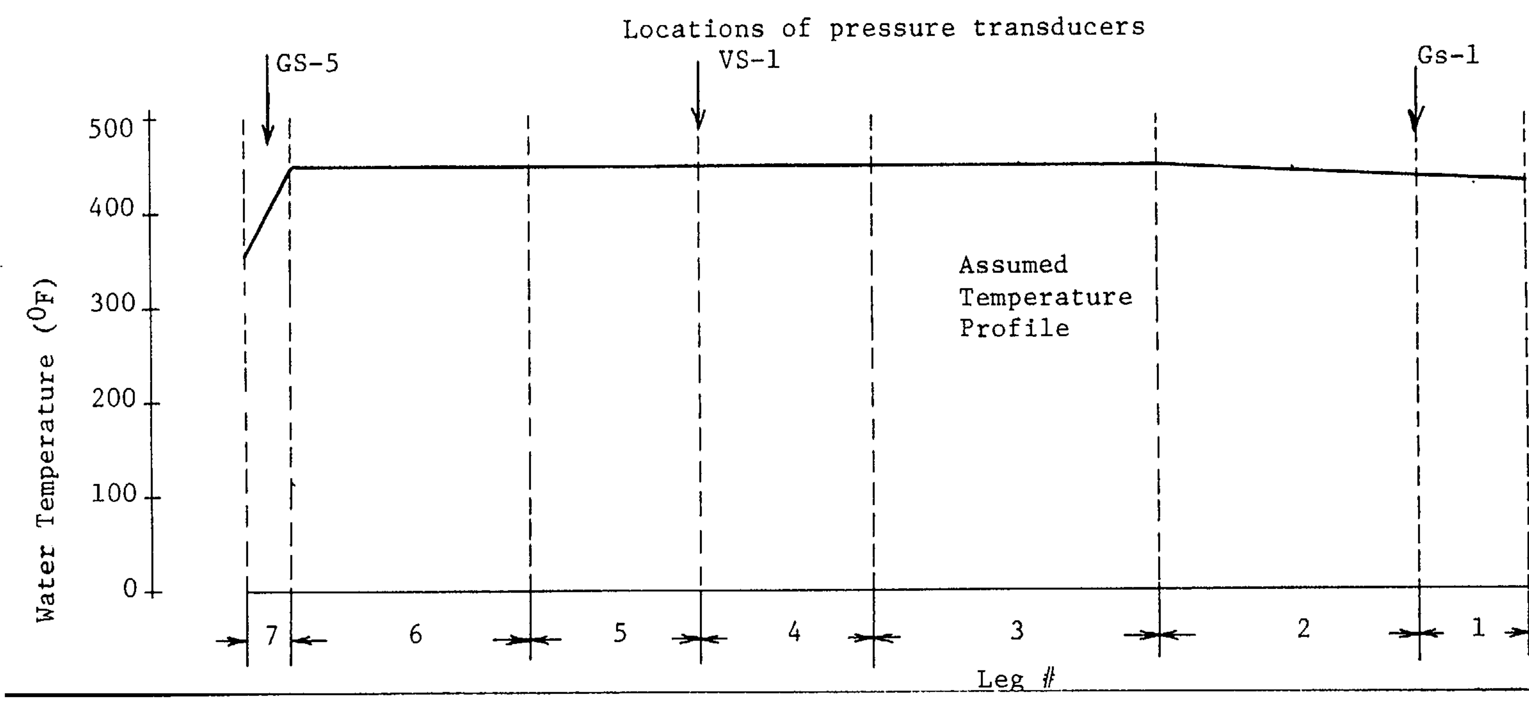

Figure A-1. British Pipe Test, BLODWN-2 Geometry and Temperature Specifications

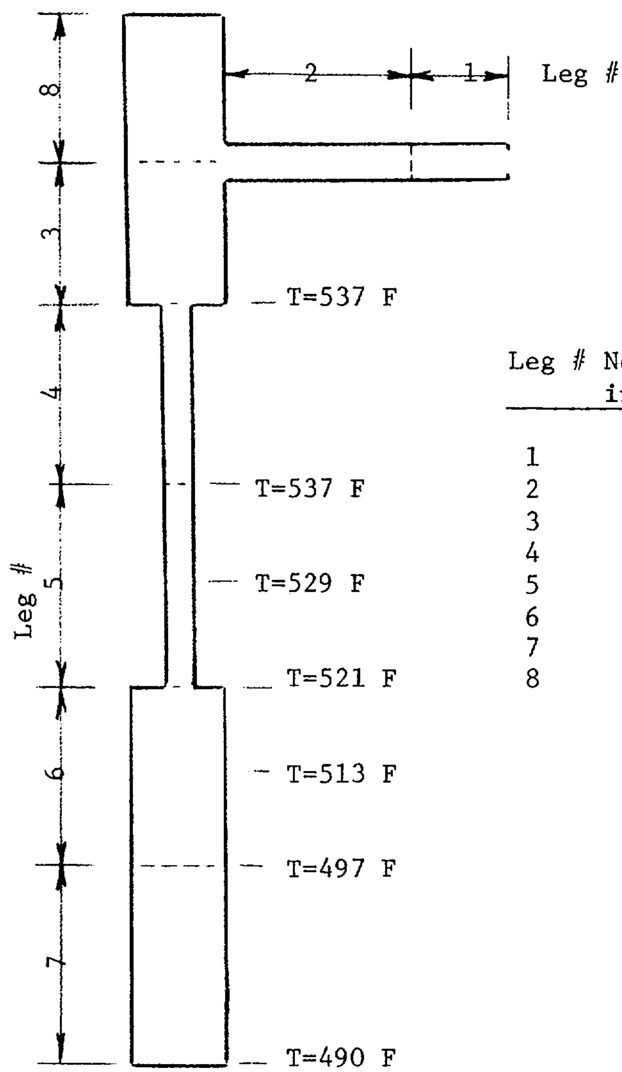

Leg #	No.of space increments	Flow area (ft^2)	DX (ft)
1	10	.087	.10526
2	19	.087	"
3	14	.700	"
4	19	.044	"
5	19	.044	"
6	14	.760	.13800
7	15	.760	"
8	16	.700	.10526

Figure A-2. Geometry Specification for BLODWN-2 Analysis of LOFT Semiscale Test No. 609

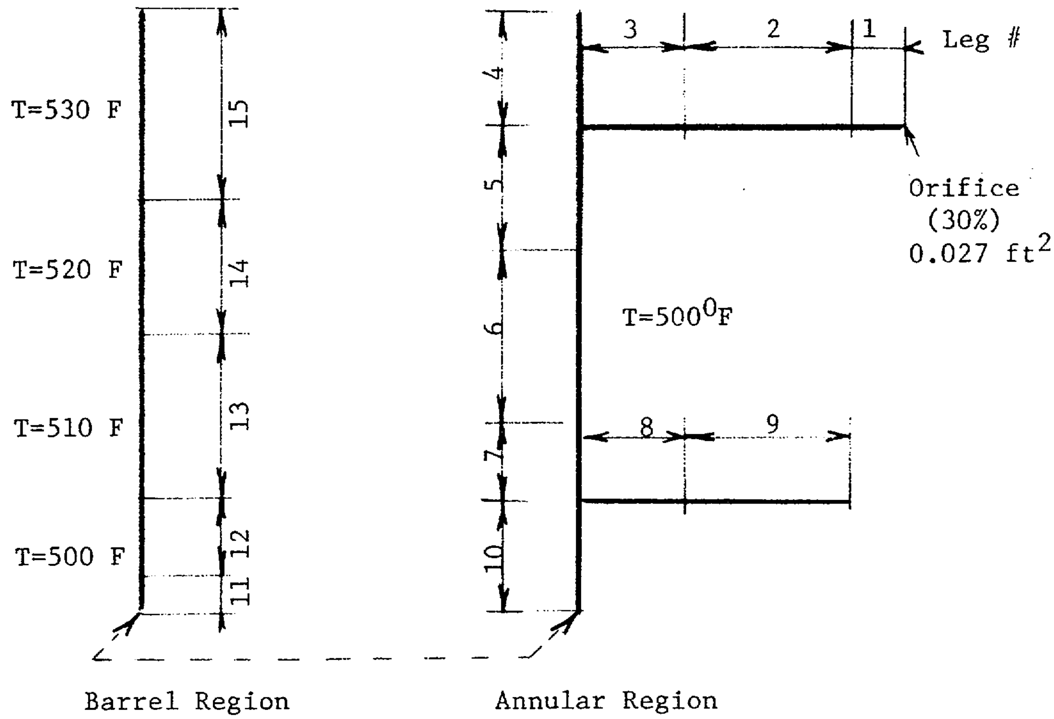

Leg #	No. of space increments	Flow area (ft^2)	DX (ft)
1	5	.090	.08333
2	18	.090	"
3	11	.130	"
4	12	.260	"
5	12	.260	"
6	18	.260	"
7	8	.260	"
8	11	.130	"
9	19	.090	"
10	12	.260	"
11	4	.8865	"
12	8	.5475	"
13	17	.5475	"
14	13	.5475	"
15	19	.7773	"

Figure A-3. Geometry Specification For BLODWN-2 Analysis of LOFT Semiscale Test No. 711

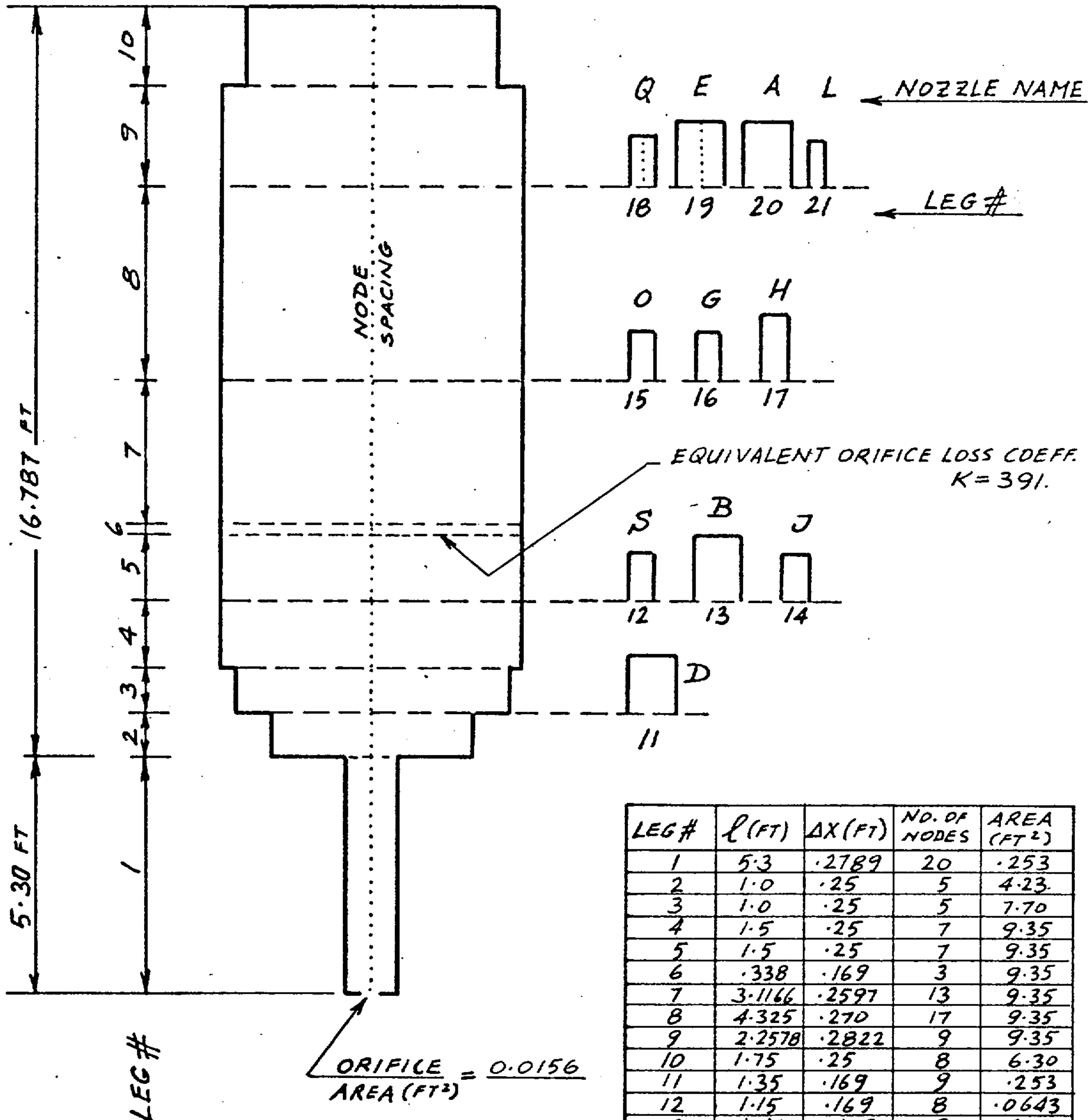

SCALE: ON LENGTH 1" = 4 FT
ON DIAMETER 1" = 2 FT

LEG #	ℓ (FT)	ΔX (FT)	NO. OF NODES	AREA (FT²)
1	5.3	.2789	20	.253
2	1.0	.25	5	4.23
3	1.0	.25	5	7.70
4	1.5	.25	7	9.35
5	1.5	.25	7	9.35
6	.338	.169	3	9.35
7	3.1166	.2597	13	9.35
8	4.325	.270	17	9.35
9	2.2578	.2822	9	9.35
10	1.75	.25	8	6.30
11	1.35	.169	9	.253
12	1.15	.169	8	.0643
13	1.43	.169	9	.253
14	1.15	.169	8	.0643
15	1.15	.169	8	.0643
16	1.15	.169	8	.0643
17	1.43	.169	9	.0643
18	1.15	.169	8	.0643
19	1.43	.169	9	.253
20	1.43	.169	9	.253
21	.833	.169	6	.015

Figure A-4. BLODWN-2 Representation of BNWL-CSE Vessel and Core Plate Arrangement (Model A)

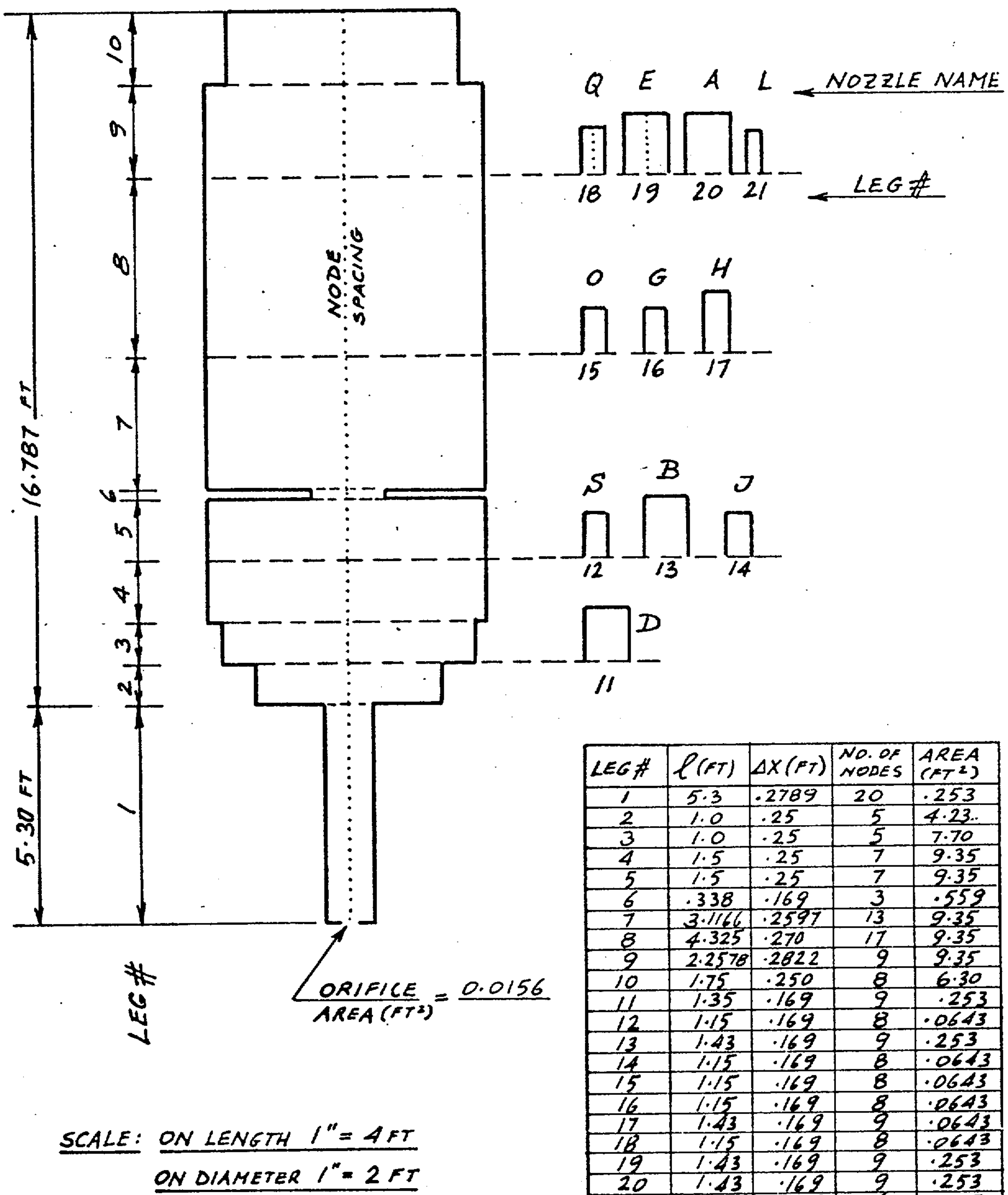

LEG #	ℓ (FT)	ΔX (FT)	NO. OF NODES	AREA (FT²)
1	5.3	.2789	20	.253
2	1.0	.25	5	4.23
3	1.0	.25	5	7.70
4	1.5	.25	7	9.35
5	1.5	.25	7	9.35
6	.338	.169	3	.559
7	3.1166	.2597	13	9.35
8	4.325	.270	17	9.35
9	2.2578	.2822	9	9.35
10	1.75	.250	8	6.30
11	1.35	.169	9	.253
12	1.15	.169	8	.0643
13	1.43	.169	9	.253
14	1.15	.169	8	.0643
15	1.15	.169	8	.0643
16	1.15	.169	8	.0643
17	1.43	.169	9	.0643
18	1.15	.169	8	.0643
19	1.43	.169	9	.253
20	1.43	.169	9	.253
21	.833	.169	6	.015

Figure A-5. BLODWN-2 Representation of BNWL-CSE Vessel and Core Plate Arrangement (Model B)

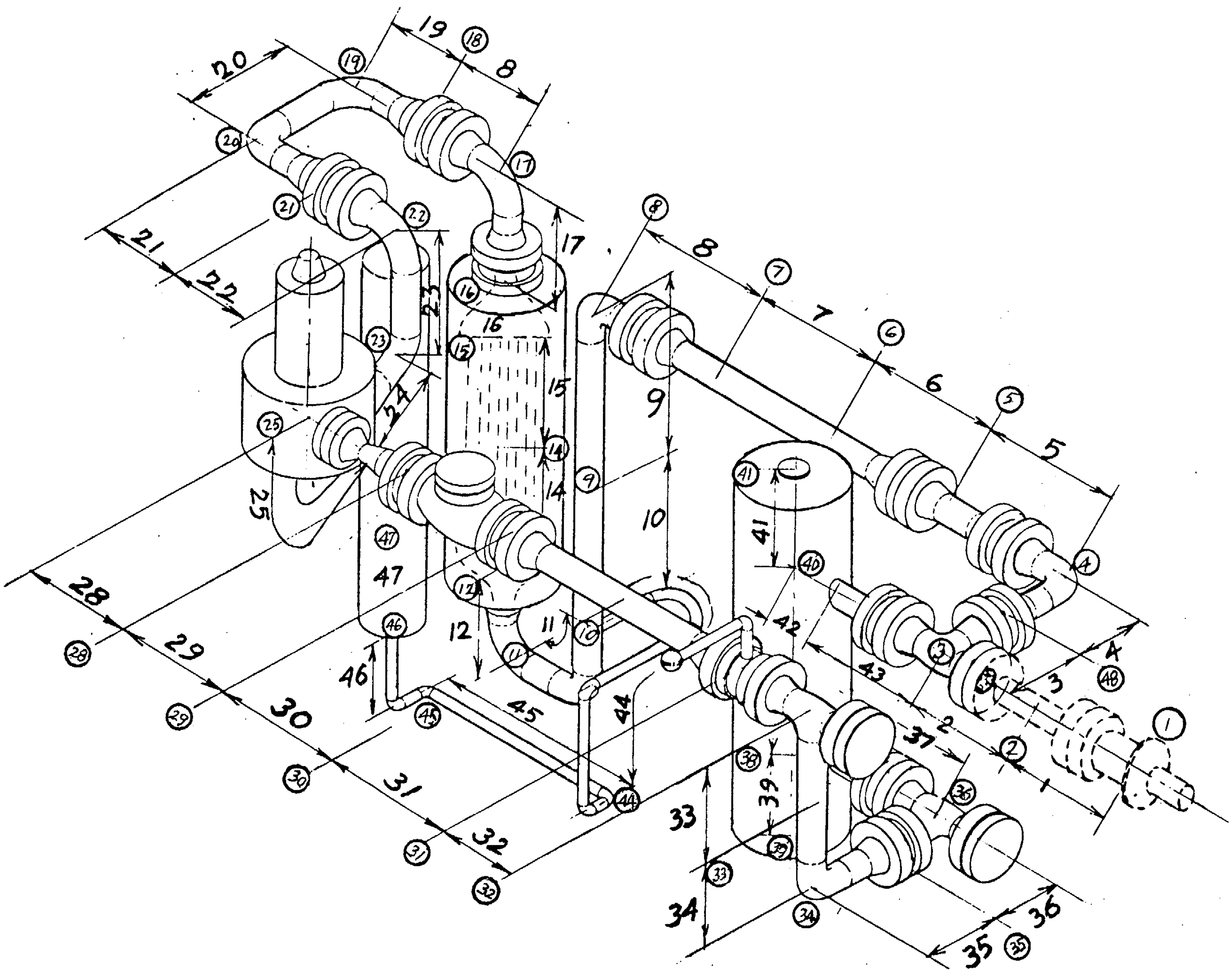

Figure A-6. LOFT 1/4 Scale Loop Map of Leg and Junction Numbers Utilized in BLODWN-2, Fine Mesh Representation

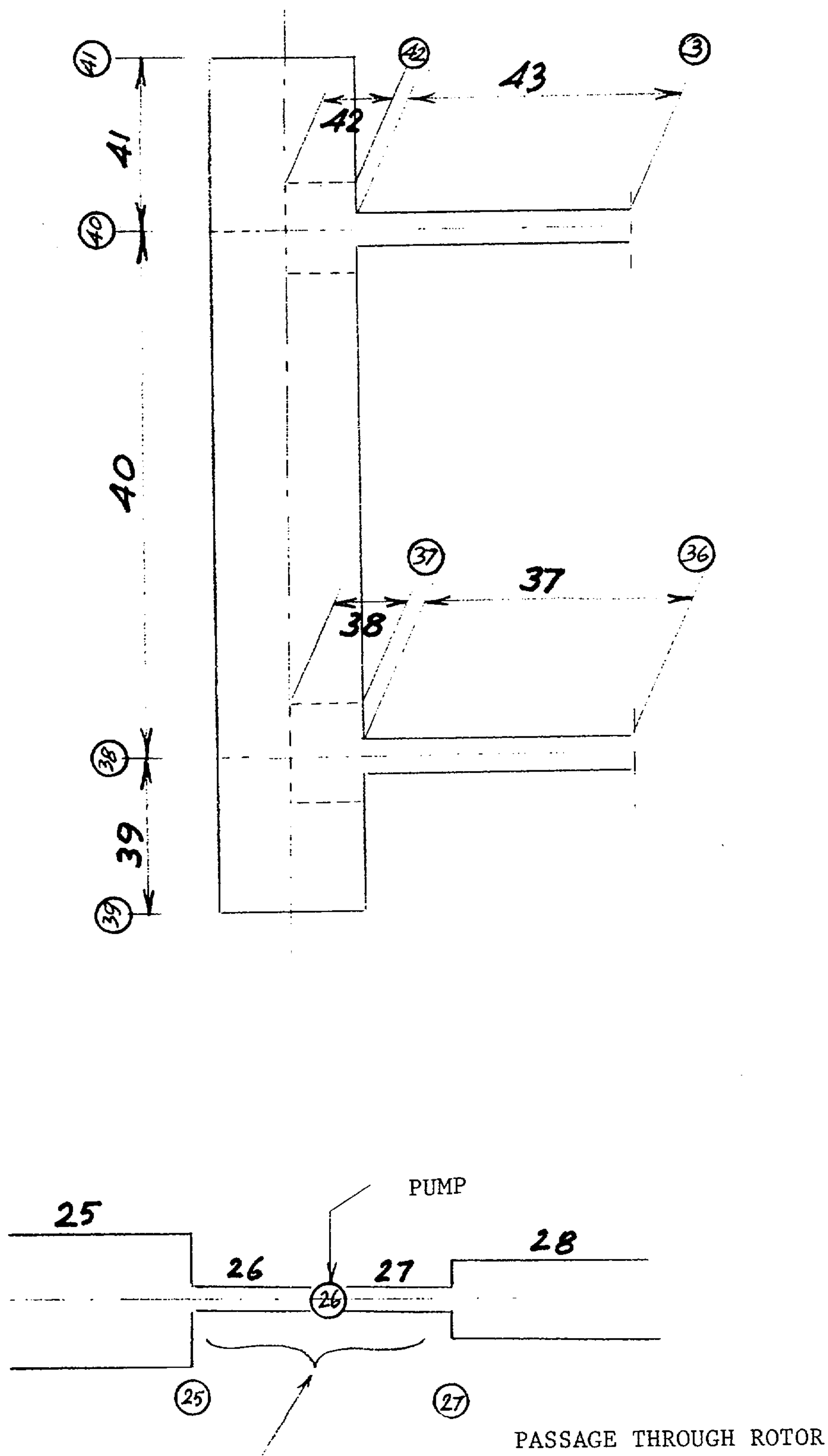

Figure A-7. LOFT 1/4-Scale Loop Vessel and Pump, Map of Leg Identification Numbers

- SYSTEM GEOMETRY -

INPUT DATA LISTING FOR BLODWN-2 ANALYSIS OF LOFT 1/4-SCALE LOOP

J	NO	NND1	NND2	LEG1	LEG2	A(SQ.FT)	DX(FT)	ELEV	DIAM(FT)	LOSS AT 1	LOSS AT N
1	20	10	2	1	2	.09000	.12737	-0.00000	.33848	0.00000	0.00000
2	9	2	3	2	3	.09000	.12737	-0.00000	.33848	-0.00000	.14450
3	10	3	2	3	48	.09000	.12855	-0.00000	.33848	.77050	-0.00000
4	14	2	2	48	4	.09000	.12855	-0.00000	.33848	-0.00000	.37300
5	20	2	2	4	5	.09000	.13555	-0.00000	.33848	-0.00000	.30000
6	20	2	2	5	6	.09000	.13555	-0.00000	.33848	0.00000	0.00000
7	20	2	2	6	7	.09000	.13555	-0.00000	.33848	0.00000	0.00000
8	20	2	2	7	8	.09000	.13555	-0.00000	.33848	-0.00000	.37300
9	17	2	2	8	9	.09000	.12500	-32.20000	.33848	0.00000	0.00000
10	17	2	3	9	10	.09000	.12500	-32.20000	.33848	0.00000	0.00000
11	20	3	2	10	11	.09000	.12500	-16.10000	.33848	.37300	.37300
12	19	2	2	11	12	.09000	.12500	32.20000	.33848	0.00000	0.00000
13	4	2	2	12	13	.75000	.16000	32.20000	.97711	0.00000	0.00000
14	15	2	2	13	14	.06638	.12500	32.20000	.04433	-0.00000	-0.00000
15	12	2	2	14	15	.06638	.12500	32.20000	.04433	-0.00000	-0.00000
16	4	2	2	15	16	.75000	.16000	32.20000	.97711	0.00000	0.00000
17	18	2	2	16	17	.09000	.12630	32.20000	.33848	-0.00000	.37300
18	11	2	2	17	18	.09000	.12630	-0.00000	.33848	0.00000	0.00000
19	16	2	2	18	19	.09000	.12630	-0.00000	.33848	-0.00000	.37300
20	17	2	2	19	20	.09000	.12630	-0.00000	.33848	-0.00000	.37300
21	16	2	2	20	21	.09000	.12630	-0.00000	.33848	0.00000	0.00000
22	11	2	2	21	22	.09000	.12630	-0.00000	.33848	-0.00000	.37300
23	20	2	2	22	23	.09000	.12280	-32.20000	.33848	-0.00000	.37300
24	13	2	2	23	24	.09000	.12280	-0.00000	.33848	0.00000	0.00000
25	20	2	2	24	25	.08200	.12280	10.40000	.32309	0.00000	0.00000
26	3	2	8	25	26	.00450	.12500	-0.00000	.07569	0.00000	0.00000
27	3	8	2	26	27	.00450	.12500	-0.00000	.07569	0.00000	0.00000
28	19	2	2	27	28	.03760	.12500	-0.00000	.21878	0.00000	0.00000
29	20	2	2	28	29	.09000	.14450	-0.00000	.33848	0.00000	0.00000
30	20	2	2	29	30	.09000	.14450	-0.00000	.33848	0.00000	0.00000
31	20	2	2	30	31	.09000	.14450	-0.00000	.33848	-0.00000	146.00000
32	11	2	2	31	32	.09000	.12000	-0.00000	.33848	-0.00000	1.00000
33	13	2	2	32	33	.09000	.13195	-32.20000	.33848	0.00000	0.00000
34	13	2	2	33	34	.09000	.13195	-32.20000	.33848	-0.00000	.37300
35	12	2	2	34	35	.09000	.12855	-0.00000	.33848	0.00000	0.00000
36	12	2	2	35	36	.09000	.12855	-0.00000	.33848	-0.00000	1.00000
37	20	2	2	36	37	.09000	.12500	-0.00000	.33848	0.00000	0.00000
38	6	2	3	37	38	.61800	.12500	-0.00000	.88697	-0.00000	1.00000
39	9	3	1	38	39	1.14674	.13540	-32.20000	1.20822	0.00000	0.00000
40	20	3	3	38	40	1.14674	.16680	32.20000	1.20822	0.00000	0.00000
41	9	3	1	40	41	1.14674	.13540	32.20000	1.20822	0.00000	0.00000

42	6	3	2	40	42	.61800	.12500	-0.00000	.88697	1.00000	-0.00000
43	20	2	3	42	3	.09000	.12500	-0.00000	.33848	-0.00000	.14450
44	20	3	2	10	44	.00499	.21050	-0.00000	.07974	1.00000	.50000
45	20	2	2	44	45	.00499	.21050	-0.00000	.07974	-0.00000	.50000
46	10	2	2	45	46	.00499	.21050	32.20000	.07974	0.00000	0.00000
47	20	2	7	46	47	.39400	.21050	32.20000	.70821	0.00000	0.00000

- INITIAL CONDITIONS OF FLUID -

J	PO(PSIA)	GO(LB/SQFT-SEC)	TEMP(F)	PSAT(PSIA)	H(BTU/LB)
1	2320.00	0.00	560.0	1377.7	562.20
2	2320.00	0.00	585.0	1377.7	592.30
3	2319.60	371.87	585.0	1377.7	592.30
4	2319.60	371.87	585.0	1377.7	592.30
5	2319.50	371.87	585.0	1377.7	592.30
6	2319.45	371.87	585.0	1377.7	592.30
7	2319.40	371.87	585.0	1377.7	592.30
8	2319.35	371.87	585.0	1377.7	592.30
9	2319.25	371.87	585.0	1377.7	592.30
10	2319.20	371.87	585.0	1377.7	592.30
11	2319.00	371.87	585.0	1377.7	592.30
12	2318.95	371.87	585.0	1377.7	592.30
13	2318.60	44.62	585.0	1377.7	592.30
14	2318.30	505.12	585.0	1377.7	592.30
15	2317.80	505.12	585.0	1377.7	592.30
16	2317.20	44.62	585.0	1377.7	592.30
17	2317.00	371.87	585.0	1377.7	592.30
18	2316.80	371.87	585.0	1377.7	592.30
19	2316.80	371.87	585.0	1377.7	592.30
20	2316.60	371.87	585.0	1377.7	592.30
21	2316.55	371.87	585.0	1377.7	592.30
22	2316.55	371.87	585.0	1377.7	592.30
23	2316.50	371.87	585.0	1377.7	592.30
24	2316.40	371.87	585.0	1377.7	592.30
25	2316.00	408.15	585.0	1377.7	592.30
26	2316.00	7437.39	585.0	1377.7	592.30
27	2356.80	7437.39	585.0	1377.7	592.30
28	2356.80	890.11	585.0	1377.7	592.30
29	2356.30	371.87	585.0	1377.7	592.30
30	2356.30	371.87	585.0	1377.7	592.30
31	2356.25	371.87	585.0	1377.7	592.30
32	2321.85	371.87	585.0	1377.7	592.30
33	2321.75	371.87	585.0	1377.7	592.30
34	2321.75	371.87	585.0	1377.7	592.30
35	2321.78	371.87	585.0	1377.7	592.30
36	2321.78	371.87	585.0	1377.7	592.30
37	2321.30	371.87	585.0	1377.7	592.30
38	2320.00	54.15	585.0	1377.7	592.30
39	2320.70	0.00	585.0	1377.7	592.30
40	2320.50	29.19	585.0	1377.7	592.30
41	2320.50	0.00	585.0	1377.7	592.30

42	2320.50	54.15	585.0	1377.7	592.30
43	2320.50	371.87	585.0	1377.7	592.30
44	2319.20	0.00	585.0	1377.7	592.30
45	2319.20	0.00	585.0	1377.7	592.30
46	2319.20	0.00	585.0	1377.7	592.30
47	2319.20	0.00	585.0	1377.7	592.30

- PUMP DATA -

I=	1	2	3	4	5	6	7	8	9
HAN(I)=	2.38000	2.05000	1.80000	1.70000	1.68000	1.65600	1.52000	1.28000	1.00000
HAD(I)=	2.38000	2.05000	1.80000	1.70000	1.68000	1.65600	1.52000	1.28000	1.00000
HVN(I)=	-0.00000	-0.00000	-0.00000	-0.00000	-.35000	-.20000	.10000	.55000	1.00000
HVD(I)=	2.38000	1.77000	1.40000	1.13000	.96000	.85000	.84000	.87000	1.00000
HVT(I)=	2.38000	1.77000	1.40000	1.13000	.96000	.85000	.84000	.87000	1.00000
BAN(I)=	1.22000	.78000	.65000	.60000	.66600	.76660	.85000	.93330	1.00000
BAD(I)=	1.22000	.78000	.65000	.60000	.66600	.76660	.85000	.93330	1.00000
BVN(I)=	-0.00000	-0.00000	-0.00000	-0.00000	-.35000	.05000	.33000	.69300	1.00000
BVD(I)=	1.22000	1.18000	1.12000	1.03000	.90000	.78000	.68000	.60000	.45000
BVT(I)=	1.22000	1.18000	1.12000	1.03000	.90000	.78000	.68000	.60000	.45000

NOMINAL PUMP HEAD(FT)= 0.12500E+03
DISCHARGE(GPM/10000.)= 0.35000E-01
SPEED(RPM)= 0.35500E+04
TORQUE(FT-LB)= 0.16670E+02
INERTIA OF ROTATING PARTS,INCLUDING ENCLOSED WATER(FT-LB-SEC.SQ)= 0.10869E+00